Earth-Science Reviews 176 (2018) 117–146

Contents lists available at ScienceDirect

Earth-Science Reviews

journal homepage: www.elsevier.com/locate/earscirev

Teleconnection of atmospheric and oceanic climate anomalies with Australian weather patterns: a review of data availability

Jasmine B.D. Jaffrés*, Chris Cuff, Cecily Rasmussen, Aimee S. Hesson

C & R Consulting, 188 Ross River Rd, Townsville, QLD 4814, Australia

ARTICLE INFO

Keywords:
Data availability
Australia
Climate indices
Extreme weather events
Satellites
Reanalysis
Weather stations

ABSTRACT

The quality and quantity of observed and reanalysed data influence the direction and accuracy of scientific research. This paper reviews the data available for the study of climate and weather patterns in Australia. A list of global reanalysis and satellite data is provided, along with a more detailed review of available in situ (weather station) data in Australia. Regularly updated climate indices are identified that have previously been linked to Australian climate and weather events. Observation of Australian weather is severely hampered by the continents' vastness and remoteness, as evidenced by heavy bias of in situ measurements that are generally clustered in the coastal high-population centres (mainly southeast of Australia), with central and northern regions often having to rely on remote sensing and reanalysis data. Data sparsity can introduce significant uncertainty in terms of extreme weather and climate change management, as variables such as rainfall exhibit high spatial and temporal variability. Several areas for future research are identified, including investigation into the impact of Australian aerosol levels, the connection between soil moisture and flooding potential, and teleconnection between Atlantic sea surface temperature and Australian climate. While this study focusses on data availability to investigate Australian climate patterns, findings are applicable at a global scale.

1. Introduction

Numerous remote climate patterns influence the climate and weather of Australia. These patterns range from daily to multi-decadal timescales (Micevski et al., 2006; Vance et al., 2015; Verdon et al., 2004a; Verdon et al., 2004b; Wheeler and Hendon, 2004), with extensive interaction between the various oceanic and atmospheric climate features (Cai et al., 2011; Meyers et al., 2007; Power et al., 1999; Risbey et al., 2009b). This high degree of interaction confounds the primary drivers of climate variation. Variability in sea surface temperature (SST), mean sea level pressure (MSLP) and wind have all been associated with distinct, region-specific climate responses in Australia (e.g. Risbey et al., 2009b). Numerous indices have been extracted from in situ and reanalysis datasets to describe and predict climate and meteorological conditions on global (Schubert et al., 2016), national (Meyers et al., 2007) and regional scales (Ummenhofer et al., 2009a). These indices often represent patterns affected by irregular periodicity, varying in timescale from multi-decadal, inter- and intra-annual to daily (Gallant et al., 2012).

Data availability for the study of climate and weather phenomena has augmented significantly since the advent of satellite surveillance in the mid-1970s and the coincident increase in computing capabilities. The emergence of satellite-based datasets, in conjunction with global in situ databases and reanalysis products, aided the identification of climate indices associated with primary climate and weather drivers and their teleconnection (e.g. Henley et al., 2015; Mantua et al., 1997; Wheeler and Hendon, 2004). The improved understanding of teleconnections has shifted the focus away from the El Niño-southern oscillation (ENSO) towards a diverse range of climate patterns (Gallant et al., 2012; Murphy and Timbal, 2008; Tozer and Kiem, 2017), including the interdecadal Pacific oscillation (IPO; Power et al., 1999), the Indian Ocean dipole (IOD; Saji et al., 1999; Verdon and Franks, 2005) and the southern annular mode (SAM; Marshall, 2003). Most indices used to explain or predict climate are based on a very limited range of data types. SST, air pressure and outgoing longwave radiation (OLR) are among the data categories commonly utilised to derive climate indices. The climate index derivation based on these data types is not arbitrary. Rather, the selection is given by decades and centuries of empirical observations triggering interest in causes. El Niño (oceanic component of the ENSO) is the most prominent example, whereby anecdotal evidence by Peruvian fishermen and sailors has pointed to the strong connection between SST and biological productivity (Barber and Chavez, 1983; Cane, 2005).

The purpose of this review is to compile comprehensive lists of

* Corresponding author.
E-mail address: jasmine@candrconsulting.com.au (J.B.D. Jaffrés).

http://dx.doi.org/10.1016/j.earscirev.2017.08.010
Received 1 December 2016; Received in revised form 24 July 2017; Accepted 17 August 2017
Available online 19 August 2017
0012-8252/ © 2017 Elsevier B.V. All rights reserved.

available remote sensing, reanalysis and in situ datasets, with a specific focus on Australia. Climate patterns and associated indices with previously reported teleconnections to Australian climate are summarised. This study is organised as follows: Section 2 presents available datasets for studying Australian weather and climate patterns, including satellite, reanalysis and in situ datasets. Section 3 is dedicated to existing atmospheric and oceanic climate indices and their associated link to Australian climate. Section 4 describes availability of climate index and Australian in situ data in detail by focussing on temporal and spatial trends in dataset observations. Lastly, Section 5 provides a synthesis and recommendations for future research.

2. Data availability

2.1. Remote sensing via satellites

The advent of satellite-based observations has greatly aided the monitoring of changes in, and interactions of, climate patterns and features (Kidd et al., 2009). Remote sensing has enabled large-scale (global) and reasonably frequent monitoring of variables impacting on climate. However, remote sensing via satellites also has several limitations. Its observations are dependent on various factors, including predetermined satellite tracks (study region may not be covered), cloud cover (obstruction of view) and scientific instrument specifications (e.g. Kidd et al., 2009; Tapiador et al., 2012; Turk et al., 2000). For instance, infrared-based methods can provide sampling at high temporal and spatial resolution and, in the case of geostationary satellite networks, also have wide coverage (Vuerich et al., 2009). However, cloud cover reduces the reliability and accuracy of infrared-based rainfall estimates. Conversely, passive microwave methods measure rainfall more directly (via microwave absorption or scattering), while their temporal and spatial resolution is relatively coarse and coverage more limited (Sapiano and Arkin, 2009). Further, there is a trade-off between increased spatial coverage and data resolution, as spatially highly fluctuating variables (e.g. rainfall) may not be captured in high enough resolution depending on the study objectives. Satellite-based observations commonly have a spatial resolution in excess of 1 km (Tapiador et al., 2012).

Satellite-derived datasets include SST, OLR, soil moisture and altimetry. The spatial and temporal resolution of gridded datasets increased significantly over time and is highly dependent on the specifications of the satellite and scientific instruments. Current projects include the National Aeronautics and Space Administration (NASA)'s Earth Observing System (EOS; http://eospso.nasa.gov) and Copernicus (Sentinel satellites; http://www.esa.int/Our_Activities/Observing_the_Earth/Copernicus). The Gravity Recovery and Climate Experiment (GRACE) mission provides information about Earth's gravity field since 2002 (Swenson and Wahr, 2002). This data type has manifold uses, including estimation of flood potential (Reager et al., 2014), terrestrial water storage (Boening et al., 2012), ocean currents (Tapley et al., 2003) and SST (Barton, 2007). Several missions have been dedicated to the monitoring and study of rainfall. The Tropical Rainfall Measuring Mission (TRMM; https://pmm.nasa.gov/data-access/downloads/trmm) has been gathering rainfall data since 1998 (Maggioni et al., 2016). The Global Precipitation Measurement (GPM), a follow-on mission of TRMM, extends coverage to higher latitudes (68°N/S) compared to TRMM (37°N/S) (Hou et al., 2014).

Individual satellites may carry multiple scientific instruments, targeting different aspects of Earth's environment. The MODIS (moderate-resolution imaging spectroradiometer) scientific instrument is carried by two EOS satellites (Terra and Aqua). Data from MODIS can be utilised to monitor bushfire potential via assessment of grassland curing (Newnham et al., 2010) and dust levels (Alizadeh Choobari et al., 2012). AVHRR (advanced very-high-resolution radiometer) sensor data have been analysed to study Australian bushfire occurrence (Russell-Smith et al., 2007). The stratospheric composition, including aerosol levels, have also been monitored via several satellite instruments, including CALIOP (cloud-aerosol lidar with orthogonal polarization) (Alizadeh Choobari et al., 2012), OSIRIS (optical spectrograph and infrared imager system) (Llewellyn et al., 2004), SAGE II (stratospheric aerosol and gas experiment II) and “SAM II” (“stratospheric aerosol measurement II”, not to be confused with the southern annular mode climate index called SAM) (Russell and McCormick, 1989). Severe hail storm activity, in turn, has been estimated based on data derived from AMSR-E (advanced microwave scanning radiometer - EOS) (Cecil and Blankenship, 2012). AMSR-E also allows for the derivation of soil moisture, with several algorithms available to retrieve soil moisture information (Draper et al., 2009; Liu et al., 2011). The SMAP (Soil Moisture Active Passive) satellite is a relatively new addition to NASA's EOS network, launched in January 2015 to primarily focus on monitoring soil moisture (Zeng et al., 2016). Satellite-derived soil moisture data have been utilised to extract connections between three commonly studied climate indices (ENSO, IOD and SAM) and Australian soil moisture (Bauer-Marschallinger et al., 2013). Satellite imagery is also analysed to determine tropical cyclone (TC) strength and position, primarily (Velden et al., 2006) by applying the Dvorak technique (Dvorak, 1975).

Satellite-derived gridded data can be freely obtained from numerous sources (Table 1), including the European Space Agency Climate Change Initiative (ESA CCI), EUMETCast (by the European Organisation for the Exploitation of Meteorological Satellites, EUMETSAT), NASA's Jet Propulsion Laboratory (JPL) and the National Snow and Ice Data Center (NSIDC).

2.2. Databases and reanalysis data

2.2.1. Databases – tropical cyclones (TCs) and in situ data

Large-scale studies commonly require data (e.g. rainfall or TCs) from several source agencies. For TC studies in the Coral Sea region east of Australia, TC information may be required from two regional specialised meteorological centres (RSMCs), as the Australian Bureau of Meteorology (BOM) is responsible for the region west of 160°E while the Fiji Meteorological Service (FMS) is in charge of the area east of that longitude. Several databases with global TC data exist (Table 2). Two international databases are commonly accessed for TC studies: 1) the International Best Track Archive for Climate Stewardship (IBTrACS;

Table 1
Online satellite data portals.

Satellite Data Provider	Abbreviation	Website
Copernicus Open Access Hub		https://scihub.copernicus.eu/
EUMETCast	EUMETCast	http://www.eumetsat.int
European Space Agency Climate Change Initiative	ESA CCI	http://cci.esa.int
Gravity Recovery And Climate Experiment Tellus	GRACE Tellus	https://grace.jpl.nasa.gov
NASA Goddard Earth Sciences Data and Information Services Center	NASA GES DISC	https://disc.gsfc.nasa.gov
NASA Langley Research Center Atmospheric Sciences Data Center	NASA LaRC ASDC	https://eosweb.larc.nasa.gov
National Snow and Ice Data Center	NSIDC	http://nsidc.org
Physical Oceanography Distributed Active Archive Center	PO.DAAC	https://podaac.jpl.nasa.gov

Table 2
Tropical cyclone and weather station databases.

Data Type	Dataset	Coverage	Comments	Reference/Source	Website
Tropical cyclones (best track)	BOM	Australian region	10-minute sustained wind speed	Bureau of Meteorology	http://www.bom.gov.au/cyclone/history
	IBTrACS	Global	Source-specific sustained wind speed period	Knapp et al., 2010	http://www.ncdc.noaa.gov/ibtracs
	JTWC	Global	1-minute sustained wind speed	Chu et al., 2002	http://www.usno.navy.mil/JTWC
	SPEArTC	Southwest Pacific	10-minute sustained wind speed	Diamond et al., 2012	http://apdrc.soest.hawaii.edu/projects/spearte
In situ (surface marine)	ICOADS	Global	Gridded products also available	Freeman et al., 2016	http://icoads.noaa.gov
In situ (weather stations)	BOM	Australia	Daily data for individual stations obtainable from CDO; entire database accessible by request	Bureau of Meteorology (Climate Data Online)	http://www.bom.gov.au/climate/data
	GHCN-Daily	Global	Source agency quality flags not provided	Menne et al., 2012	ftp://ftp.ncdc.noaa.gov/pub/data/ghcn/daily
	GSN	Global	High-quality GCOS reference stations (subset)	Peterson et al., 1997	http://www.wmo.int/pages/prog/gcos
	HQACDs	Australia	High-quality datasets, including ACORN-SAT	Bureau of Meteorology	http://www.bom.gov.au/climate/change/datasets/datasets.shtml

http://www.ncdc.noaa.gov/ibtracs) and 2) the Joint Typhoon Warning Center (JTWC; http://www.usno.navy.mil/JTWC; also accessible via Unisys Weather; http://weather.unisys.com/hurricane). The JTWC data is based on the Saffir–Simpson hurricane wind scale (Chu et al., 2002). Thus, their severe TC classification is based on 1-minute sustained wind speeds, rather than the World Meteorological Organization (WMO) standard of 10-minute sustained wind speeds (Knapp et al., 2010; WMO, 1983) as practised in the Australian region. IBTrACS provides two main datasets. IBTrACS-WMO only contains data from organisations sanctioned by the WMO, including BOM and FMS. IBTrACS-All, in turn, comprises data from all available sources (Knapp et al., 2010), including JTWC. A new database, the Southwest Pacific Enhanced Archive for Tropical Cyclones (SPEArTC; http://apdrc.soest.hawaii.edu/projects/spearte), was recently compiled (Diamond et al., 2012). SPEArTC incorporates existing IBTrACS TC data for the southwest Pacific region (including the Gulf of Carpentaria and Coral Sea) and also contains TC track information recovered from various Pacific Island national meteorological services. A detailed quality control has been applied to all individual TC tracks contained in SPEArTC. Magee et al. (2016) compared IBTrACS-All, JTWC and SPEArTC and determined that SPEArTC is the most complete repository of TCs for the southwest Pacific region. As the present paper's focus is on Australia, TC data will be directly accessed from BOM (http://www.bom.gov.au/cyclone/history).

Global databases are also available for various in situ data types (Table 2). The International Comprehensive Ocean-Atmosphere Data Set (ICOADS; formerly COADS) is reputedly the most extensive and most widely used database of in situ (ships, buoys, etc.) surface marine observations (Freeman et al., 2016). The database contains 22 observed and derived variables, including SST, sea ice, sea level pressure, air temperature and cloud cover (Worley et al., 2005). ICOADS is a freely available archive (http://icoads.noaa.gov) that is routinely utilised for scientific analysis (Wolter and Timlin, 1993; Wolter and Timlin, 1998) and construction of gridded datasets (e.g. Huang et al., 2015; Kennedy et al., 2011a). The Global Historical Climatology Network (GHCN)-Daily dataset, in turn, contains records from weather stations worldwide, with an estimated two-thirds only registering rainfall (Menne et al., 2012). The GHCN-Daily database also contains all daily temperature and rainfall data maintained by BOM, although the associated quality flags are excluded.

BOM maintains a large number of weather stations throughout Australia, recording a range of variables. Gathered data generally includes daily rainfall, with some stations recording additional data, including temperature, wind speed and relative humidity. Daily rain and temperature data are freely available from BOM via their Climate Data Online (CDO) website (http://www.bom.gov.au/climate/data). Data not accessible via the CDO database (including data recordings exceeding daily frequency) can be purchased on request by contacting BOM. For the present paper, data were accessed from both sources (CDO and BOM).

Following a request by the WMO in 1990 (Trewin, 2013) to identify high-quality in situ and remote sensing data, the Global Climate Observing System (GCOS) was established (Spence and Townshend, 1995). The associated GCOS Surface Network (GSN) contains approximately 1000 weather stations, selected according to their perceived data quality, record length and globally uniform spatial coverage (Peterson et al., 1997). GSN also contains weather station data supplied by BOM (cf. full list in GCOS, 2013). The GSN represents only a subset of identified weather stations with high-quality, long-term data records. BOM have compiled extended lists of weather stations suitable for inclusion in high-quality Australian climate datasets (HQACDs; http://www.bom.gov.au/climate/change/datasets/datasets.shtml). Separate lists are available for daily rainfall (Lavery et al., 1992) and temperature (Trewin, 2001), monthly rainfall (Lavery et al., 1997), pan evaporation (Jovanovic et al., 2008) and cloud amount (Jovanovic et al., 2011), and annual temperature (Della-Marta et al., 2004; Torok and

Nicholls, 1996). The original daily and annual temperature datasets have been superseded by the Australian Climate Observations Reference Network – Surface Air Temperature (ACORN-SAT; Trewin, 2013), which includes data from 112 weather stations (Bureau of Meteorology, 2011). All data within HQACDs, including ACORN-SAT, are freely accessible from BOM (http://www.bom.gov.au/climate/change/hqsites).

2.2.2. Gridded data – modified in situ observations and reanalysis products

Derivation of global gridded datasets by aggregating and reanalysing historic observations (in situ, remote sensing and numerical model data) has facilitated investigation and interpretation of regional and global climate patterns by filling spatial and temporal gaps in data availability. For the purpose of this review, we distinguish between gridded datasets derived entirely from in situ observations that underwent minimal modifications, and gridded reanalysis (or retrospective analysis) products created by more extensive data transformation. Reanalysis methods include a vast array of statistical procedures (e.g. data assimilation by optimal interpolation; Daley, 1993) and the final product may result from a blend of data from multiple platforms (e.g. numerical models, satellites and in situ monitoring). Basic gridding techniques include cell-averaging of in situ observations (Worley et al., 2005) and interpolation for data gap reduction (Jones et al., 2009). More elaborate methods are applied to obtain reanalysis products, involving multi-step processes and commonly incorporating data from several sources (e.g. Maggioni et al., 2016). Various gridded datasets are in existence, with the spatial resolution ranging from 0.05° to 5° (Table 3). The European Centre for Medium-Range Weather Forecasts (ECMWF) has produced several global ERA (ECMWF re-analysis) datasets (http://apps.ecmwf.int/datasets), including ERA-40 (Kållberg et al., 2004), its successor ERA-Interim (Dee et al., 2011), and the more land-oriented ERA-Interim/Land (Balsamo et al., 2015). The National Centers for Environmental Prediction–National Center for Atmospheric Research (NCEP–NCAR) reanalysis (NNR; http://www.esrl.noaa.gov/psd) project also offers various gridded datasets (Kalnay et al., 1996). Additional gridded products are available from Princeton University (http://hydrology.princeton.edu/data.php), including global meteorological forcing data (Sheffield et al., 2006).

ICOADS (cf. Section 2.2.1) includes a wide range of non-interpolated monthly gridded climatology products, derived from basic statistics for each of the observed near-surface meteorological and oceanographic variables contained in the extensive ICOADS in situ database (Freeman et al., 2016). The ICOADS in situ database also formed the basis for several gridded datasets that have been created with focus on SST (e.g. Huang et al., 2015; Kennedy et al., 2011a). SST datasets include the global sea-ice and SST (GISST) dataset (Rayner et al., 1996), now superseded by Hadley Centre sea ice and sea surface temperature (HadISST; Rayner et al., 2003), extended reconstructed sea surface temperature (ERSST; Huang et al., 2015; Smith et al., 2008), optimum interpolation sea surface temperature (OISST; Reynolds, 2009; Reynolds et al., 2007) and Hadley Centre SST (HadSST; Kennedy et al., 2011a; Kennedy et al., 2011b). These gridded surface marine datasets have been used to derive a wide range of climate indices (Table 4), including Niño indices (Smith and Sardeshmukh, 2000; Wolter and Timlin, 1993), the IOD (Saji et al., 1999), the IPO tripole index (TPI; Henley et al., 2015) and the Pacific decadal oscillation (PDO; Mantua et al., 1997).

Various gridded datasets are available for atmospheric studies. Gridded MSLP data are offered by ERA-40 and NNR, both of which have been utilised to derive indices for the SAM (cf. Marshall, 2003). Global tropospheric variability estimates derived from assimilated observations of synoptic surface pressure are provided by the Twentieth Century Reanalysis (20CR) project (Compo et al., 2011). This international project is let by National Oceanic and Atmospheric Administration (NOAA)'s Earth System Research Laboratory (ESRL) and the Cooperative Institute for Research in Environmental Sciences (CIRES). Both ERA-Interim (Allen and Karoly, 2014) and NNR (Brooks et al., 2003) data have been applied to severe storm analysis encompassing Australia. Global rainfall data grids derived from interpolated in situ observations are provided by the Global Precipitation Climatology Centre (GPCC; Schneider et al., 2014) and the Climatic Research Unit (CRU; Harris et al., 2014). While the monthly GPCC climatology rainfall product is based on considerably more weather stations than CRU TS (CRU time series) (Schneider et al., 2014), CRU TS offers a wider range of variables, including potential evapotranspiration and various temperature fields (Harris et al., 2014).

Several higher resolution (0.05°) gridded Australian products are also offered. The Scientific Information for Land Owners (SILO) dataset (Jeffrey et al., 2001) is maintained by the Queensland Department of Science, Information Technology and Innovation (DSITI; www.longpaddock.qld.gov.au/silo), while the Australian Water Availability Project (AWAP) dataset can be accessed from BOM (http://www.bom.gov.au/jsp/awap; Jones et al., 2009). The AWAP products are obtained with weather station data (e.g. rainfall), satellite data (solar radiation) and a water-carbon model (evaporation) (Jones et al., 2009). SILO provides gridded datasets as well as patched point records (filling of temporal data gaps at point locations by spatial interpolation) (Jeffrey et al., 2001) for approximately 4800 BOM weather station sites. Both AWAP and SILO exhibit a small positive bias on dry days and a negative bias on wet days (Beesley et al., 2009). Beesley et al. (2009) determined that SILO tends to outperform AWAP in the east coast of Australia where the rain gauge density is higher. A close fit between SILO and BOM station data is generally expected, as the SILO derivation method explicitly aims at reproducing individual observation points, while AWAP targets the replication of area-averaged values (Tozer et al., 2012). However, Tozer et al. (2012) found that SILO performs relatively poorly when compared to independent rainfall gauge data. Further, they noted that both AWAP and SILO tend to overestimate rainfall during dry periods and fail to accurately capture extreme rainfall events. Both SILO and AWAP data are commonly utilised in Australian studies (e.g. Klingaman et al., 2013; Tozer et al., 2014; Vance et al., 2015).

Individual rainfall observation methods are associated with strengths and weaknesses (cf. Section 2.1 and Section 2.2.3). To overcome these limitations, infrared, microwave and in situ rainfall products are commonly merged (Sapiano and Arkin, 2009). The TRMM Multisatellite Precipitation Analysis (TMPA) dataset combines observations from TRMM with rain gauge data (Huffman et al., 2007). A different approach to the creation of a global gridded rainfall dataset was taken by the University of California, Irvine (UCI) with their PERSIANN (Precipitation Estimation from Remotely Sensed Information using Artificial Neural Networks) product (Hsu et al., 1997; Sorooshian et al., 2000). UCI primarily use infrared satellite data, in conjunction with artificial neural networks, to obtain operational estimates of rainfall rate at a 0.25° spatial resolution, with data available from March 2000 (http://chrsdata.eng.uci.edu). Additional satellite precipitation products include the Climate Prediction Center (CPC) morphing technique (CMORPH; Joyce et al., 2004) and the Global Satellite Mapping of Precipitation (GSMaP; Ushio et al., 2009) by the Japan Aerospace Exploration Agency (JAXA). Maggioni et al. (2016) provide a detailed review of these rainfall products.

Numerical models are utilised for the creation of gridded datasets by assimilating diverse datasets and interpolating sparse observations (Rintoul et al., 2012). Yasunaka and Hanawa (2011) compared seven SST datasets, highlighting the various gridding methods (from simple grid averaging to more technical interpolation approaches) applied to create the gridded datasets. ICOADS (Worley et al., 2005) and HadSST (Kennedy et al., 2011a) are among the datasets that underwent simple grid averaging and therefore contain numerous data gaps (missing grid values) in undersampled regions, especially during the pre-satellite era. Application of more technical interpolation methods allows filling data

Table 3
Details of gridded datasets. Datasets are categorised as 1) "modified in situ" (MIS) if the original terrestrial (in situ) data underwent minimal alteration or 2) as a reanalysis (rean.) product if the original data were satellite-derived or underwent significant, multi-step modification.

Dataset	Type	Period	Coverage	Spatial Resolution	Temporal Resolution	Reference	Source	Website
20CRv2c	Rean.	1851–2014	Global	2°	6-hourly	Compo et al., 2011	NOAA ESRL/CIRES	https://www.esrl.noaa.gov/psd/data/20thC_Rean
AWAP	MIS/rean.	1900–present	Australia	0.05°	Daily	Jones et al., 2009	BOM	http://www.bom.gov.au/jsp/awap
CMORPH	Rean.	December 2002–present	60°N - 60°S	0.0727°	30 minutes	Joyce et al., 2004	NOAA/CPC	http://www.cpc.ncep.noaa.gov/products/janowiak/cmorph_description.html
CRU TS	MIS	1901–2015	Global	0.5°	Monthly	Harris et al., 2014	CRU	http://www.cru.uea.ac.uk/cru/data/hrg
ERA-Interim	Rean.	1979–present	Global	0.75°	3-hourly	Dee et al., 2011	ECMWF	http://apps.ecmwf.int/datasets
ERA-Interim/Land	Rean.	1979–2010	Global	80 km	3-hourly	Balsamo et al., 2015	ECMWF	http://apps.ecmwf.int/datasets
ERSSTv4	Rean.	1854–present	Global	2°	Monthly	Huang et al., 2015	NOAA-NCEI	https://www.ncdc.noaa.gov/ersst
GPCC	MIS/rean.	1901–present	Global	0.25°	Monthly	Schneider et al., 2014	Deutscher Wetterdienst	http://gpcc.dwd.de
GSMaP	Rean.	March 2000–present	60°N - 60°S	0.1°	Hourly	Ushio et al., 2009	JAXA	http://sharaku.eorc.jaxa.jp/GSMaP
HadISST1	Rean.	1871–present	Global	1°	Monthly	Rayner et al., 2003	Met Office Hadley Centre	http://www.metoffice.gov.uk/hadobs/hadisst
HadSST	MIS	1850–present	Global	5°	Monthly	Kennedy et al., 2011a,b	Met Office Hadley Centre	http://www.metoffice.gov.uk/hadobs/hadsst3
ICOADSv3	MIS	1662–present	Global	2°	Monthly	Freeman et al., 2016	NOAA/NCAR	http://icoads.noaa.gov
NNR	Rean.	1948–present	Global	2.5°	6-hourly	Kalnay et al., 1996	NOAA-NCEP/NCAR	http://www.esrl.noaa.gov/psd
OISSTv2	Rean.	1981–present	Global	0.25°	Daily	Reynolds, 2009	NOAA-NCEI	https://www.ncdc.noaa.gov/oisst
PERSIANN	Rean.	March 2000–present	Global	0.25°	Hourly	Hsu et al., 1997; Sorooshian et al., 2000	UCI	http://chrsdata.eng.uci.edu
Meteorological forcings	Rean.	1948–2008	Global	1°	3-hourly	Sheffield et al., 2006	Princeton	http://hydrology.princeton.edu/data.php
SILO	MIS	1890–present	Australia	0.05°	Daily	Jeffrey et al., 2001	DSITI	www.longpaddock.qld.gov.au/silo
TMPA	Rean.	1998–present	50°N - 50°S	0.25°	3-hourly	Huffman et al., 2007	NASA GES DISC	https://disc.gsfc.nasa.gov

Table 4
Climate index details (SLP: sea level pressure; Niño indices: oceanic component of ENSO).

Climate Feature	Data Type	Index Abbreviation	Dataset/Source	Publications	Website
Aerosol optical depth (AOD)	Aerosols	AOD	"SAM II"; SAGE; OSIRIS	Sato et al., 1993	http://data.giss.nasa.gov/modelforce/strataer
El Niño-southern Oscillation (ENSO)	MSLP/SST	BEST	HadISST1.1	Smith and Sardeshmukh, 2000	http://www.esrl.noaa.gov/psd/people/cathy.smith/best
	SST/SLP/wind/air temperature/ cloudiness	MEI	ICOADS	Wolter and Timlin, 1993, 1998	http://www.esrl.noaa.gov/psd/enso/mei
Indian Ocean dipole (IOD)	SST	DMI	ERSSTv4; HadISST1; OISSTv2	Saji et al., 1999	http://climexp.knmi.nl; http://www.jamstec.go.jp/frcgc/research/d1/iod/e/index.html
Interdecadal Pacific oscillation (IPO)	SST	IPO	HadISST1	Parker et al., 2007	http://cola.gmu.edu/c20c
		TPI	ERSSTv4; HadISST1	Henley et al., 2015	http://www.esrl.noaa.gov/psd/data/timeseries/IPOTPI
Madden–Julian oscillation (MJO)	Velocity potential	EOF1-10	NRR	Xue et al., 2002	http://climexp.knmi.nl; http://www.cpc.noaa.gov/products/precip/CWlink/daily_mjo_index/mjo_index.html
		VPM	ERA-Interim	Ventrice et al., 2013	http://www.esrl.noaa.gov/psd/mjo/mjoindex
	Wind/OLR	RMM1-2	NRR	Wheeler and Hendon, 2004	http://www.bom.gov.au/climate/mjo
	OLR	ROMI	ERA-Interim	Kiladis et al., 2014	http://www.esrl.noaa.gov/psd/mjo/mjoindex
Niño indices (El Niño/La Niña)	SST	CTI	ICOADS	Deser and Wallace, 1990	http://research.jisao.washington.edu/enso
		EMI	HadISST	Ashok et al., 2007	http://www.jamstec.go.jp/frcgc/research/d1/iod/DATA/emi.monthly.txt
		Niño 1 + 2; Niño 3; Niño 3.4; Niño 4	ERSSTv4; HadISST1; OISSTv2	Trenberth, 1997	http://climexp.knmi.nl; http://www.cpc.ncep.noaa.gov/data/indices
		ONI	ERSSTv4	Dahlman, 2016	http://www.esrl.noaa.gov/psd/data/correlation/oni.data
		TNI	HadSST1.1; OISST	Trenberth and Stepaniak, 2001	http://www.esrl.noaa.gov/psd/data/correlation/tni.data
Outgoing longwave radiation (OLR)	OLR	OLRI	AVHRR	Gruber and Krueger, 1984	https://www.ncdc.noaa.gov/teleconnections/enso/indicators/olr
Pacific decadal oscillation (PDO)	SST	PDO	HadSST; OISST	Mantua et al., 1997	http://research.jisao.washington.edu/pdo/PDO.latest
Quasi-biennial oscillation (QBO)	Zonal wind	QBO	NRR	Baldwin et al., 2001	http://www.esrl.noaa.gov/psd/data/climateindices/list
Solar activity	Solar radio emission	SRF	Solar radio telescope	Tapping, 2013	http://www.spaceweather.ca/solarflux/sx-en.php
	Sunspot count	SSN	SSNv2	Clette et al., 2014	http://sidc.oma.be/silso
Southern annular mode (SAM)	MSLP	AOI; AOIR	ERA-40	Meneghini et al., 2007	–
	Geopotential height	AAOI/EOF1	NRR	Mo, 2000; Thompson and Wallace, 2000	www.cpc.ncep.noaa.gov/products/precip/CWlink/daily_ao_index/aao/aao.shtml
	MSLP	SAM	Station data	Marshall, 2003	http://www.nerc-bas.ac.uk/icd/gjma/sam.html
Southern oscillation index (SOI)	MSLP	SOI (Troup index)	Station data	Ropelewski and Jones, 1987	http://www.cpc.noaa.gov/data/indices
				Ropelewski and Jones, 1987	https://crudata.uea.ac.uk/cru/data/soi
				McBride and Nicholls, 1983	http://www.bom.gov.au/climate/enso
South Pacific convergence zone (SPCZ)	MSLP	SPI/SPCZI	Station data	Folland et al., 2002; Salinger et al., 2014	–
	Wind	–	ERA-Interim	Kidwell et al., 2016	–

gaps, although special attention is required on maintaining sufficient detail based on original observations (Rayner et al., 2003), as gridding is inherently associated with smoothing-associated loss of information (Tozer et al., 2012). Fully interpolated reanalysis datasets (e.g. ERSSTv4 and HadISST1) are commonly utilised to force numerical models (Chaudhuri et al., 2013). Hence, numerical models rely on accurate, unbiased reanalysis datasets to facilitate more accurate predictions and analysis.

2.2.3. The importance of in situ data

While some climate variables are represented well by reanalysis and coarsely gridded satellite datasets, other variables are either highly reliable on model specifications for their derivation or exhibit high spatial variability. Gridded data are inherently smoothed and extreme events (e.g. intense, localised rainfall) are often not captured as a consequence (Tozer et al., 2012). Rainfall is among variables that are only indirectly measured by satellites (Huffman et al., 2007; Maggioni et al., 2016) and other remote sensing techniques (e.g. weather radar; Sinclair and Pegram, 2005). Highly heterogeneous rainfall patterns are often captured insufficiently in global (Chaudhuri et al., 2013) and higher resolution Australian (Jones et al., 2009) gridded datasets when applied to small-scale regional studies. Kalnay et al. (1996) categorised precipitation as a Class C variable in their NRR description, signifying a reliance on the model specifications used to derive the reanalysis rainfall grid. A recent study (Chaudhuri et al., 2013) has confirmed high errors involved in reanalysis rainfall (and wind stress) estimates, especially in tropical regions, as a result of inaccurate interpretation of cloud cover and volcanic emissions. Further, remote sensing techniques also have difficulty with correctly assessing orographic enhancement of rainfall (Chen et al., 2013a; Chen et al., 2013b; Maggioni et al., 2016). In situ data are therefore crucial to evaluate and validate remote sensing, reanalysis and modelling datasets, and are also required for effective calibration and bias correction of erroneous data fields. However, in situ measurement techniques are also flawed. During a WMO-initiated international precipitation measurement intercomparison project, systematic error sources were investigated (Sevruk et al., 2009). The most significant precipitation errors are associated with wind-induced losses but systematic errors are also introduced by evaporation, wetting (water drops adhering to the inner walls of the gauge) and gauge design (Peck, 1997; Sevruk et al., 2009; Strangeways, 2004; Tapiador et al., 2012; Vuerich et al., 2009). Torok and Nicholls (1996) have noted that some weather stations were affected by changes in instrumentation, location (altitude and position), observing practice (e.g. data truncation), and local station environment (e.g. urbanisation and vegetation growth). Some of these changes occurred widespread rather than in isolation. For instance, weather stations were commonly relocated from built-up areas to airports around the middle of the 20th century, while Stevenson screens (thermometer shelters) were introduced in Australia earlier in the century (Torok and Nicholls, 1996). Imprecision and human error (e.g. erroneous data logging, duplicate records or incorrect recording of station coordinates) also reduce the quality of in situ data (Jeffrey et al., 2001). For example, the coordinates for weather station #004051 (20.60°S/117.80°E) position this decommissioned site over the ocean, while the actual location was likely about 10 km further south. As gridding methods rely heavily on accurate positioning (and values) of individual data points, errors in observed in situ data will also generate flawed gridded and reanalysis products. Efforts to identify and aggregate high-quality in situ data into databases like GSN and ACORN-SAT (Section 2.2.1 and Table 2) aim to offset caveats associated with in situ observations.

AWAP is among recent efforts to combine remote sensing and model data with in situ observations to increase the accuracy of the reanalysis products. Jones et al. (2009) have demonstrated improved accuracy in the reanalysis fields of AWAP when in situ data were available at higher density. However, they have also shown that AWAP still suffers from significant inaccuracy in rainfall estimates despite the incorporation of in situ data and higher grid resolution. Further, reanalysis products have relatively low temporal resolution (hourly to monthly; cf. Table 3) and are therefore unable to consistently capture brief bursts of localised rainfall events and associated high rainfall intensities (King et al., 2013). Hence, in situ data are highly advantageous for small-scale regional studies. However, in situ data are often scarcely available, especially in less populated and mountainous regions.

In situ data also allow for indirect monitoring of extreme weather impacts (e.g. streamflow response to rainfall). Information on stream gauge sites and data availability is generally not easily extractable and will be the subject of a future publication.

3. Indices describing climate features impacting on Australia

Numerous indices exist to describe atmospheric and oceanic climate variability, of which the ENSO is arguably the most well-known. These indices are commonly used to explain observed terrestrial climate and weather patterns, including drought, flood, bushfire (term for wildfires in Australia) and TC risk (e.g. Kiem et al., 2003; Palmer et al., 2015; Schubert et al., 2016; Vincent et al., 2011). Many climate indices have previously been linked to Australian climate (e.g. Kiem et al., 2003; Palmer et al., 2015; Ummenhofer et al., 2009a; Verdon et al., 2004a) and will be discussed in this review. The temporal availability of these climate indices is displayed in Fig. 1. Some climate indices extend back to the 19th century (e.g. SST-based Niño indices) while other indices cover a relatively short period (e.g. OLR-based indices), have been discontinued or are not regularly updated (e.g. IPO indices) (Fig. 1).

3.1. El Niño/La Niña – El Niño-southern oscillation (ENSO)

El Niño and La Niña are the oceanic components of ENSO (cf. Section 3.2 for the atmospheric component) and are obtained from SST data (Fig. 2). Numerous climate indices have been derived based on different regions and statistical methods (Cane, 2005). Several indices are provided by NOAA CPC (http://www.cpc.ncep.noaa.gov/data/indices), including the traditional or eastern Pacific El Niño (Niño 1+2), the eastern equatorial Pacific El Niño (Niño 3), the central equatorial Pacific El Niño (Niño 4), the central-eastern equatorial Pacific El Niño (Niño 3.4; Trenberth, 1997) and the Oceanic Niño index (ONI; Dahlman, 2016). Additional climate indices include the ENSO Modoki index (EMI; Ashok et al., 2007), the cold tongue index (CTI; Deser and Wallace, 1990), the multivariate ENSO index (MEI; Wolter and Timlin, 1993; Wolter and Timlin, 1998) and the Trans-Niño index (TNI; Trenberth and Stepaniak, 2001).

Calculation of SST anomalies (SSTAs) over a specific region (e.g. Trenberth, 1997) is the most common oceanic Niño index derivation method. Differences between these indices are solely attributed to the observation area (e.g. the region for Niño 3.4 is partially overlapping those for Niño 3 and Niño 4; Fig. 2). Further, some indices are based on the same area, while the derivation method differs. The NOAA CPC derives the ONI by measuring the running 3-month mean SSTA for the Niño 3.4 region (http://www.esrl.noaa.gov/psd/data/correlation/oni.data), while the TNI is obtained from the difference in normalised anomalies of SST between Niño 1+2 and Niño 4 regions (Fig. 2) (Trenberth and Stepaniak, 2001). The EMI refers to a central equatorial Pacific SST pattern that is distinct from conventional ENSO characteristics. The EMI-associated SST has a horseshoe pattern rather than an ENSO-like tongue shape (e.g. Cai and Cowan, 2009; Takahashi et al., 2011), with the Japanese term “Modoki” meaning “a similar but different thing” (Ashok et al., 2007). The EMI is obtained by calculating the area-averaged SSTA over each of three regions (Fig. 2: $EMI = SSTA_{Region\text{-}A} - 0.5 \times SSTA_{Region\text{-}B} - 0.5 \times SSTA_{Region\text{-}C}$) (Ashok et al., 2007). The MEI incorporates data from both the ocean (SST) and atmosphere (sea level pressure, zonal and meridional surface wind components, surface air temperature and cloudiness) via principal component analysis (Wolter and Timlin, 1993; Wolter and Timlin,

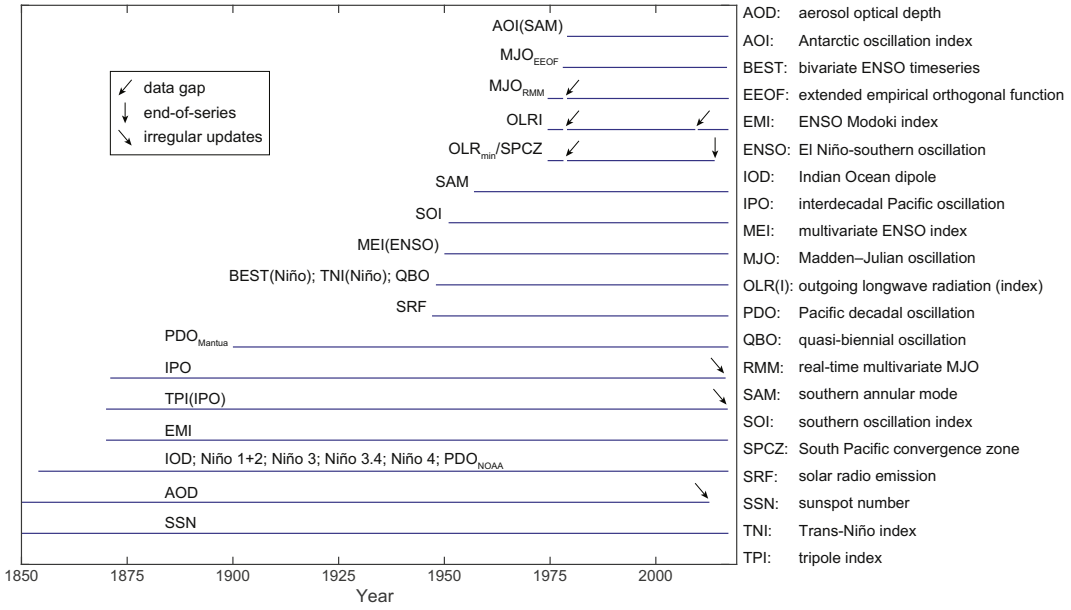

Fig. 1. Climate indices with reported links to Australian climate and their temporal availability. Subscripts refer to data source (NOAA; Mantua) or derivation method (RMM; EEOF; min: minima) while index family groups are listed in brackets (ENSO, Niño, IPO, SAM).

1998). Hence, this index is referred to as an ENSO index (ocean and atmosphere) rather than solely a Niño index (oceanic only). Wolter and Timlin (2011) have more recently published an extended version of the MEI (MEI.ext) that covers the period 1871–2005. The extended temporal coverage was achieved by producing a simplified MEI variety based only on SST and sea level pressure. Similarly, the bivariate ENSO timeseries (BEST) incorporates SST and pressure data by combining standardised Niño 3.4 and SOI data (Smith and Sardeshmukh, 2000).

Conventional (canonical) La Niña events (cold phase; negative ENSO index) are associated with above average SSTs in western tropical Pacific and below average SSTs in the eastern tropical Pacific, while easterly trade winds strengthen in the Pacific (Philander, 1990). Conversely, classical El Niño events (warm phase; positive ENSO index) are characterised by above average SSTs in the eastern tropical Pacific (Bjerknes, 1966; Cane, 2005; Philander, 1990). Easterly trade winds weaken or reverse in the Pacific (Bjerknes, 1966). The Australian summer monsoon trough is relatively weak and displaced equatorward during El Niño events (Evans and Allan, 1992). Specifically, the warm, positive phase of ENSO Modoki was linked to shorter and more intense Australian monsoons (Taschetto et al., 2009).

Australian climate is strongly linked to oceanic ENSO indices (Chiew et al., 1998). El Niño events (warm/positive phase) are associated with lower rain over southern and eastern inland areas of Australia (Risbey et al., 2009b). Risbey et al. (2009b) observed a negative correlation between rainfall and oceanic ENSO indices in the east and northeast of Australia, while the relationship between rainfall and oceanic ENSO indices was not found to be significant in the west. Trenberth and Stepaniak (2001) suggested that two ENSO indices (in their case, TNI and Niño 3.4) should be used in conjunction in order to capture the distinct character and evolution of an ENSO event.

El Niño events are associated with drought in Australia, although the relationship is not linear (drought severity is not significantly related to El Niño strength) (Power et al., 2006). TC occurrence is generally reduced in Queensland during El Niño, while northern and northwestern regions of Australia (area with above average SSTs) experience an increase in both cyclogenesis and land crossings (Evans and Allan, 1992). Persistently warm SSTs in the central Pacific associated with El Niño event result in a shift in the Walker circulation and tropical convection, moving away from Australian longitudes (Murphy and Timbal, 2008). The Walker circulation (or Walker cell) describes zonal overturning in the equatorial troposphere (Bjerknes, 1969). Normally, air rises over the western equatorial Pacific and Indian Ocean and sinking over the eastern equatorial Pacific (Oort and Yienger, 1996), producing easterlies in the Pacific and westerlies in the Indian Ocean. During an El Niño event, the Walker circulation weakens or even reverses (Julian and Chervin, 1978; Oort and Yienger, 1996), with air ascending over the central/eastern equatorial Pacific and descends over the Atlantic and Indo-western Pacific (Wang et al., 2004).

La Niña events are linked to greater flood risk in Australia (Kiem et al., 2003; Ward et al., 2014) and higher TC incidences in the Coral Sea region (Basher and Zheng, 1995). TC tracks also tend to persist further south, with more crossings observed on the east coast of

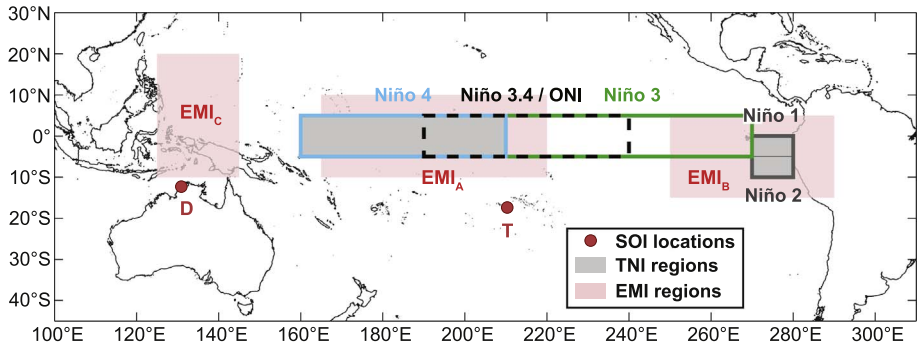

Fig. 2. Niño regions and mean sea level pressure locations for the SOI (Troup index). Darwin (D) and Tahiti (T) are denoted by filled circles.

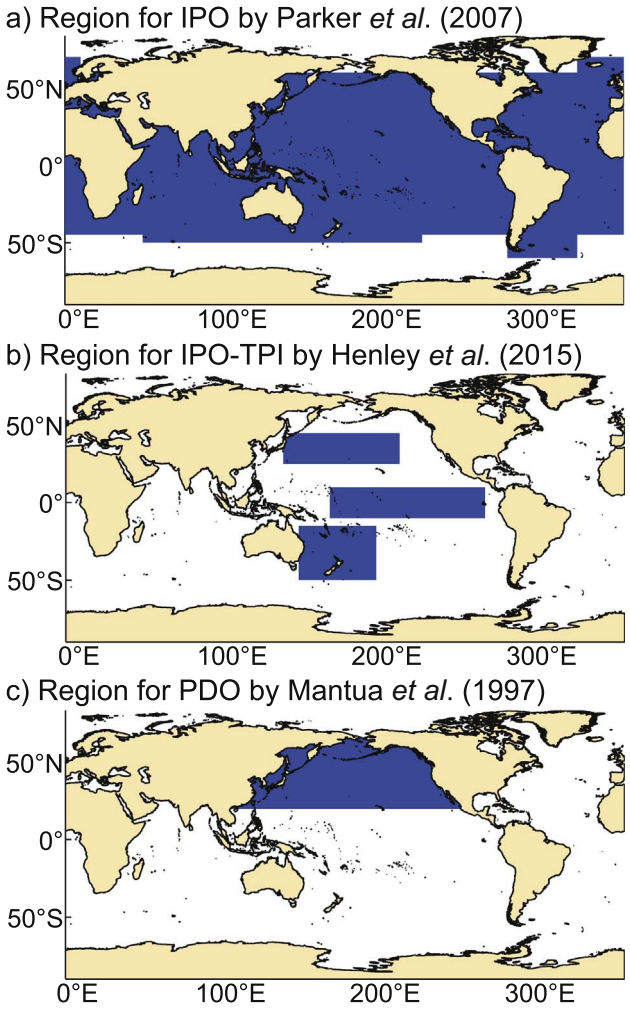

Fig. 3. Sea surface region (in blue) used to obtain a) the IPO index by Parker et al. (2007), b) the TPI by Henley et al. (2015) and c) the PDO by Mantua et al. (1997).

Australia, and fewer TCs in northern Australia (Evans and Allan, 1992). West coast TCs, in turn, tend to track offshore (Evans and Allan, 1992). La Niña events also impact on human health since these events are associated with a greater risk of mosquito-borne disease outbreaks (Russell, 1998) such as Australian encephalitis, dengue and Ross River fever (e.g. Kovats et al., 2003; Lindsay et al., 1993).

In recent years, several notably strong ENSO events impacted on Australian climate (Hendon et al., 2014; Murphy and Timbal, 2008; Whelan et al., 2013). In the spring of 2010, eastern Australia experienced its highest rainfall since 1900 (Hendon et al., 2014). These rainfall events coincided with a very strong La Niña event and an extreme positive excursion of the SAM (Hendon et al., 2014). Strong El Niño events were reported in Australia in 1997–1998 and again in 2002–2003 (Murphy and Timbal, 2008), with the earlier event described as the "El Niño of the century" (Murphy and Timbal, 2008) and associated with very large SSTAs in the east Pacific. However, rainfall in the southeast of Australia was only minimally affected during the earlier (1997–1998) ENSO event. In contrast, Murphy and Timbal (2008) note that the latter event (2002–2003) resulted in arguably the worst drought in Australian recorded history, and was characterised by very low rainfall and very warm temperatures.

3.2. Southern oscillation – El Niño-southern oscillation (ENSO)

The southern oscillation is the atmospheric component of ENSO (cf. Section 3.1 for the oceanic component). Its indices are commonly derived from sea level pressure (Cane, 2005). Only one index name, southern oscillation index (SOI), is regularly used. Several types of SOI exist. The SOI can be obtained by the Troup index, the Wright index, the Darwin index, or the Papeete index (McBride and Nicholls, 1983). All four index types use MSLP data at one (Darwin and Papeete Indices) two (Troup index) or eight (Wright index) locations (McBride and Nicholls, 1983).

The most well-known SOI is the Troup index (Troup, 1965) that describes the oscillation in surface air pressure between eastern and western Pacific by recording the pressure difference between Tahiti and Darwin (Fig. 2) (Allan et al., 1991; McBride and Nicholls, 1983; Ropelewski and Jones, 1987). Henceforth, the Troup index is referred to as SOI. The SOI sign is positive when the Darwin pressure is lower (Allan et al., 1991) and is characterised by stronger Pacific trade winds (Hanley et al., 2003). As the SOI and oceanic ENSO indices are negatively correlated, positive SOI tend to coincide with La Niña episodes (negative oceanic ENSO index) (Hanley et al., 2003). The southern oscillation is linked to the fluctuations in the intensity of the Walker circulation (Tanaka et al., 2004), as well as SST, rainfall and wind strength (McBride and Nicholls, 1983).

The SOI is well-known for its use as a seasonal rainfall predictor, with its austral winter and spring values used to estimate rainfall for subsequent seasons (e.g. McBride and Nicholls, 1983). Strong correlations between the SOI and rainfall are mainly restricted to the eastern half of Australia and are dependent on season (Risbey et al., 2009b), index and lag (McBride and Nicholls, 1983). In addition, the relationship varies on interdecadal timescales (Risbey et al., 2009b).

The relationship between SOI and rainfall varies depending on whether the SOI value is positive or negative. When positive, the SOI tends to be positively correlated to Australian annual mean rainfall (Murphy and Timbal, 2008). Thus, positive SOI values are generally associated with above mean rainfall over Australia. Conversely, no clear relationship between the magnitude of observed negative SOI values and Australian rainfall has been observed (Murphy and Timbal, 2008). Specifically, while more positive SOI values tend to coincide with more rain (compared to rainfall at lower positive SOI values), extremely negative SOI values do not consistently overlap with very low rainfall (compared to rainfall at moderately negative SOI levels). Drought and bushfire risk is generally higher during strong negative SOI (i.e. El Niño events) as a consequence of higher maximum temperatures and lower relative humidity (Verdon et al., 2004a; Williams and Karoly, 1999).

A very strong negative correlation has been observed between TC numbers and Darwin spring/summer MSLP (Nicholls, 1985). Negative (positive) SOI correlates with fewer (more) (Nicholls et al., 1998) and late-season (early-season) TCs (Hastings, 1990; Nicholls, 1984). The TC occurrence is shifted north-eastward (south-westward) during negative (positive) SOI (Basher and Zheng, 1995) and Coral Sea TC incidences are greater.

3.3. Interdecadal Pacific oscillation (IPO)

Several indices called interdecadal Pacific oscillation (IPO) have been calculated by various research groups. Although the name is often identical, the methods for the IPO derivation differ. IPO indices are commonly derived from empirical orthogonal function (EOF) analyses (Power et al., 1999) of near-global SST (Parker et al., 2007; Zhang et al., 1997) (Fig. 3a). Henley et al. (2015) recently developed a monthly IPO index (the tripole index, TPI) based on differences between the SSTAs averaged over the central equatorial Pacific and the average of the SSTAs in the northwest and southwest Pacific (Fig. 3b). A 6- to 13-year low-pass filter is commonly applied in conjunction with the EOF analyses (cf. Table 1 in Henley et al., 2015). The positive IPO is characterised by warm water in the tropical Pacific that is flanked by cold water to the north and south (Power et al., 1999). This feature is potentially driven by solar irradiance cyclicity (Franks, 2002).

Several studies have shown a strong link between the IPO and

Australian climate (Kiem and Franks, 2004; Kiem et al., 2003; Micevski et al., 2006; Palmer et al., 2015; Power et al., 1999; Verdon et al., 2004a; Verdon et al., 2004b). However, notably, no regularly updated monthly IPO indices are currently accessible, with updates for both the Parker et al. (2007) IPO and the Henley et al. (2015) TPI provided on an ad hoc basis. Traditionally, IPO indices have been derived from principal component analysis (PCA), with the TPI (Henley et al., 2015) being a notable exception. Four TPI indices extending to near-present are available (http://www.esrl.noaa.gov/psd/data/timeseries/IPOTPI), of which two are unfiltered (TPI_{unf}) and, thus, comparable to IPO and, to a lesser extent, the Pacific decadal oscillation (PDO; cf. Section 3.4). These two TPI indices are based on the difference between the SSTAs averaged over the central equatorial Pacific and the average of the SSTAs in the northwest and southwest Pacific (Henley et al., 2015). Their values are therefore expressed in °C. The two TPI indices are derived from two separate reconstructed global SST datasets, 1) ERSSTv4 and 2) HadISST1. A low-pass (13-year) filter was applied to both TPI indices to produce two additional filtered indices (TPI_{filt}). As was observed for other climate indices derived separately from ERSST and HadISST data, ERSST-derived TPI indices are slightly more up-to-date compared to HadISST-based indices. ERSST-derived TPI have an estimated yearly update frequency based on monthly review of data availability.

According to Power et al. (1999), the predictability of short-term (monthly to yearly) Australian rainfall is significantly improved during the negative (cool) phase of the IPO, while the ENSO-rain relationship is weakened during the positive (warm) IPO phase. The positive phase is characterised by less severe ENSO impacts (Kiem and Franks, 2004) although El Niño events are more frequent and enhanced (Salinger et al., 2001). The South Pacific convergence zone (SPCZ) moves northeast, with the furthest northeast positioning occurring during an El Niño (Folland et al., 2002). During the negative phase, the SPCZ moves southwest, resulting in greater flood risk (Kiem et al., 2003). The greatest flood risk occurs when the negative IPO coincides with La Niña. During these events, the SPCZ is in its most south-westerly position and the ITCZ also moves south. Further, the observed link between ENSO and spatial variation of cyclogenesis (cf. Section 3.1 and 3.2) in the southwest Pacific is significantly modulated by the IPO phase. The negative (positive) IPO phase is associated with a westward (eastward) shift in the southwest Pacific cyclogenesis, irrespective of the ENSO sign (Magee et al., 2017). This shift is most prominent during the late-season (February–April) TC genesis in the southwest Pacific and is likely connected to the IPO-associated SPCZ migration (Magee et al., 2017).

Based on the filtered TPI, a positive (warm) phase occurred during the 1978–1997 (Fig. 4c). Negative (cool) IPO phases are associated with the periods 1944–1977 and 1998–onwards. Less agreement among the various indices is observed for the periods prior to the mid-1940s, with the HadISST-derived filtered TPI mainly exhibiting positive values during 1913-1943, while the filtered ERSST TPI oscillates between positive and negative values during the same period. These differences are attributable to the low data density available for the TPI derivation during the earlier periods.

3.4. Pacific decadal oscillation (PDO)

The PDO describes interdecadal SSTAs in the North Pacific (Mantua et al., 1997). Thus, the PDO (Fig. 4b) is closely related to the IPO (Fig. 4a; cf. Section 3.3), although specifically focussing on the northern hemisphere (Fig. 3c). The PDO is derived from the leading EOF of monthly SSTAs in North Pacific (Mantua et al., 1997). Several PDO indices are available, including the PDO index by Mantua et al. (1997) and a PDO index by NOAA's NCEI (National Centers for Environmental Information; http://www.ncdc.noaa.gov/teleconnections/pdo). Patterns (consistently positive or negative PDO values) persist for 20–30 years (Mantua and Hare, 2002). It has been suggested that the PDO may be forced by solar irradiance (Franks, 2002; McGowan et al., 2010), with the positive PDO phase linked to lower solar irradiance. The strong link between the PDO and climate is most prominent in the North Pacific/North American region, with secondary signatures existing in the tropics, including Queensland (Fig. 3 in Mantua and Hare, 2002).

3.5. Indian Ocean dipole (IOD)

Previous studies have highlighted the strong connection between tropical Indian Ocean SST (including Indonesian waters) and Australian climate (Cai and Cowan, 2008; Nicholls, 1989; Verdon and Franks, 2005). The Indian Ocean interannual SST variability can be broadly grouped into monopole and dipole (i.e. IOD) modes (Behera et al., 2003). A basin-wide monopole SST pattern is the leading mode in the Indian Ocean and closely associated with the ENSO, lagging the Pacific SST signal by approximately four months (Venzke et al., 2000). The IOD mode, in turn, refers to the SST gradient between western equatorial Indian Ocean and the southeastern Indian Ocean (Fig. 5). The IOD signal is strongest during austral winter and spring (Behera et al., 2006; Behera et al., 2003). A subtropical Indian Ocean dipole (SIOD) has also been identified (Behera and Yamagata, 2001), although the SIOD does not appear to be significantly linked to Australian climate (Ummenhofer et al., 2009b).

An ongoing debate surrounds the nature of the relationship between the IOD mode and ENSO (e.g. Gallant et al., 2012; Stuecker et al., 2017). While several studies have highlighted a close association between the IOD and ENSO (c.f. Stuecker et al., 2017 and references therein), other publications have indicated that the IOD mode operates largely independently from the ENSO (Behera et al., 2006; Rao et al., 2002). Cai et al. (2011) determined that the IOD-ENSO relationship varies seasonally, with significant correlation in austral spring and weaker relationship in winter. Moreover, Verdon and Franks (2005) demonstrated the connection between Indonesian SST variability and east Australian winter rainfall, suggesting that an index based solely on Indonesian SST may have even greater value for Australian climate studies than IOD indices based on the anomalous east-west temperature gradient. Similarly, Tozer et al. (2017) found a strong link between Indonesian SST and South Australia winter rain, while the influence of IOD patterns is mainly restricted to spring.

Several indices are available to represent the IOD. The dipole nature of Indian Ocean SST variability was first identified by Nicholls (1989). Based on these findings, Verdon and Franks (2005) have calculated the Nicholls Dipole Index (NDI) from SST anomaly differences between the central Indian Ocean and Indonesian waters (Fig. 5). Large-scale cloud bands oriented northwest-southeast across Australia are associated with the NDI (Nicholls, 1989; Verdon and Franks, 2005). The dipole mode index (DMI) is arguably the most well-known IOD proxy. The DMI is derived from the difference between SSTAs in the western and eastern equatorial Indian Ocean (Fig. 5) (Saji et al., 1999). The DMI is referred to as the IOD for the remainder of this paper.

During the positive IOD phase, western equatorial Indian Ocean SSTs are anomalously warm compared to south-equatorial, eastern Indian Ocean SSTs near Indonesia (Murphy and Timbal, 2008). Consequently, easterlies (instead of westerlies) are present in the Indian Ocean during the positive IOD phase (Cai et al., 2009), along with anomalous upwelling along the Sumatra-Java coast (Feng and Meyers, 2003). It has been hypothesised that IOD changes may be predictable via equatorial easterly anomalies, which induce gravity (Rossby/Kelvin) waves (Cai et al., 2009), although the pattern of the preceding gravity waves changes.

The IOD is linked to rainfall variability in eastern Africa, Indonesia and Australia (Murphy and Timbal, 2008). In southern and western Australia, a negative correlation with autumn and winter rain was observed, with these regions experiencing higher rainfall amounts during the negative IOD phase (Ashok et al., 2003; Meyers et al., 2007;

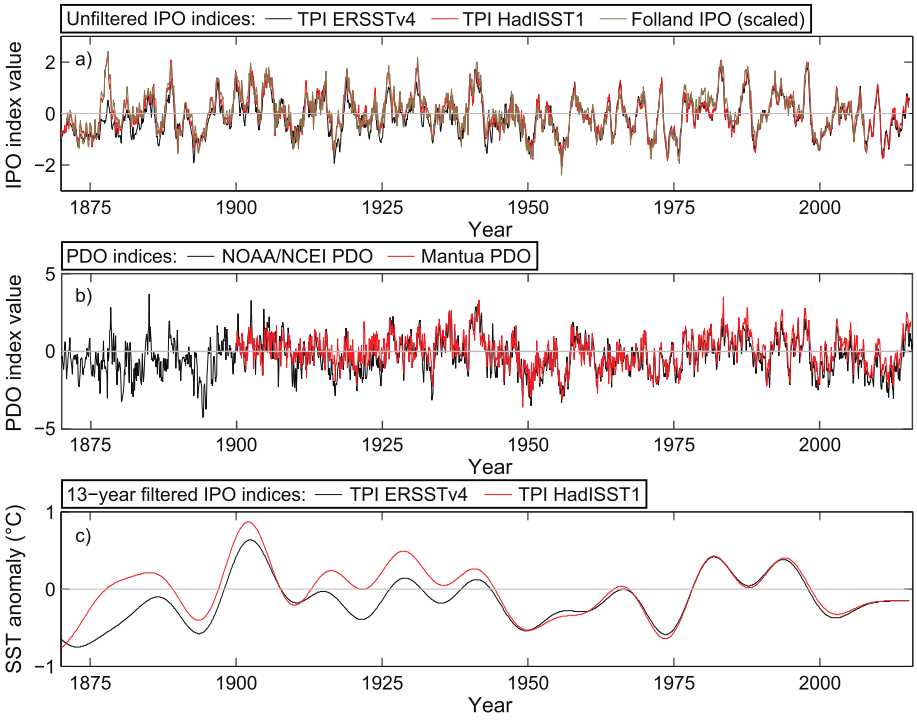

Fig. 4. Time series of a) unfiltered IPO indices except for a scaled Folland et al. (1999) IPO index, b) unfiltered PDO indices and c) filtered IPO indices. The IPO and PDO indices are based on different SST reconstruction datasets and index derivation methods (cf. Table 1 in Henley et al., 2015). TPI units are °C while Folland's IPO values and the PDO indices were derived from PCA.

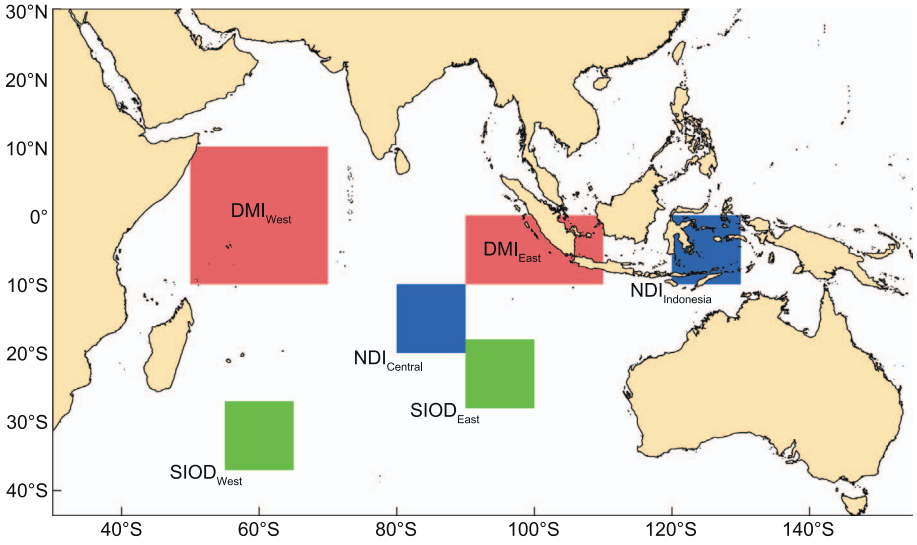

Fig. 5. Sea surface regions used for the derivation of tropical Indian Ocean dipole (IOD) and subtropical Indian Ocean dipole (SIOD) indices. The respective areas are shown for the dipole mode index (DMI), the Nicholls Dipole Index (NDI) and the SIOD index.

Risbey et al., 2009b; Saji and Yamagata, 2003). Concomitantly, lower rain levels are recorded in the far north (Top End) and eastern Australia (Queensland and New South Wales) (Meyers et al., 2007; Risbey et al., 2009b). Notably, Tozer et al. (2017) determined that the Nicholls Dipole (NDI), as opposed to the IOD (DMI), is a key driver of South Australian rainfall from autumn to spring, a finding likely connected to specific atmospheric characteristics associated with the SST anomalies in the NDI and DMI regions. The risk of a severe or prolonged drought is increased during multi-year absences of negative IODs (Ummenhofer et al., 2009a), when Indonesian waters exhibit cooler to average SSTs and easterly winds tend to be present in the Indian Ocean, reducing moisture advection into the Australian region. IOD and land temperature are also connected, with a negative correlation observed in the north, and a positive correlation in the south (Saji and Yamagata, 2003). The correlation is strongest in winter in the north and in spring in the south (Table 2 in Saji and Yamagata, 2003).

3.6. Outgoing longwave radiation (OLR)

OLR is a proxy for deep tropical convection (Wheeler et al., 2009) and identifies tall, thick, convective rain clouds (Hall et al., 2001). Satellite instruments have observed OLR since June 1974 (Gruber and Krueger, 1984). Satellite-derived OLR has been utilised to monitor several atmospheric climate features, including the Madden–Julian oscillation (MJO; Section 3.7) (Wheeler and Hendon, 2004) and the Walker circulation (Lau and Chan, 1983; Stechmann and Ogrosky, 2014). An OLR index (OLRI) based on standardised OLR anomaly is available for a region centred across the equator from 160°E to 160°W (http://www.ncdc.noaa.gov/teleconnections/enso/indicators/olr). An early study based on OLR data demonstrated the teleconnection between equatorial central Pacific OLR and Australian rain patterns (Lau and Chan, 1983).

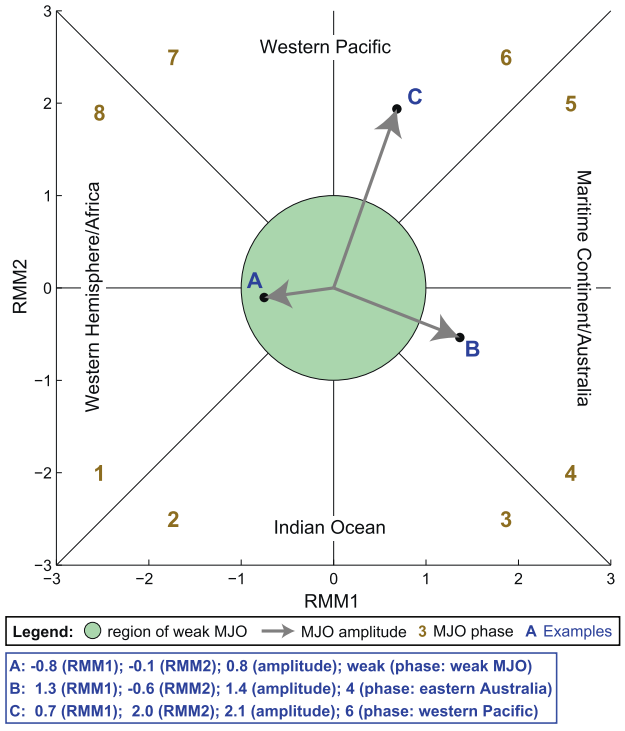
Western Pacific
Western Hemisphere/Africa
Maritime Continent/Australia
Indian Ocean
RMM1
RMM2
A
B
C
Legend: region of weak MJO MJO amplitude 3 MJO phase A Examples
A: -0.8 (RMM1); -0.1 (RMM2); 0.8 (amplitude); weak (phase: weak MJO)
B: 1.3 (RMM1); -0.6 (RMM2); 1.4 (amplitude); 4 (phase: eastern Australia)
C: 0.7 (RMM1); 2.0 (RMM2); 2.1 (amplitude); 6 (phase: western Pacific)

Fig. 6. MJO phase diagram showing three examples (A, B and C) for real-time multivariate MJO (RMM) values, including RMM1, RMM2, MJO amplitude and MJO phase.

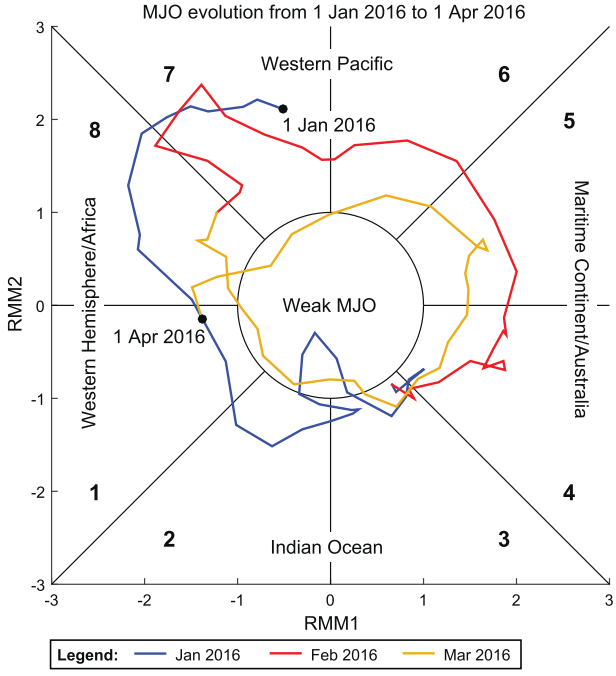

Fig. 7. MJO phase diagram for a 3-month period (January–March 2016).

3.7. Madden–Julian oscillation (MJO)

The MJO was first described by Madden and Julian (1971). The position, strength and phase of the MJO are inferred from zonal (east-west) wind and OLR. Several MJO indices have been derived. A group of indices obtained via the real-time multivariate MJO (RMM) method (Wheeler and Hendon, 2004; Wheeler et al., 2009) is considered the standard for monitoring the MJO (Kiladis et al., 2014). These indices include a pair of daily RMM indices, usually referred to as RMM1 and RMM2 (Fig. 6) (Wheeler and Hendon, 2004; Wheeler et al., 2009), the RMM-associated MJO amplitude and the MJO phase (phases 1 to 8) (Wheeler et al., 2009). While MJO indices are commonly obtained based on OLR data (e.g. real-time OLR-based MJO index or ROMI; Kiladis et al., 2014), some rely instead on velocity potential, including the velocity potential MJO (VPM; Ventrice et al., 2013) and a set of ten daily MJO indices derived by NOAA CPC from ten time-lagged patterns of the first extended EOF (EEOF) of pentad velocity potential anomalies (Xue et al., 2002). Because of the dependence on satellite data availability, MJO indices are not available prior to 1974 (Wheeler and Hendon, 2004).

The RMM pair, MJO amplitude and MJO phase indices are all interlinked (Wheeler and Hendon, 2004; Wheeler et al., 2009). The pair of RMM indices are derived from EOF analysis and describe the location of enhanced convection (Wheeler and Hendon, 2004). For example, a positive RMM1 value signifies that enhanced convection is situated over the maritime continent (i.e. Australian region), while a positive RMM2 value is related to enhanced convection over the Pacific. The RMM pair can be visually combined to obtain more detailed information of the MJO position (Fig. 6). In instances where both RMM values are positive, enhanced convection is situated over eastern Australia and the Coral Sea region (zones 5 or 6; cf. example C in Fig. 6). The MJO amplitude, in turn, is derived from the RMM indices via $\sqrt{RMM1^2 + RMM2^2}$, with high values (> 1) denoting strong MJO activity and low values (< 1) indicating weak MJO phases (cf. example A vs B and C in Fig. 6) (Wheeler et al., 2009). Finally, the MJO phase refers to the location of the MJO (Wheeler and Hendon, 2004; Wheeler et al., 2009). Eight different phases are associated with the MJO, reflecting the position of the region of enhanced convection, plus a central, weak region for all phases (Fig. 6). During the active phase, an eastward moving "pulse" of cloud and rainfall is observed near the equator, typically recurring every 30 to 60 days (Fig. 7) (Matthews et al., 2010; Zhang, 2005). Zhang (2005) describes it as an isolated, discrete pulse-like event rather than a sinusoidal wave. The active phase is normally confined to the Indian and western Pacific oceans.

The MJO undergoes a seasonal cycle with interannual fluctuations and reaches its primary peak in the austral summer, in association with the Australian monsoon (Zhang, 2005). ENSO events change the spatial extent and strength of MJO. MJO is strong before the El Niño peak, but weak after the peak (and weak in general during La Niña) (Zhang, 2005). MJO may induce El Niño events by triggering Kelvin waves (Hendon and Salby, 1994; Zhang, 2005). Risbey et al. (2009b) have stated that the MJO can impact rain throughout the Australian continent but predominantly influences monsoonal rain. Rain increases in the Australian tropics when the MJO phase is in the Australian/Coral Sea region (phase 5 and 6; Figs. 6 and 7), and decreases when the MJO is more remote (Murphy and Timbal, 2008; Wheeler et al., 2009). Impacts on southeast Australia rainfall are not spatially widespread and are seasonally limited (Murphy and Timbal, 2008).

During the convective (active) MJO phase, more TCs tend to occur in the area of enhanced convection (Hall et al., 2001; Liebmann et al., 1994). This signifies elevated TC risk for Australia when the MJO is located in or near the Maritime Continent/Australian region (zones 3 to 6; cf. examples B and C in Fig. 6). The observed connection between TCs and MJO makes TC risk estimation more predictable if MJO can be forecast with sufficient accuracy. The location of the active MJO phase is flanked, both east and west, by regions of weak deep convection and precipitation (Zhang, 2005).

3.8. South Pacific convergence zone (SPCZ)

The SPCZ is connected to the intertropical convergence zone (ITCZ). The ITCZ refers to the zone just north of the Equator that is characterised by lower pressure where the converging and rising air produces cloud and rainfall (Salinger et al., 1995). The SPCZ, in turn, is a band of strong low-level convergence, high cloudiness and precipitation

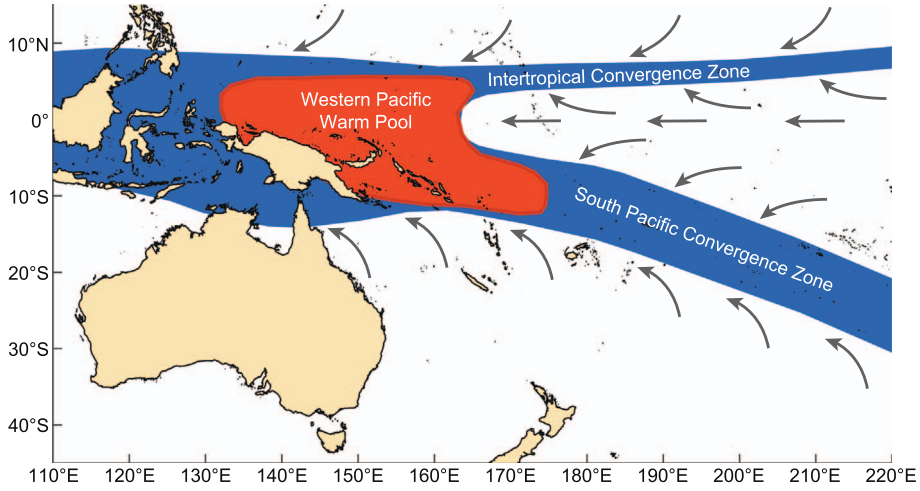

Fig. 8. Approximate positions of the South Pacific convergence zone, intertropical convergence zone and western Pacific warm pool.

positioned from the western Pacific warm pool south-eastwards towards French Polynesia (Fig. 8) (Folland et al., 2002). The SPCZ is present throughout the year, but is best developed during austral summer (Vincent et al., 2011). The SPCZ tends to fuse into the ITCZ in the central equatorial Pacific (Folland et al., 2002). On rare occasions, when the warm pool extends east of 160°W, the SPCZ changes to a zonal orientation (e.g. during some strong El Niño events), merging with the ITCZ (Vincent et al., 2011). Seasons with zonal SPCZ include 1982/83, 1991/92 (moderate El Niño) and 1998/97. Zonal SPCZ recurrence rate is expected to increase because of climate change (Cai et al., 2012).

The position of the SPCZ can be estimated by several proxies, including minimum OLR (Fig. 9), maximum rainfall, maximum of low level convergence, and maxima of the 500 hPa vertical motion. Monthly SPCZ indices were calculated by Folland et al. (2002) and Salinger et al. (2014) via MSLP differences between Apia (Samoa) and Suva (Fiji), while Kidwell et al. (2016) derived several parameters from surface wind convergence to describe the SPCZ in terms of strength, area and centroid location. However, none of these indices appear to be kept up-to-date and made available from a website. Fig. 9 displays several examples of OLR minima and algorithmically defined SPCZ position. The SPCZ is sometimes poorly defined (visually and algorithmically) based on OLR minima (Fig. 9b, d) and the estimated SPCZ position is therefore not always accurate.

Strong rain gradients are evident in the vicinity of the SPCZ (Vincent et al., 2011). Consequently, its position is closely linked to the regional distribution and occurrence of floods, bushfires and cyclones (Cai et al., 2012). The SPCZ is located furthest southwest during La Niña episodes with a negative IPO (Fig. 9c) (Folland et al., 2002). The SPCZ moves northward during El Niño and is furthest northeast when the IPO is in its positive phase. In addition, the SPCZ not only moves northward but may also change to a more zonal structure (Fig. 9a) during strong El Niño events, increasing drought, bushfire and TC risk for Pacific Islands (French Polynesia) (Cai et al., 2012; Vincent et al.,

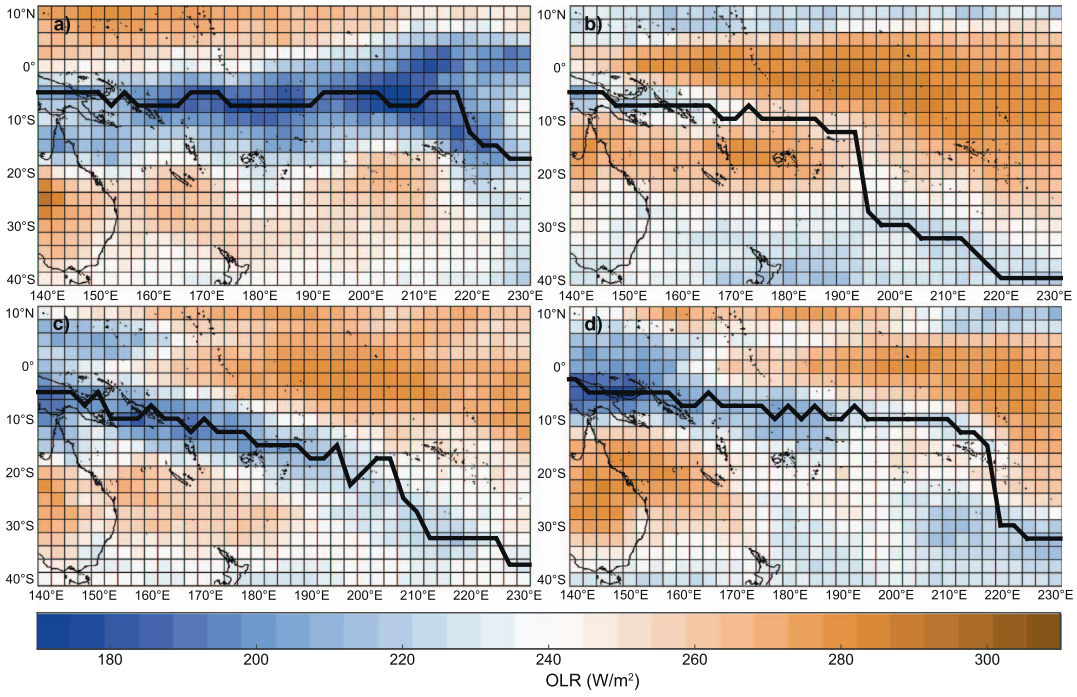

Fig. 9. Interpolated outgoing longwave radiation for a) January 1998, b) September 2010, c) February 2012 and d) December 2013 (data source: NOAA/OAR/ESRL PSD, Boulder, Colorado, USA, www.esrl.noaa.gov/psd/data/gridded; cf. Liebmann and Smith, 1996 for further details). The solid black lines denote the algorithmically estimated position of the South Pacific convergence zone.

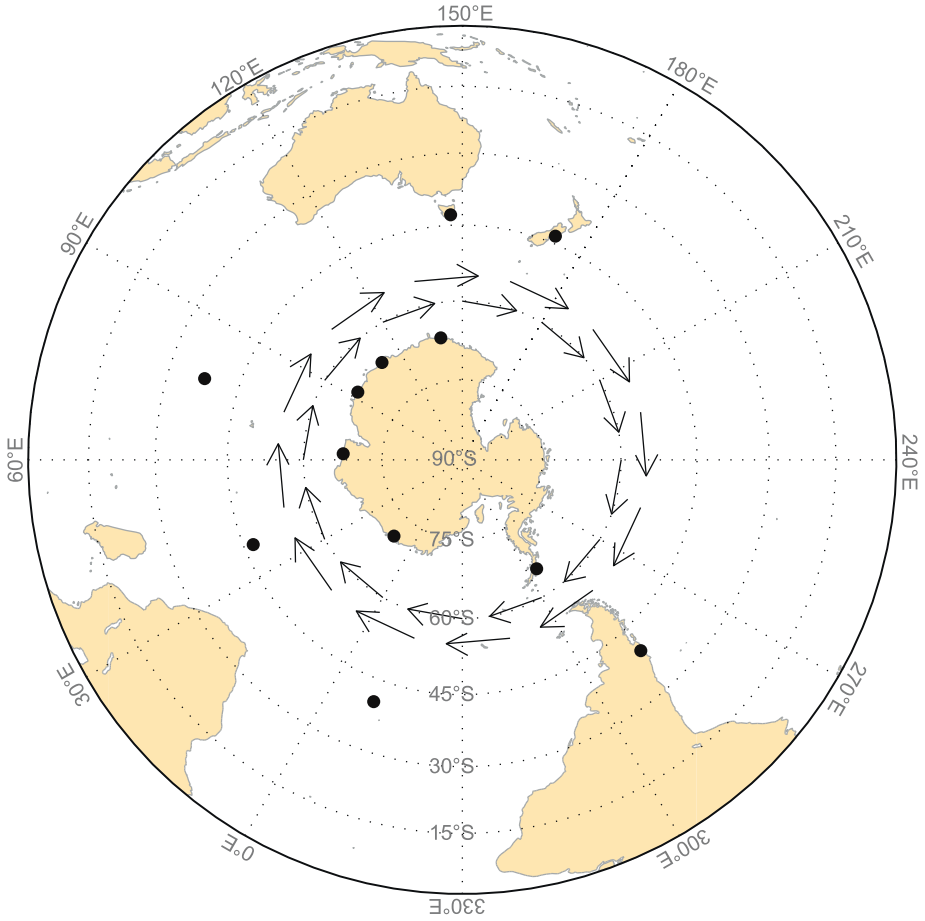

Fig. 10. Region of wind anomaly (arrows) over the Southern Ocean. The filled circles mark the weather station locations used by Marshall (2003) to obtain the SAM.

2011). In north Queensland, the northward movement of the SPCZ amplifies rainfall (Cai et al., 2012), although, in general, the rain area rather than rainfall intensity is increased by the northward movement of the SPCZ (Vincent et al., 2011).

Cyclogenesis (TC formation) is generally limited to within 10° south of the SPCZ (Vincent et al., 2011). Hence, cyclogenesis in the central Pacific only occurs when the SPCZ displays a zonal orientation, while fewer TCs develop in the Coral Sea during northward and zonal SPCZ shifts (normally coinciding with El Niño events). Cyclogenesis similarly moves southward during southern SPCZ shifts (normally coinciding with La Niña events), augmenting the chance of TCs forming in the Coral Sea.

3.9. Rossby and Kelvin waves

Rossby and Kelvin waves occur both in the ocean and the atmosphere (Holton and Hakim, 2013). Different types of Rossby and Kelvin waves exist, including equatorial Kelvin waves, oceanic coastal Kelvin waves, Rossby waves (including equatorial Rossby waves) and Rossby-gravity (Yanai) waves. These waves differ in regard to the forces (waveguides) applied (e.g. coastal boundary, thermocline and Coriolis effect/equatorial wave trapping) and in their physical characteristics (wave and energy propagation, wave period, etc.) (Fedorov and Brown, 2009).

Oceanic equatorial (Rossby and Kelvin) waves are produced by (and are producing) wind forcing (Cai et al., 2009; Kim et al., 2011) and can be described as a 'delayed oscillator' mechanism (Cane, 2005). These wave-types cause variations of sea surface height and are therefore observable by high precision satellite altimetry (Chelton and Schlax, 1996). The presence of Rossby or Kelvin waves is also evident in subsurface temperature anomalies, produced by the waves' ability to alter the thermocline depth (resulting in up-/downwelling of cooler/warmer water) (Fedorov and Brown, 2009).

Rossby waves are also referred to as 'planetary waves' (Rossby, 1949). Oceanic equatorial Rossby waves move westward along the thermocline (Fedorov and Brown, 2009). They are characterised by a long period and low velocity (0.6–0.8 m/s) and take months/years to cross ocean basins. When a Rossby wave reaches the western ocean boundary, it reflects as an upwelling equatorial Kelvin wave (i.e. raising the thermocline and reducing upper ocean temperature) (Fedorov and Brown, 2009).

Equatorial Kelvin waves move eastward along the thermocline (Fedorov and Brown, 2009). They are 5 or 10 cm high, have a long wavelength and a velocity of 2–3 m/s (Matthews et al., 2010). Kelvin waves are non-dispersive (phase speed of the wave crests is equal to the group speed of the wave energy) (Fedorov and Brown, 2009).

As a result of the connection with wind forcing, Rossby and Kelvin waves are associated and interlinked with various climate indices, including the MJO (Matthews et al., 2007; Matthews et al., 2010), ENSO (Cai et al., 2011; Kim et al., 2011; McPhaden, 1999) and IOD (Cai et al., 2009). Matthews et al. (2007, 2010) discussed the link between MJO-related winds and the generation of Kelvin waves, while van Rensch and Cai (2014) highlighted that Rossby wave trains are generated by ENSO and IOD patterns (individually or in combination), affecting mid-latitude Australian rainfall via the waves' ability to alter ocean temperature. Kim et al. (2011), in turn, found that equatorial Kelvin waves can be a precursor of La Niña events, hence indirectly impacting on the Australian climate.

3.10. Southern annular mode (SAM)

The southern annular mode (SAM) and available SAM indices have

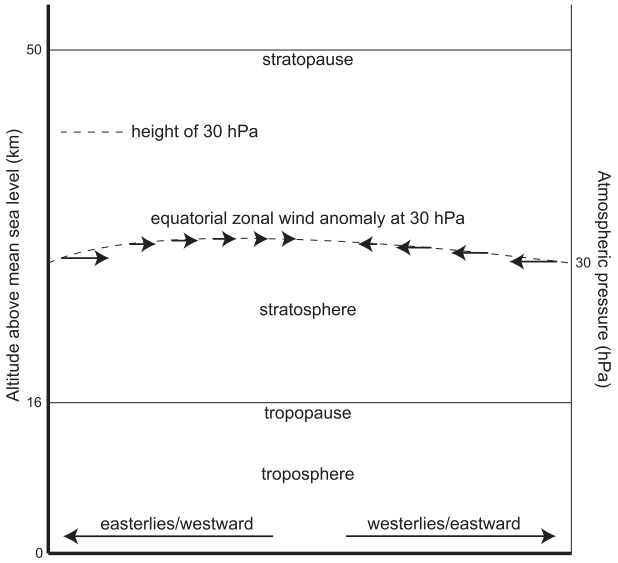

Fig. 11. Zonal wind anomaly at 30 hPa in the tropical stratosphere as a proxy for the quasi-biennial oscillation.

been reviewed previously by Ho et al. (2004). The SAM is essentially a measure of the pressure gradient between mid- (~40°S) and high-latitudes (~65°S) in the southern hemisphere (Marshall, 2003; Thompson and Wallace, 2000). The positive (high index) phase of the SAM is characterised by pressures that are lower than normal in the polar region with enhanced westerly winds along 55°S–60°S latitude (Fig. 10) (Risbey et al., 2009b). Meneghini et al. (2007) stated that the SAM has a greater influence on zonal wind (heat transport) than on temperature. Alternative names in use for the characteristics described by the SAM are Antarctic oscillation and the high-latitude mode (Marshall, 2003). Throughout the present paper, the feature will be referred to as the SAM.

Several reanalysis datasets and indices are in use to describe the SAM (Ho et al., 2012). Indices include the Antarctic oscillation index (AOI) and AOI regional (AOIR) by Meneghini et al. (2007), the Antarctic oscillation index (abbreviated as AAOI; http://www.cpc.ncep.noaa.gov/products/precip/CWlink/daily_ao_index/aao/aao.shtml) by Mo (2000) and a SAM index derived using MSLP data from twelve weather stations located near 40°S or 65°S (Fig. 10) (Marshall, 2003). Marshall (2003) determined that SAM indices based on ERA-40 (Meneghini et al., 2007) or NCEP–NCAR reanalysis data (Mo, 2000) needed to be used cautiously, as both datasets contain spurious high-latitude pressure data. Marshall (2003) further pointed out that, while there has been a trend toward the positive phase of the SAM between 1958 and 2000, it is not necessarily as strong a shift as reported in many publications that used the discredited data.

Previous research found that the SAM is positively correlated to rainfall in northern Australia and, for part of the year, negatively in southern Australia (Hendon et al., 2007; Meneghini et al., 2007). More specifically, rainfall in southern Australia (i.e. southwest Western Australia, Victoria and Tasmania) is reduced (Hendon et al., 2007; Meneghini et al., 2007) during the positive phase of the SAM, while rainfall in certain southeastern locations, particularly New South Wales (Risbey et al., 2009b) and northern Australia, is increased (Hendon et al., 2007; Meneghini et al., 2007). The inverse relationship in the southern part of Australia is most prominent during winter (Meneghini et al., 2007). Temperature anomalies are also connected to the SAM, with the strongest impact observed during austral spring and summer (Hendon et al., 2007). Most of Australia experiences cooler temperatures during the positive phase of the SAM, while Tasmania tends to be warmer (Gillett et al., 2006). These results were confirmed by Hendon et al. (2007), who attributed the positive SAM phase to lower maximum temperatures over central and eastern subtropical Australia. During the negative phase of the SAM, the storm track expands towards the equator (Murphy and Timbal, 2008).

3.11. Subtropical ridge (STR)

The subtropical ridge (STR) is a belt of atmospheric high pressure that encircles the globe in the mid-latitudes (Timbal and Drosdowsky, 2013). The position of the STR is strongly linked to synoptic scale weather features (cf. Section 3.15). Dry and stable weather conditions are normally observed along the ridge, with cold fronts located poleward of the STR. During austral summer, the STR is generally located to the south of the Australian continent (Whan et al., 2014), promoting drier conditions. The STR shifts abruptly northwards in austral autumn and remains over the Australian mainland during the cooler season, allowing cold fronts and storm tracks to pass over Australia. Several indices have been created based on MSLP to characterise the STR in terms of location and, less commonly, intensity (Drosdowsky, 2005; Larsen and Nicholls, 2009). These indices are commonly referred to as the *L*-index (for latitude of the STR). Drosdowsky (2005) showed a delay in the northward shift of the STR position during autumn from 1975 onwards, along with a general more northern location during the other seasons and strengthening of the STR. The decrease in autumn rainfall in southern Australia (Murphy and Timbal, 2008) has been attributed to the delayed northward movement (Drosdowsky, 2005) and strengthening of the STR (Larsen and Nicholls, 2009; Timbal and Drosdowsky, 2013). Larsen and Nicholls (2009) determined that the STR intensity during the cooler period is more closely related to southern Australia rainfall than the STR latitudinal position. Similarly, Tozer et al. (2014) found that a more intense STR is linked with reduced winter rainfall in South Australia.

3.12. Quasi-biennial oscillation (QBO)

The quasi-biennial oscillation (QBO) most commonly refers to a quasi-periodic oscillation of the equatorial zonal wind between easterlies and westerlies in the tropical stratosphere (Fig. 11) (Baldwin et al., 2001). Its tropospheric counterpart (Kwan and Samah, 2003), the tropospheric biennial oscillation (TBO; Meehl, 1997), is occasionally also referred to as QBO (Nicholls, 1978). A regularly updated QBO index is available, with the index based on the NNR-derived zonal average of the equatorial 30 hPa zonal wind (http://www.esrl.noaa.gov/psd/data/climateindices/list). The QBO has a periodicity of 2–2.5 years (Allan et al., 2003), with a mean period of 28–29 months (Baldwin et al., 2001). Gravity waves are believed to force the stratospheric QBO as they propagate vertically from the tropical troposphere (Baldwin et al., 2001). The tropospheric QBO is linked to interannual variability in the Asian-Australian monsoon (Meehl and Arblaster, 2011) and has also been indirectly associated with Ross River virus (vector-borne disease) incidence in Queensland (Done et al., 2002).

3.13. Aerosol optical depth (AOD)

The aerosol load in the atmosphere impacts climate via radiative forcing (scattering and absorption of solar radiation), change in cloud composition and altering rainfall levels (Ramanathan et al., 2001). A global aerosol optical depth (AOD) index has been derived based on satellite and historic volcanic eruption data (Sato et al., 1993). Peaks in AOD values are associated with large volcanic eruptions (Fig. 12). Numerical simulations have demonstrated that Australian rainfall is connected to remote forcing of atmospheric aerosol levels (Rotstayn et al., 2007).

3.14. Solar cycle – sunspot number (SSN) and solar radio flux (SRF)

Several solar cycles operating at various temporal scales have been

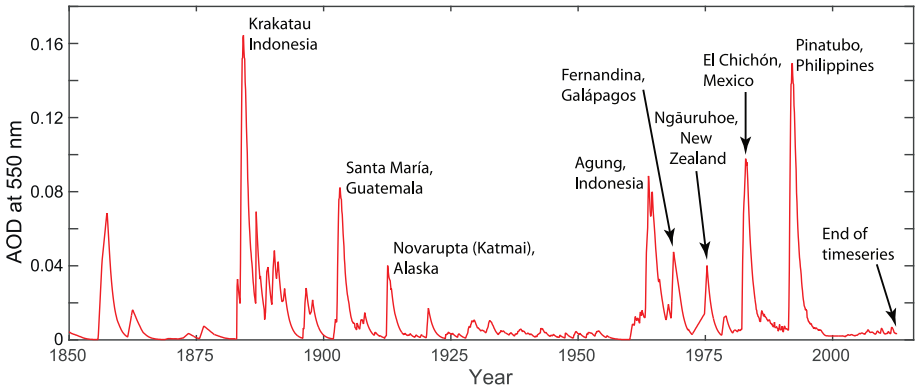

Fig. 12. Temporal evolution of global mean stratospheric aerosol optical depth (AOD) at 550 nm and associated explosive volcanic events (AOD data obtained from data.giss.nasa.gov/modelforce/strataer).

identified. These include the Schwabe cycle (Schwabe, 1844), the Hale cycle (Hale et al., 1919), the Gleissberg cycle (Gleissberg, 1939) and the Suess wiggles (De Jong et al., 1979; Suess, 1978). The Schwabe cycle (Schwabe, 1844) is an 11-year decadal solar oscillation, characterised by a gradual increase and more rapid decrease of the number of sunspots over a period ranging from 8 to 15 years (Fröhlich and Lean, 2004). The cycle's existence has been linked to the alignment of Jupiter, Earth and Venus (Hung, 2007). The Schwabe cycle is believed to be forcing the quasi-decadal oscillation (QDO) (Bal et al., 2011), which also has an approximately 11 year cycle. The quasi-decadal oscillation, in turn, is associated with El Niño-La Niña pairs occurring during the 11 year cycle (White and Liu, 2008). The Hale cycle operates on a 22 year cycle - double the temporal length of the Schwabe cycle (Scafetta, 2010). The Hale cycle is caused by the reversal of the Sun's magnetic field during each Schwabe cycle (Babcock, 1961). The Gleissberg cycle has a 80–90 year cycle that is believed to be an amplitude modulation of the Schwabe cycle (Friis-Christensen and Lassen, 1991). The Suess wiggles (also called de Vries cycle) have a relatively long cycle of 180-210 years (Raspopov et al., 2008; Usoskin, 2013).

Several indices are in use to represent variation in solar activity, including the international sunspot number (SSN; http://sidc.oma.be/silso) and the solar radio flux (SRF; www.spaceweather.ca/solarflux/sx-en.php). The SSN and SRF indices are described in detail by Clette et al. (2014) and Tapping (2013), respectively. SST variations corresponding to solar changes with periods of 9–13 (Mufti and Shah, 2011; Reid, 1991; Roy and Haigh, 2010) and 80–90 years (Mufti and Shah, 2011; Weng, 2005) have been detected. The solar maxima of the Schwabe cycle often coincide with La Niña-like conditions (cf. Fig. 3 in Roy and Haigh, 2010), followed by El Niño-like patterns two years later (Bal et al., 2011). Similarly, peaks in the Gleissberg cycle tend to correspond with La Niña events (Weng, 2005). Solar cycles have also been linked to cloud cover (Erlykin et al., 2010) and the ability of the clouds to produce precipitation (Tinsley and Yu, 2004). However, the solar influence on cloud cover is deemed to be minor (Erlykin and Wolfendale, 2011). Increases in stratospheric temperature in response to enhanced solar irradiance corresponding to the solar maximum of the Schwabe cycle result in stronger summer easterly winds, which penetrate into the tropical upper troposphere (Haigh, 1996). This results in the poleward shift of subtropical westerly jets, STR and storm tracks, as well as a broadening of the tropical Hadley cell. Some recent studies have found an increased disconnect between SSN and temperature from about 1985 (e.g. Stauning, 2011). Stauning (2011) also noted that there is a causality problem between SSN and terrestrial temperatures, with the latter sometimes leading SSN.

3.15. Synoptic meteorological features

Synoptic scale features, such as high- and low-pressure areas, as well as related frontal zones, can significantly impact the location, timing and severity of extreme events such as flooding, bushfires and TCs. One of the synoptic scale features linked to Australian extreme events is atmospheric blocking (Pook and Gibson, 1999). Atmospheric blocking is associated with a splitting of the upper-tropospheric western airstream into two distinct branches (anti-cyclonic and cyclonic) (Trenberth and Mo, 1985), with the degree of splitting represented by an index (blocking index: BI) developed by BOM (Pook and Gibson, 1999). The frequency of atmospheric blocking is linked to the ENSO (Ashok et al., 2009; Risbey et al., 2009a), with more blocking observed during La Niña events (Risbey et al., 2009b).

Atmospheric blocking most commonly occurs in winter in the Tasman Sea and the New Zealand region (Pook and Gibson, 1999). Periods of atmospheric blocking are often associated with extended dry spells in southern Australia (Risbey et al., 2009b), with the location of the atmospheric blocking feature influencing the location of rainfall. For example, atmospheric blocking over the Great Australian Bight (approximately 130°E) favours rainfall in Western Australia, while atmospheric blocking around 140°E can result in elevated rainfall in southeast Australia associated with cut-off lows to the north of the blocking high (Risbey et al., 2009b).

3.16. Interconnection of climate indices and extreme weather

Numerous publications have shown strong relationships and climate interactions between ENSO, IPO, IOD, SPCZ, oceanic Rossby and Kelvin waves, and Walker and Hadley circulations (e.g. Cai et al., 2009; Gallant et al., 2012; Murphy and Timbal, 2008). For example, decreased rainfall over southern Australia has often been associated with El Niño, while relatively recent studies have found that southern winter precipitation anomalies are linked to the IOD (Ashok et al., 2003; Risbey et al., 2009b) and Rossby waves (Cai et al., 2011) instead. In addition, Pepler et al. (2014) determined that coastal rainfall in southeast Australia exhibits a weak relationship with ENSO because of modulation of zonal wind flow associated with the IOD. Cai et al. (2011) have also observed that SSTs in the IOD and ENSO regions are positively correlated in austral spring (i.e. co-occurrence of El Niño and positive IOD, or La Niña and negative IOD), but more independent in winter.

The accuracy of seasonal climate forecasting is also impacted by interactions of various climate drivers. Risbey et al. (2009b) showed that rainfall predictability is improved during the negative phase of the IPO in terms of expansion of regions displaying significant ENSO-rainfall correlation (predominantly central and eastern Australia; cf. their Fig. 3a, c). Conversely, the ENSO-rain relationship is weakened during positive IPO, with areas exhibiting significant correlation generally limited to eastern Queensland, eastern New South Wales and, to a lesser extent, northern Australia (Fig. 3b, d in Risbey et al., 2009b). The greatest spatial extent of positive rainfall anomalies is observed when both the ENSO (La Niña) and IOD are negative (Meyers et al., 2007). Queensland and Victoria were affected by severe and large-scale flood events during December 2010 and January 2011. Months preceding

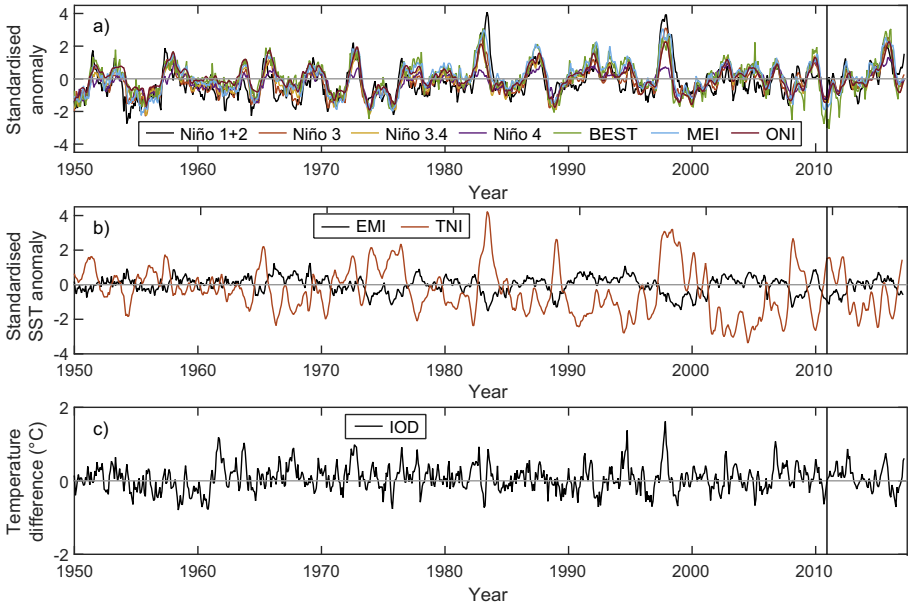

Fig. 13. Timeseries of a–b) nine ENSO indices and c) IOD from 1950 to present. The vertical lines mark the large-scale flood events of December 2010. All ENSO indices were standardised based on an index-specific reference period. Units are °C except for MEI (1st unrotated principal component) and BEST (combined Niño 3.4 and SOI). The index sources are provided in Table 4.

December 2010 coincided with a negative IOD and La Niña (positive SOI) (Fig. 13). Negative rainfall anomalies occur when either or both the IOD and oceanic ENSO (El Niño) are in their positive phases (i.e. neither negative), with the spatial extent of rain anomaly being comparable while the regions that are most impacted vary (Meyers et al., 2007; Risbey et al., 2009b).

Elevated flood risk in Queensland is associated with La Niña events (Kiem et al., 2003). The flood risk is further increased if a La Niña coincides with a negative IPO phase, pushing the SPCZ to its most southwestern position (Folland et al., 2002), with a concomitant southward movement of the ITCZ. Further, ENSO exhibits significant correlation with the SAM (Cai and van Rensch, 2013). During spring 2010 (September-November), eastern Australia received the highest rainfall since 1900 (Hendon et al., 2014). Hendon et al. (2014) showed that the record rainfall was largely commensurate with the occurrence of a very strong La Niña event and an extreme positive excursion of the SAM. Cai and van Rensch (2013) illustrated that the strong coherence of the SAM and ENSO reinforces the individual impact of the two climate patterns.

Droughts and concomitant decrease in crop productivity are commonly linked to El Niño events (Stone, 2014). Ummenhofer et al. (2011) noted distinct differences in southeastern Australia drought response on interannual and decadal timescales. While extended drought periods in southeastern Australia are more closely associated with IOD patterns (Ummenhofer et al., 2009a), interannual water availability is also driven by Pacific conditions (Ummenhofer et al., 2011). An elevated risk of severe and prolonged droughts is attributed to multi-year absences of negative IODs (Ummenhofer et al., 2009a). A negative IOD in the absence of ENSO coincides with the most striking SST characteristics in waters surrounding the Australian continent, as positive SSTAs are recorded throughout the Australian region (cf. Fig. 3c in Meyers et al., 2007). The greatest positive SSTAs are observed in Indonesian waters to the north of Australia and in the Southern Ocean south of the Australian mainland (south of 40°S and west of the dateline), while tropical waters further away from Australia/Indonesia tend to be cooler. In comparison, a positive IOD in the absence of an ENSO event is similar to a neutral SST state, with the exception of cold SSTAs in the Sumatra-Java region (cf. Fig. 3d, e in Meyers et al., 2007).

TC occurrence (including location of cyclogenesis) also heavily depends on various climate cycles, notably ENSO, IPO, SPCZ and MJO (Hastings, 1990; Liebmann et al., 1994; Magee et al., 2017; Solow and Nicholls, 1990; Vincent et al., 2011). More TCs develop in the Coral Sea during La Niña events when the SPCZ has shifted southward. During strong El Niño events, the SPCZ not only moves northward but may also change to a more zonal structure, increasing precipitation in north Queensland (Cai et al., 2012) while reducing cyclogenesis in the Coral Sea (Vincent et al., 2011). The zonal SPCZ recurrence rate is expected to increase because of climate change (Cai et al., 2012), resulting in fewer TCs forming in the Coral Sea and more in the central Pacific (Vincent et al., 2011).

4. Reliability and accessibility of climate indices and weather data

Several problems have been identified in regard to climate index and weather data availability during the compilation of this review. These issues relate to 1) data errors by intermediary data providers, 2) data hosting by a new website, 3) altered climate index derivation method, 4) discontinued indices and 5) changes to baseline periods. In some instances, the difficulty lies more in the selection of the most suitable index (e.g. Niño indices as a result of numerous available indices, whose suitability may vary depending on the study specifications) rather than obtaining any index representative of a specific feature (e.g. up-to-date IPO index). Further, funding cuts are behind discontinued datasets in some cases (e.g. NOAA's interpolated OLR data, available until 2013; http://www.esrl.noaa.gov/psd/data/gridded/data.interp_OLR.html), while restructuring or cessation of an organisation may result in the termination, movement or alteration of a dataset. Importantly, no data should be taken at face-value as technical or human errors may be present in any dataset, whether gathered independently or as part of a large organisation. Objective evaluation of any dataset and investigation of any unexpected feature facilitate continued data improvements and concomitant reliability of study results.

4.1. Caveats associated with climate indices

While many climate indices can only be obtained directly from the index creators, several websites exist that provide access to numerous indices from various sources (e.g. http://climexp.knmi.nl) or within the same organisation (e.g. http://www.esrl.noaa.gov/psd/data/climateindices/list). While some climate indices are updated on a monthly basis (e.g. various ENSO and MJO indices), others are sporadically (e.g. IPO indices, Section 3.3) or never updated. During the course of this study, several versions and changes were noted for some

climate indices. The AOD index (Sato et al., 1993) has not been updated since October 2012 (http://data.giss.nasa.gov/modelforce/strataer), although a value of zero is routinely assigned during periods of low volcanic activity. No alternative AOD index appears to be available. Further, several links to climate indices became defunct during this review, either as a result of 1) renaming the index, 2) restructuring the host's website or 3) shifting the index hosting responsibility to another organisation. The link to the RMM (MJO) indices became invalid in late October 2015, with the original data website source no longer accessible when the data hosting was shifted from the Centre for Australian Weather and Climate Research (CAWCR) to BOM (http://www.bom.gov.au/climate/mjo). Further, the climate index values (RMM1, RMM2 and RMM amplitude) for March 2003 onwards changed slightly, with no information provided for the reason for either the shift or the data changes. A second climate index (SSN v1.0) also had its data website link discontinued, with an entirely revised and recalibrated SSN index (v2.0) replacing the SSN v1.0 as of 1 July 2015 (http://www.sidc.be/silso/datafiles) following identification of biases in the original v1.0 SSN index (Clette et al., 2014).

Several studies revealed issues with data availability or quality. Henley et al. (2015) determined four distinct oceanic regions relevant to the development of their IPO TPI, including an area in the Southern Ocean (cf. their Fig. 1). As this region has been undersampled, particularly during the pre-satellite era, the Southern Ocean region was ignored when defining the IPO TPI (Henley et al., 2015). Discrepancies have also been found in reanalysed southern hemisphere high-latitude pressure data as a result of observational data sparsity in the Southern Ocean (Nicolas and Bromwich, 2011), impacting on the quality of SAM indices that rely on accurate Southern Ocean data (Ho et al., 2012; Marshall, 2003).

Climate indices, including the majority of ENSO indices, are commonly derived by calculating standardised anomalies of a variable (e.g. SST; Trenberth, 1997). The calculation of standardised anomalies requires a baseline period as a reference (Arguez and Vose, 2011). WMO has long recommended a 30-year baseline period, updated every ten years to reflect changing climate conditions (Hulme et al., 2009; WMO, 2007). Thus, many organisations (e.g. NOAA) have changed the baseline period for their products on a decadal basis, most recently from 1971–2000 to the current 1981–2010 period (Arguez et al., 2012), with a change to 1991–2020 expected in 2021. Table 5 lists various standardised ENSO indices and their corresponding baseline period. The differences in these ENSO indices highlight that baseline periods not only vary among identically-named indices (e.g. SOI) but may also differ among separate products within the same organisation (e.g. ONI vs Niño 3.4, NOAA CPC). For ONI, a moving 30-year reference period is applied on the running 3-month SST mean instead of a fixed baseline period (Lindsey, 2013). Each ONI value is centred on a 30-year baseline period, which is shifted every five years. As climate patterns are non-stationary, the climatology mean and variability will depend on the selected baseline period. Consequently, historical anomaly values are altered when a different reference period is selected. For example, a season hitherto categorised as neutral may be classed as an El Niño event with respect to the new baseline period. Hence, the interpretation of past, present and future climate patterns are specific to the chosen reference period and may alter with a new baseline. Further, the comparison of studies is hindered when their data are based on different baseline periods.

Table 5
ENSO indices and associated baseline periods (JAMSTEC: Japan Agency for Marine-Earth Science and Technology; JISAO: Joint Institute for the Study of the Atmosphere and Ocean).

ENSO index	Baseline Period	Organisation
BEST	1898–2000	NOAA ESRL
MEI	1950–1993	NOAA ESRL
CTI	1950–1979	JISAO
EMI	1979–2005	JAMSTEC
Niño 3; Niño 3.4; Niño 4	1961–1990	BOM
Niño 1 + 2; Niño 3; Niño 3.4; Niño 4	1981–2010	NOAA CPC
ONI	30-year sliding	NOAA CPC
TNI	1981–2010	NOAA CPC
SOI	1933–1992	BOM
	1951–1980	CRU
	1981–2010	NOAA CPC

4.2. Tropical cyclone (TC) trends

Long-term TC trend analyses are hampered by incomplete pre-satellite TC records. Several studies (e.g. Harper et al., 2008; Kuleshov et al., 2010) have discussed data gaps and false trends in TC occurrence and intensity as a result of changes and improvements in TC observation over time. Albeit satellite observations have been available since 1966, only twice-daily images were provided until 1978 (Harper et al., 2008). The poor temporal resolution was concomitant with low spatial resolution (~9 km instead of 1–4 km). Hence, TC data prior to the 1980s in particular have to be evaluated cautiously. In addition, Harper et al. (2008) noted that BOM did not consistently obtain data based on 10-minute sustained wind speeds prior to 2000. Instead, some data were obtained based on 1-minute sustained wind speed, adding further inaccuracy and ambiguity to the TC database.

Tropical low pressure systems are usually classified in terms of the sustained wind speeds near the centre. The first TCs in the Australian region were observed and recorded in 1907 according to the BOM TC database (http://www.bom.gov.au/cyclone/history). However, the first wind data only became available in 1973, with extensive wind data gaps persisting in the BOM database until the mid-1980s. Hence, classification of tropical disturbance severity is hindered considerably prior to the mid-1980s. Efforts have been undertaken to identify and catalogue additional TCs from the pre-satellite era to obtain more complete datasets, including SPEArTC that covers the southwest Pacific region and extends back to the 1840/1841 TC season (Diamond et al., 2012). Fig. 14 presents the number of severe TCs within the Australian exclusive economic zone (AEEZ) and over the Australian continent (Fig. 15) based on BOM's database. Each TC record was classified as severe if a) they contained wind data that exceeded 33 m/s (64 knots) or, in the absence of wind data, if b) pressure dropped to at least 970 hPa. For TCs with neither wind nor pressure data, track positions classified as severe (CYC_TYPE Code 40 in the BOM database) were also collated. This step added no further TCs to the severe TC record (earliest TC assigned Code 40 is severe TC Fiona, 2003). The BOM database contains relatively few severe TCs prior to the 1970s as a result of limited observation capability (Fig. 14). Hence, the shift towards more TCs in Fig. 14 reflects improved observation capabilities rather than an

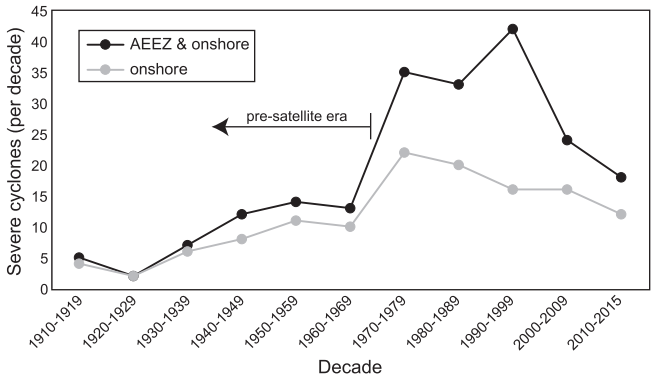

Fig. 14. Number of severe tropical cyclones (TCs) per decade in the Australian region (AEEZ: Australian Exclusive Economic Zone) based on the BOM TC database. TC numbers during the pre-satellite era are underestimated. 'Onshore' includes the area ≤ 20 km from land.

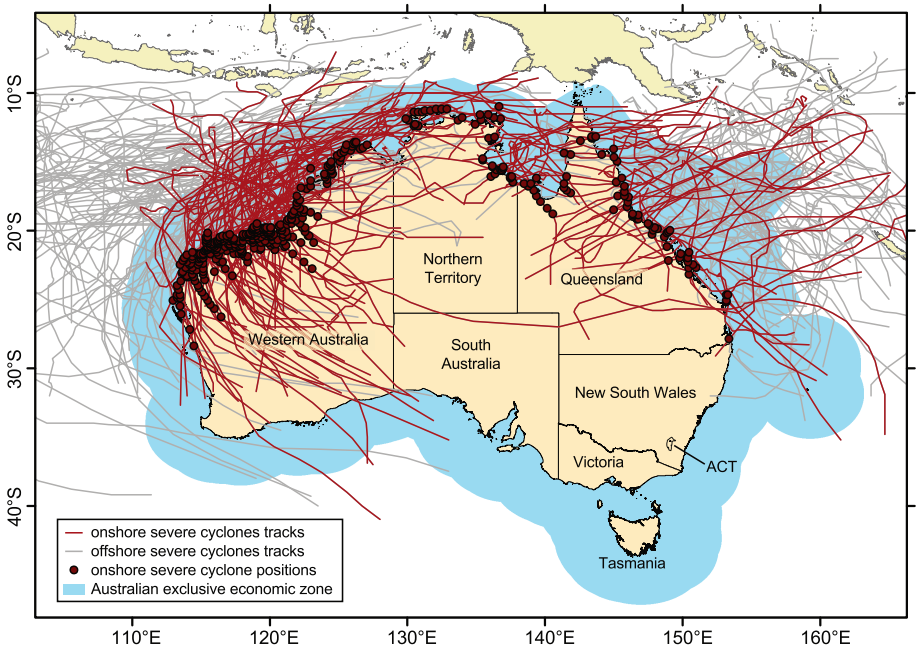

Fig. 15. Severe tropical cyclone (TC) tracks and onshore positions in the Australian region. Tracks for TCs categorised as severe when crossing over land are displayed in red, while offshore severe TCs are shown in grey. The filled circles mark the track positions while TCs are severe and onshore. 'Onshore' is defined as including the area ≤ 20 km from land. TC track positions were derived from BOM (www.bom.gov.au/cyclone/history).

increase in historical TC occurrence. Since 1970, 152 TCs have been categorised as severe within the AEEZ or over the Australian mainland, with a majority of these TCs concentrated in the Western Australia region (Fig. 15).

4.3. In situ data

4.3.1. Weather stations

In Australia, the highest number of operational weather stations were available in the mid-1970s (8051 active rain gauges in 1973; Fig. 16a). Since then, there has been a gradual decline in operational weather stations and, concomitantly, in weather stations with data records covering at least 30 years (Fig. 17). Of the 17,877 BOM-supplied individual data files, 9407 weather stations, or 52.6%, had a minimum rainfall record length of 30 years. Since 1985, 2954 new weather stations have been collecting data. Of these, 2150 were still operational in February 2015. Fig. 18 displays the life span of the weather stations still operational in 2016. The maximum, mean and median are 182, 66.3 and 56 years, respectively. Notably, the period between installation and decommissioning of a weather station does not necessarily coincide with the period for which data is available from that station. For instance, a Tasmanian weather station (#91040) has the distinction of the earliest installation year (1835) among weather stations that are still operational (based on weather station lists obtained from BOM and CDO). However, data for weather station #91040 are only available from November 1916, reducing the period for which data can be obtained from 182 years to 100 years. Rainfall exhibits high inter-annual and long-term variability. Hence, extended rainfall records are required to estimate average recurrence intervals (ARIs) of extreme rainfall events with greater certainty. A short rainfall record only constitutes a snapshot of multi-centennial rainfall variability and is unlikely to have captured a fully representative sample of long-term rainfall patterns. Thus, any statistical estimation of ARIs in excess of about 10 years is inherently unreliable. Nonetheless, ARIs are commonly estimated based on rainfall records that are significantly shorter than the ARI (e.g. a 50-year long rainfall record used to estimate a 100-year ARI). Ideally, the reverse scenario should apply (rainfall record exceeding the targeted ARI several-fold).

Similarly, a dense network of weather stations is needed to capture the spatial variability of rainfall more accurately, allowing a more realistic estimation of flood risk in terms of runoff volume, flow velocity and timing. Rain gauge spatial density has decreased in parallel with the total number of active weather stations. The maximum density within a 1° grid cell was 203 rain gauges in 1970 (Fig. 19), dropping to 155 by 2014. Coastal regions in the southeast and southwest of Australia had the highest density of operational rain gauges. These areas generally coincide with the higher population centres. A similar bias towards high-density centres is also observed in other countries. Fig. 20 compares the density network of weather stations recording rainfall in Australia and the United States based on data contained within the GHCN-Daily dataset (Menne et al., 2012). The number of weather stations in the mountainous region of the western United States is comparatively low compared to the rest of the country, with weather station numbers closely reflecting population density.

4.3.2. McArthur forest fire danger index (FFDI) data requirements

Rainfall data are routinely collected by most weather stations (Fig. 16a). Conversely, other data types, including temperature (Fig. 16c–d), wind (Fig. 16g–h) and relative humidity (Fig. 16e), are relatively scarce despite their usefulness in many research fields (e.g. bushfire risk analysis). To estimate bushfire risk, the McArthur forest fire danger index (FFDI) is commonly utilised. This index requires daily data for rainfall, relative humidity at 3 p.m. (RH_{3pm}), maximum temperature (T_{max}), temperature at 3 p.m. (T_{3pm}) and wind speed at 3 p.m. (V_{3pm}). Of the 17,877 weather station files provided by BOM in February 2015, only 1264 gauges (7.1%) contained sufficient data to calculate the FFDI. RH_{3pm} was the main constraining factor in limiting FFDI derivation between 1964 and 1987 (Fig. 21a), as evidenced by the FFDI time series closely matching the RH_{3pm} availability pattern (Fig. 21b).

The number of operational rain gauges that recorded all required data (rainfall, T_{3pm}, V_{3pm}, etc.) increased significantly from 1959 (Fig. 16a, c–e, g–h and Fig. 21b). The 2003–2009 period had the greatest number of relevant active rain gauges (500–600). As observed for rain data availability (Fig. 19), the highest density of operational rain gauges was consistently associated with high population centres in southeastern and southwestern Australia (Fig. 22). The density peak occurred relatively late in 2008 (17 rain stations within a 1° grid cell) as a result of greater availability of all required data types (Fig. 21a).

4.3.3. Severe storm data

BOM has compiled a severe storm archive based on anecdotal

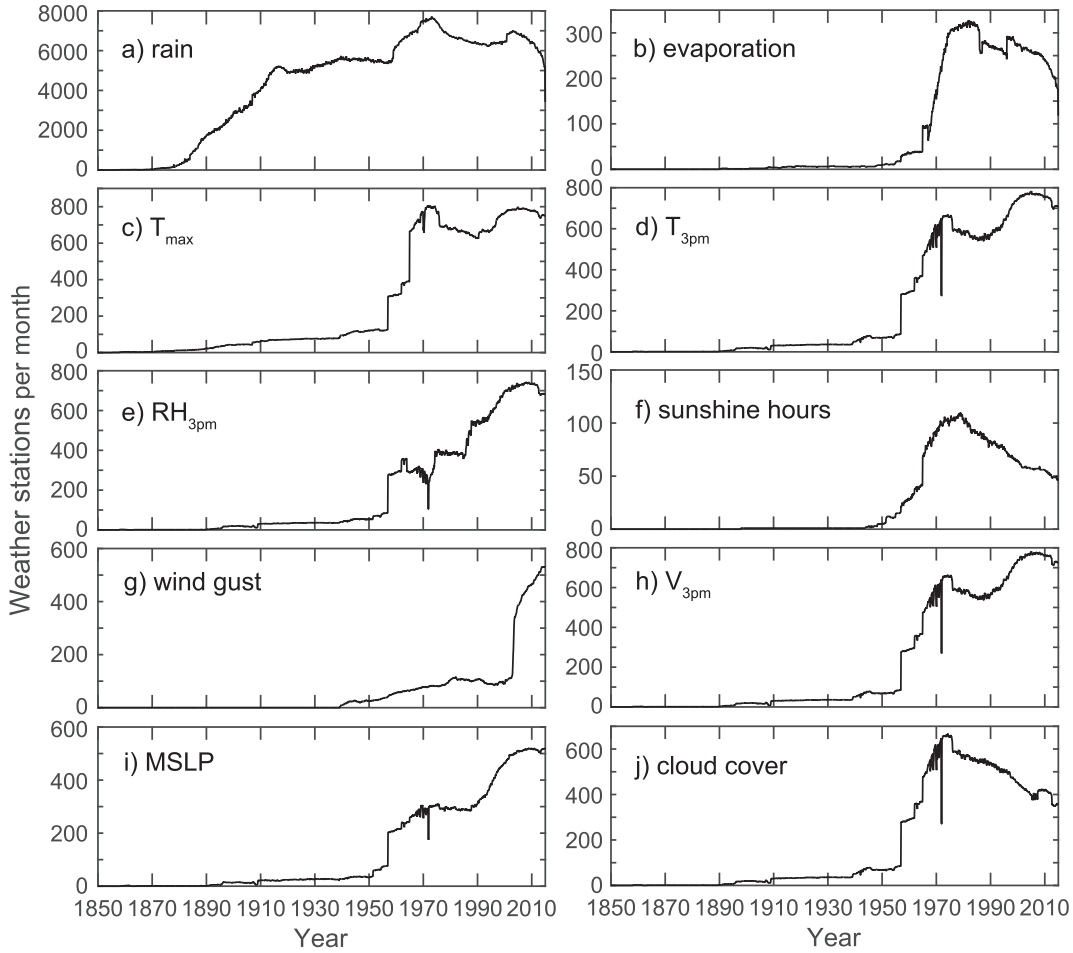

Fig. 16. Number of weather stations with relevant data in Australia for each month between January 1850 and January 2015. The subplots display data availability for a) rainfall, b) evaporation, c) maximum temperature (T_{max}), d) temperature at 3 p.m. (T_{3pm}), e) relative humidity at 3 p.m. (RH_{3pm}), f) sunshine hours, g) wind gust, h) wind speed at 3 p.m. (V_{3pm}), i) mean seal level pressure (MSLP) and j) cloud cover.

information of severe storm activity in Australia dating back to the 18th century (Bureau of Meteorology, 2016). This database includes information about historic events based on observed rain, hail, wind, tornadoes, lightning, waterspouts and dust devils. The archive quality is heavily dependent on the accuracy and detail of reporting by the general public, and on careful data evaluation prior to addition to the archive. Wind gust data units, for instance, may be knots, km/h or, in many cases, left unspecified. The location, in terms of coordinates, may also be unspecified or incorrect, although these can usually be rectified by consulting the "Nearest town" attribute (e.g. Forrest, Western Australia, was assigned an offshore latitude of 33.74°S for observations from 2013 instead of 30.84°S based on pre-2013 entries). Further, some data were filed incorrectly (e.g. wind direction and speed estimates switched around).

Wind gust data are commonly used to assess storm activity. Figs. 16g and 17g highlight the relative scarcity of wind gust data availability. Out of the 17,877 weather station files obtained from BOM, only 689 (3.9%) observed wind gust data. The number of operational weather stations that recorded wind gust data increased substantially from about September 2002 (Figs. 16g and 23a), significantly later compared to most other data types collected by weather stations (Fig. 16a–e, h–j). Fig. 23b displays spatial density distributions of operational weather stations that observed wind gust during 2014. Fig. 23c lists the equivalent density map for observations catalogued in the severe storm archive. Both datasets display temporal and spatial bias in data availability and density, with data availability mainly limited to the more populous southeastern Australia and post-2002 period.

4.3.4. Source-dependent data content

As mentioned in Section 2.2.1, certain weather station data (chiefly rainfall and temperature) can be obtained both via CDO and BOM. Some notable differences exist between the two datasets. A main difference between the CDO- and BOM-derived data consists in the data filtering. While no filtering is applied to data purchased from BOM, CDO only contains data deemed of good quality. In the absence of quality flags, data are automatically excluded in CDO. Conversely, quality flags are provided with purchased BOM data, enabling the user to select data based on their perceived quality. However, data that passed quality checks are not necessarily free of errors. Hence, unusual data patterns should always be treated with additional scrutiny. For instance, 10-minute averaged wind speed at 3 p.m. was sometimes found to exceed the daily maximum wind gust, suggesting that one or both values are flawed. Conversely, an absence of quality checks should not necessarily encourage the removal of unexamined data. CDO-derived rainfall data display a negative spike in rain gauge numbers in late 1994 (Fig. 24a), a feature that is absent in BOM-purchased rainfall data (Fig. 24b). Examination of the CDO-derived data revealed that, during August-November 1994, a large number of weather stations only contained a rainfall value for rain days, while days without rainfall were not assigned any value. Days without any rain are normally assigned a value of 0 mm in data sourced from BOM. Further investigation showed that the quality flags were missing in the affected weather stations during non-rain days in certain months. As CDO only contains data that

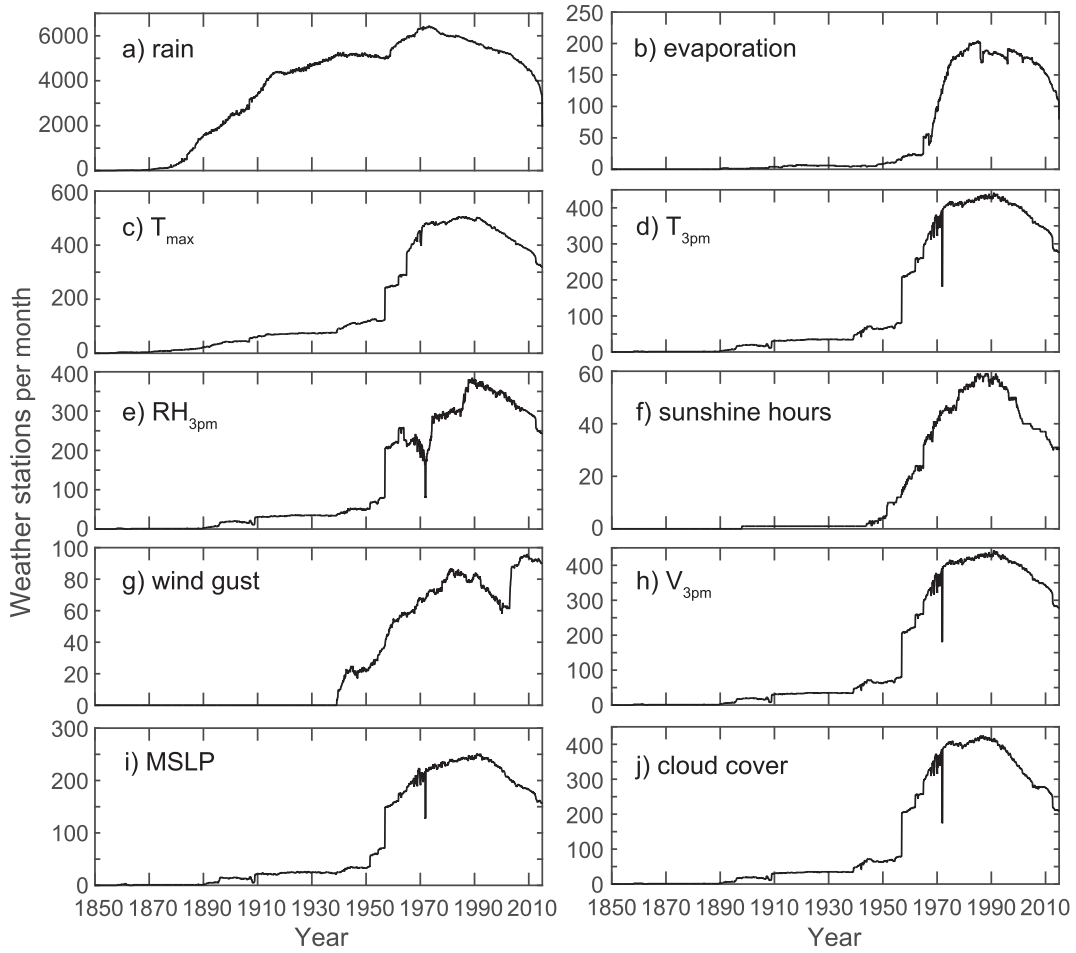

Fig. 17. Number of weather stations operational with at least 30 years of relevant data in Australia for each month between January 1850 and January 2015. The subplots display data availability for a) rainfall, b) evaporation, c) maximum temperature (T_{max}), d) temperature at 3 p.m. (T_{3pm}), e) relative humidity at 3 p.m. (RH_{3pm}), f) sunshine hours, g) wind gust, h) wind speed at 3 p.m. (V_{3pm}), i) mean seal level pressure (MSLP) and j) cloud cover.

passed BOM's quality checks, any data without a quality flag were automatically discarded. Hence, studies incorporating CDO rainfall data from late 1994 should consider that a significant amount of rejected rain-free days are likely genuine.

5. Synthesis, conclusions and future research

5.1. Synthesis

This review examined data available to observe and interpret climate and weather patterns in Australia. Reviewed data include in situ, reanalysis and satellite data. The advent of satellites has enabled large-scale data observation, encompassing not only populated areas but also regions that were hitherto neglected due to logistical restraints. Satellite data are commonly accessed after assimilation into a reanalysis product, for which many sources exist (cf. Table 3). Global databases and reanalysis datasets greatly facilitate scientific studies by collating data from various sources (instruments and organisations) and, in the case of several reanalysis datasets, by providing estimates for regions that continue to be undersampled (data attribution by interpolation for remote regions). Nonetheless, great uncertainty persists in many aspects, including data accuracy, climate variability and long-term trends. In terms of data accuracy, uncertainty is evidenced by the differences in variable estimates among the various global, gridded datasets.

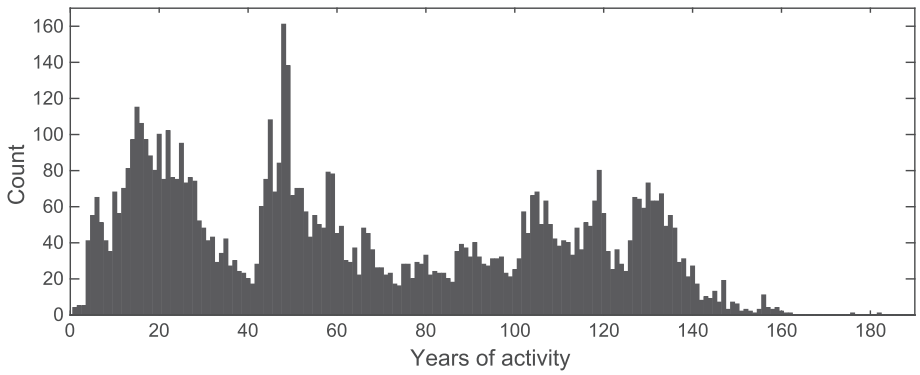

Fig. 18. Record length (based on installation date) of weather stations that were operational in 2016. The tally is based on weather station data provided by BOM in February 2015 and an updated list of available weather stations downloaded from Climate Data Online in November 2016.

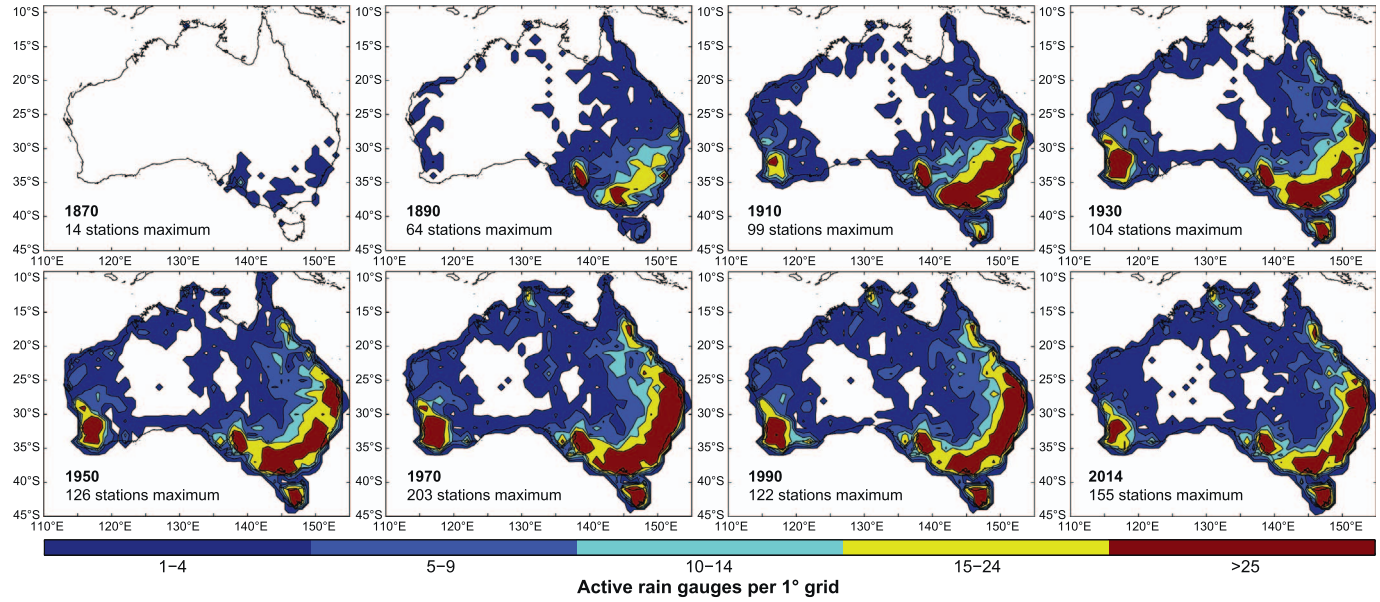

Fig. 19. Evolution of weather station density per 1° grid cell between 1870 and 2014 in Australia.

Disparities arise from the selection of a subset of available data sources for the construction of a gridded dataset, and are further exacerbated by different interpolation and assimilation techniques. Further, while these datasets have advanced research considerably, including in more remote regions, their relatively coarse spatial grid precludes their use for some studies, especially those requiring local rainfall information, as rainfall is known to be highly heterogeneous. However, a significant bias towards coastal, high-population centres has been identified among in situ data, highlighting the importance of remotely sensed or reanalysed data for remote locations in Australia. Furthermore, the large size of Australia precludes a one-size-fits-all approach, with significantly different teleconnections observed in various regions of the country.

Climate indices have been identified that have previously been linked to Australian climate and weather events. These links can be used to estimate probabilities of extreme events occurring. However, the indices' connections to Australian climate and weather events are dependent on the interaction of various remote climate patterns (Meyers et al., 2007). Several studies (Kiem et al., 2003; Risbey et al., 2009b) have shown, for example, that the strength of index connection to Australian climate is dependent on decadal and multi-decadal SST patterns in the Pacific Ocean. Further, the relationship between indices and Australian climate and weather patterns are also regionally and seasonally constrained.

Despite the importance of in situ data, highlighted in Section 2.2.3, the number of active weather stations has been on the decline since the early 1970s (Fig. 16). Some weather stations that were taken offline boasted a relatively long data record for Australian standards and their removal is expected to hamper investigations into long-term climate variability. As weather stations are decommissioned, there is increased reliance on remotely sensed (radar, satellite) data to facilitate long-term and immediate forecasting. Remote sensing has been an invaluable resource for furthering our understanding of climate, especially in regard to global coverage. However, remote sensing and derived data (reanalysis products and numerical modelling) do not always represent actual values realistically and accurately, especially in relation to rainfall (Chaudhuri et al., 2013). Hence, in situ observations are vital for calibration and bias correction of remote sensing products to maximise their accuracy. Further, data products derived from remote sensing tend to have coarse temporal and spatial resolution (Table 3) and are therefore unable to capture the intricacies of small-scale, transitory events. As precipitation is spatially and temporally highly heterogeneous, estimation and management of flood risk associated with extreme rainfall events is problematic and exacerbated by the relatively

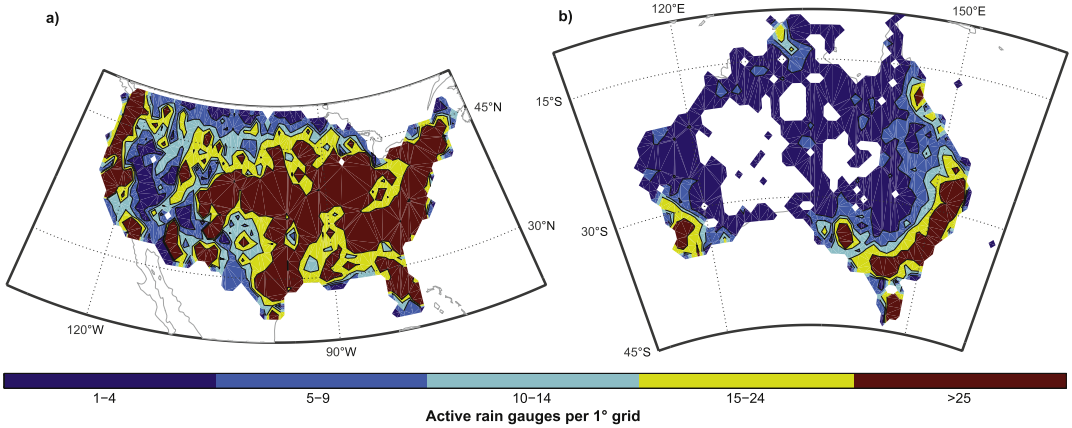

Fig. 20. Number of weather stations (per 1° grid cell) recording rainfall in a) the United States and b) Australia during 2015 based on weather stations contained in the GHCN-Daily dataset (Menne et al., 2012). The area associated with each grid cell increases towards the equator.

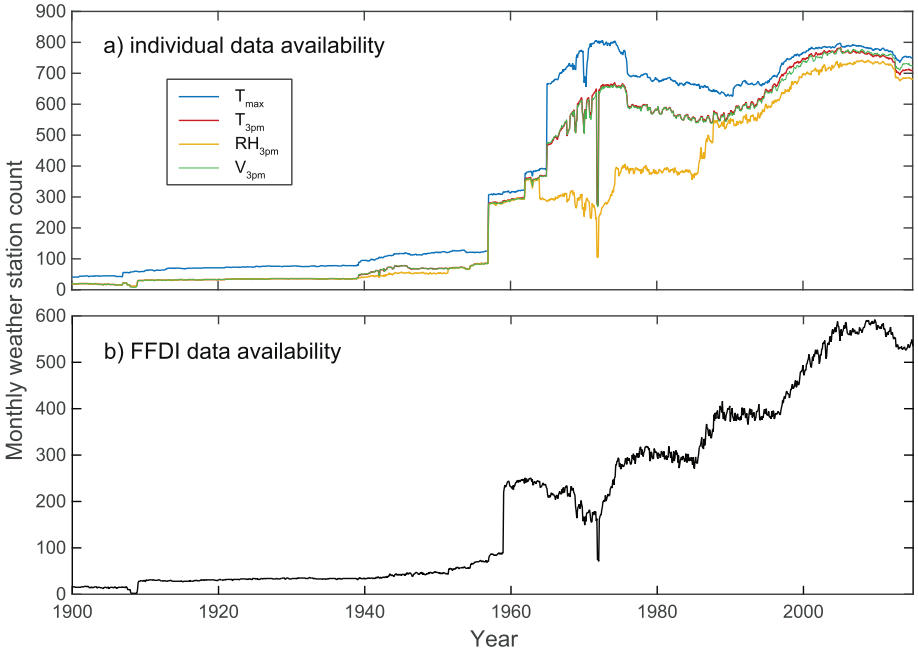

Fig. 21. Time series of total monthly number of a) individual data (T_{max}, T_{3pm}, RH_{3pm} and V_{3pm}) relevant to the McArthur forest fire danger index (FFDI) and b) weather stations that observed all relevant data per month.

sparse network of direct rainfall observations by weather stations in remote areas.

5.2. Concluding remarks

Based on this review, the following conclusions can be drawn based on patterns of data availability discussed earlier.

- Remote sensing and reanalysis datasets greatly advanced the understanding of climate and weather patterns by providing data on a global scale, including for regions hitherto underrepresented. However, certain data types (most notably rainfall) are estimated indirectly by satellite instruments and therefore rely on in situ surveillance for direct observations and validation. Nevertheless, the global gridded datasets are invaluable for large scale studies.
- Significant spatial gaps in in situ data availability persist, especially in scarcely populated regions of Australia. The size and complexity of Australian river systems, the intensity of rainfall and the lack of monitoring stations (including stream gauges) in upper catchments limit the ability to realistically interpret flow velocity, timing and runoff volume. While higher concentration of scientific equipment in populated areas is reasonable to cater to the immediate needs of urban areas, the lack of monitoring stations in scarcely populated areas not only hampers research and management in general but can also jeopardise industry, infrastructure and personal safety (e.g. underestimation of extreme rain events resulting in flash flooding).
- While some variables are spatially relatively uniform (e.g. evaporation), variables such as rainfall exhibit significant variability even at small regional scale. Hence, remote sensing and reanalysis datasets at relatively high resolution (0.25°) will still be subject to significant uncertainty for rainfall. The currently available network of in situ observations can only partially improve the estimates, as few weather monitoring stations exist outside urban areas. Maintenance of the current network of weather stations and instalment of supplementary rain gauges at key sites are vital for accurate estimates of rainfall and associated impact, especially at a local scale.
- In Australia, time series for individual locations and variables are relatively short and cannot adequately resolve low frequency climate variability. The brevity of available observational data therefore introduces great uncertainty when investigating climate variability on a decadal and longer timescale. The non-stationarity of climate was confirmed by several recent Australian paleoclimate studies that showed more frequent and prolonged wet (higher flood risk) and dry (higher drought risk) periods in the pre-instrumental era (Allen et al., 2015; Ho et al., 2015; Vance et al., 2015). Consequently, management of climate risk, including preparedness for low frequency rain events (e.g. 1-in-100-year flood event), is significantly hampered by the lack of accurate historic data. Any studies incorporating long ARI estimates should highlight the high uncertainty associated with long-term rainfall fluctuation.

5.3. Future research

The advent of the satellite era facilitated more detailed studies of oceanic and atmospheric teleconnections with Australian climate. Existing climate indices are most commonly based on SST, atmospheric pressure, wind or OLR data that are usually derived from reanalysis datasets (Table 4). Increased data availability will likely lead to the revelation of additional climate indices linked to Australian weather patterns. Specifically, soil moisture is strongly linked to flooding and bushfire potential (Holgate et al., 2016) and satellite-based observations are thus expected to increase our understanding of flood and bushfire risk. Further, studies into regional dust patterns may also reveal relevant teleconnections to Australian climate.

The rate of change in atmospheric and oceanic conditions also impacts on remote climate and weather patterns. Consequently, a greater focus on investigating absolute or relative changes in monthly climate index values is encouraged. In addition, while some studies have investigated interhemispheric association with Australian climate (Miller et al., 2005; Wu et al., 2009), links between Australian climate and oceanic-atmospheric patterns in the Atlantic Ocean region have hitherto only received limited attention. A preliminary study (results not shown) between Atlantic SST patterns and Australian severe TC occurrence returned significance (p-value < 0.001) at various lead times by the chosen climate indices (tropical North and South Atlantic indices by Enfield et al., 1999). Conversely, the link between the SPCZ position and Australian rainfall is well documented and, although SPCZ indices have previously been derived (Folland et al., 2002; Kidwell et al., 2016; Salinger et al., 2014), regularly updated SPCZ indices do not appear to

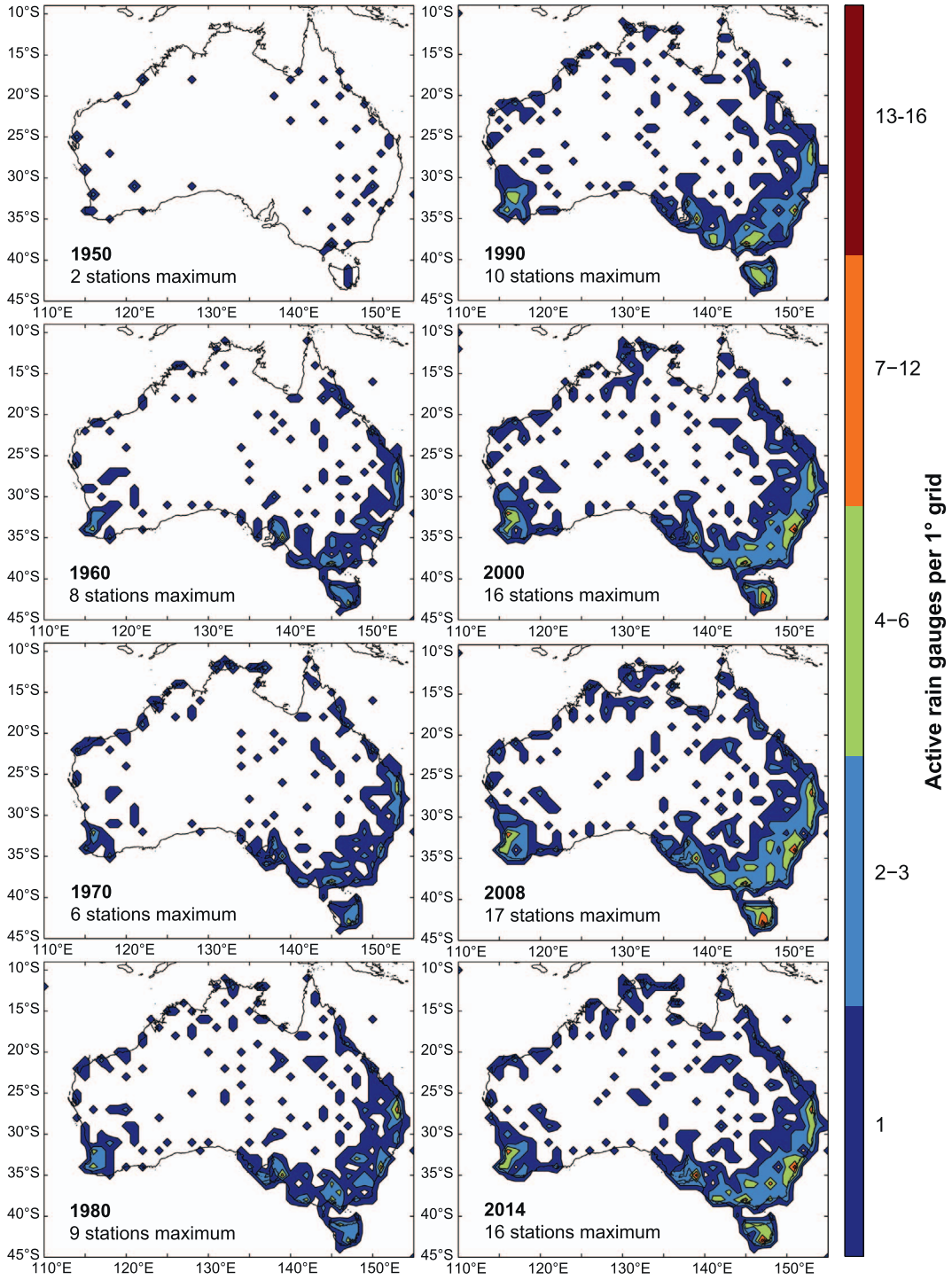

Fig. 22. Density maps of suitable weather stations (collecting all data required for the McArthur forest fire danger index) per 1° grid cell during eight individual years.

be readily available.

A significant amount of uncertainty is involved in climate patterns and terrestrial response, especially in fields associated with rainfall variability, and the relatively short data records available in Australia can only provide a limited picture of expected recurrence interval of risks like flooding. Further, the vastness and clustered population of the continent has hitherto resulted in the neglect of remote areas as a result of perceived low risk to more urbanised regions. Further emphasis is required on data gathering in underrepresented regions to obtain a more complete and accurate view of processes interacting on the Australian continent.

Acknowledgements

The discovery and acquisition of climate indices were greatly helped by a website maintained by Geert Jan van Oldenborgh (http://climexp.knmi.nl). Additional climate index sources include http://www.esrl.noaa.gov/psd/data/climateindices/list and http://www.esrl.noaa.gov/psd/mjo/mjoindex. The best track tropical cyclone and weather station data were provided by the Australian Bureau of Meteorology (http://www.bom.gov.au), with additional in situ data obtained via the Climate Data Online website (http://www.bom.gov.au/climate/data). Global information on weather stations was obtained from the GHCN-

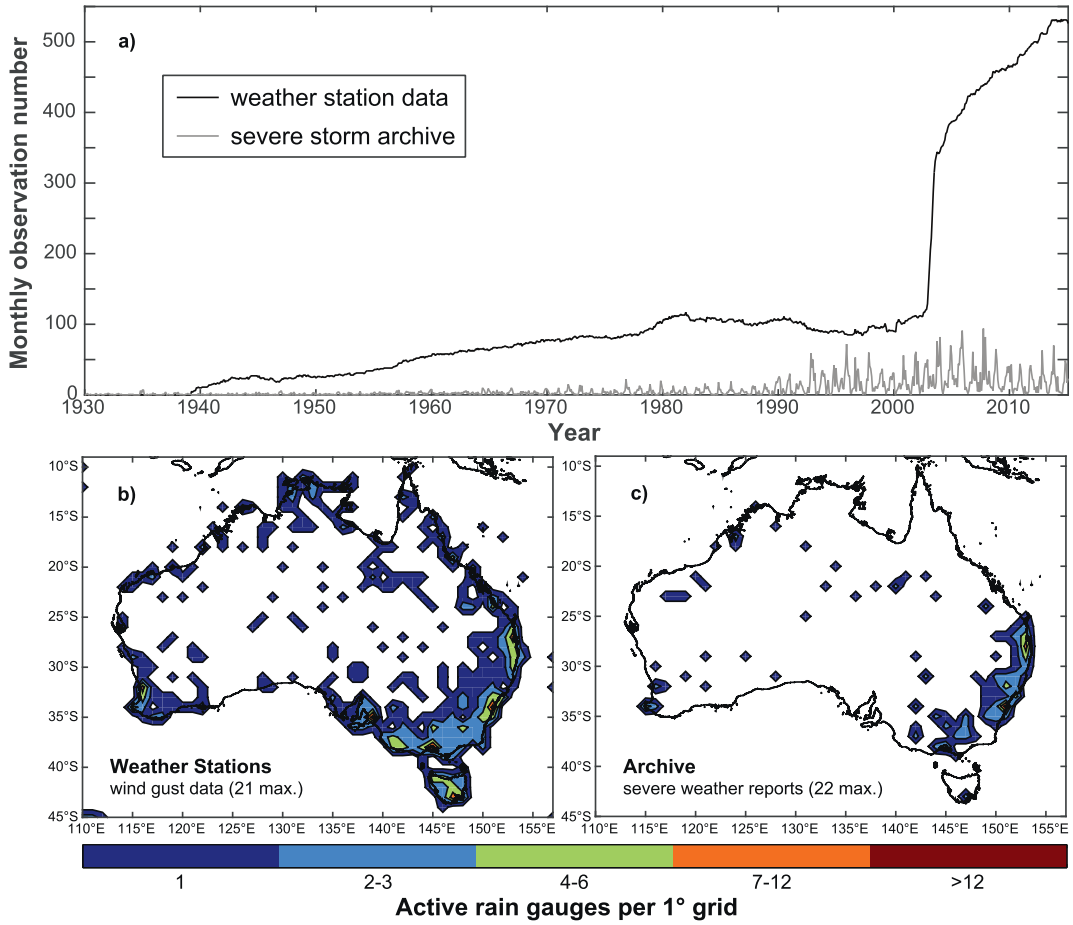

Fig. 23. a) Temporal (1930–2015) and b–c) spatial (2014) severe storm data availability. The data were derived from a–b) weather stations with wind gust data in Australia and a, c) the Bureau of Meteorology's severe storm archive. The density maps (b–c) are provided on a 1° grid cell resolution.

Daily inventory (ftp://ftp.ncdc.noaa.gov/pub/data/ghcn/daily). Interpolated OLR data were provided by the NOAA/OAR/ESRL PSD, Boulder, Colorado, USA, from their Web site at http://www.esrl.noaa.gov/psd. The authors appreciate the instructive comments of two anonymous reviewers. This study was financially supported by Suncorp Insurance.

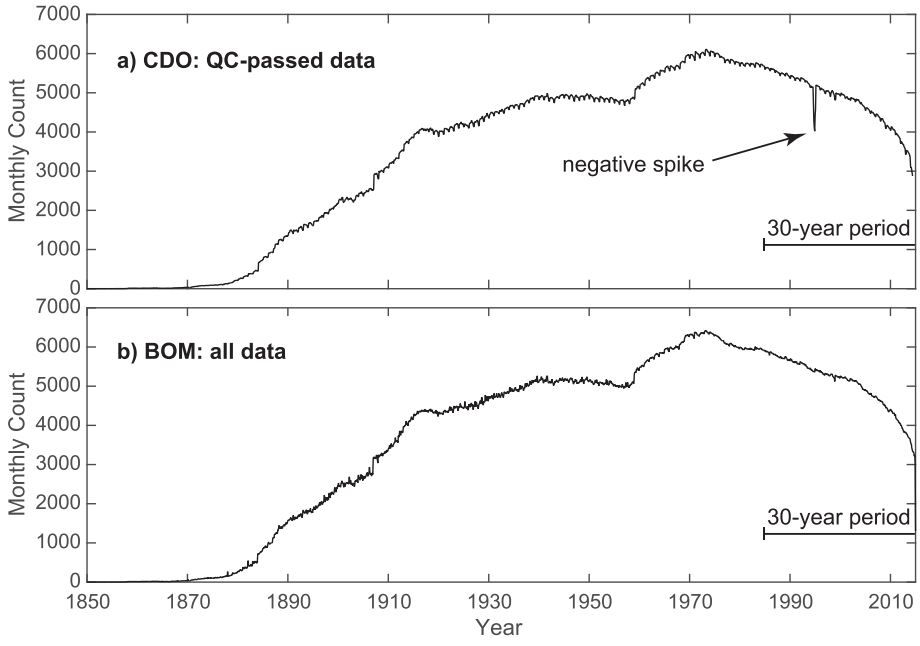

Fig. 24. Time series of monthly total number of active weather stations in Australia with a minimum of 30-year rainfall data record length based on a) data derived from Climate Data Online (CDO; QC: quality control) and b) purchased from BOM. Weather stations with fewer than twenty observations during an individual month were not counted towards the monthly total.

References

Alizadeh Choobari, O., Zawar-Reza, P., Sturman, A., 2012. Atmospheric forcing of the three-dimensional distribution of dust particles over Australia: a case study. J. Geophys. Res. Atmos. 117 (D11).

Allan, R.J., Nicholls, N., Jones, P.D., Butterworth, I.J., 1991. A further extension of the Tahiti-Darwin SOI, early ENSO events and Darwin pressure. J. Clim. 4 (7), 743–749.

Allan, R.J., Reason, C.J.C., Lindesay, J.A., Ansell, T.J., 2003. Protracted' ENSO episodes and their impacts in the Indian Ocean region. Deep-Sea Res. II Top. Stud. Oceanogr. 50 (12-13), 2331–2347.

Allen, J.T., Karoly, D.J., 2014. A climatology of Australian severe thunderstorm environments 1979–2011: inter-annual variability and ENSO influence. Int. J. Climatol. 34 (1), 81–97.

Allen, K.J., Nichols, S.C., Evans, R., Cook, E.R., Allie, S., Carson, G., Ling, F., Baker, P.J., 2015. Preliminary December–January inflow and streamflow reconstructions from tree rings for western Tasmania, southeastern Australia. Water Resour. Res. 51 (7), 5487–5503.

Arguez, A., Vose, R.S., 2011. The definition of the standard WMO climate normal: The key to deriving alternative climate normals. Bull. Am. Meteorol. Soc. 92 (6), 699–704.

Arguez, A., Durre, I., Applequist, S., Vose, R.S., Squires, M.F., Yin Jr., X., R.R.H. and Owen, T.W., 2012. NOAA's 1981–2010 US climate normals: An overview. Bull. Am. Meteorol. Soc. 93 (11), 1687–1697.

Ashok, K., Guan, Z., Yamagata, T., 2003. Influence of the Indian Ocean Dipole on the Australian winter rainfall. Geophys. Res. Lett. 30 (15), 1821.

Ashok, K., Behera, S.K., Rao, S.A., Weng, H., Yamagata, T., 2007. El Niño Modoki and its possible teleconnection. J. Geophys. Res. Oceans Atmos. 112 (C11), C11007.

Ashok, K., Tam, C.Y., Lee, W.J., 2009. ENSO Modoki impact on the Southern Hemisphere storm track activity during extended austral winter. Geophys. Res. Lett. 36 (12).

Babcock, H.W., 1961. The topology of the Sun's magnetic field and the 22-year cycle. Astrophys. J. 133, 572–587.

Bal, S., Schimanke, S., Spangehl, T., Cubasch, U., 2011. On the robustness of the solar cycle signal in the Pacific region. Geophys. Res. Lett. 38 (14), L14809.

Baldwin, M.P., Gray, L.J., Dunkerton, T.J., Hamilton, K., Haynes, P.H., Randel, W.J., Holton, J.R., Alexander, M.J., Hirota, I., Horinouchi, T., Jones, D.B.A., Kinnersley, J.S., Marquardt, C., Sato, K., Takahashi, M., 2001. The quasi-biennial oscillation. Rev. Geophys. 39 (2), 179–229.

Balsamo, G., Albergel, C., Beljaars, A., Boussetta, S., Brun, E., Cloke, H., Dee, D., Dutra, E., Muñoz-Sabater, J., Pappenberger, F., de Rosnay, P., Stockdale, T., Vitart, F., 2015. ERA-Interim/Land: a global land surface reanalysis data set. Hydrol. Earth Syst. Sci. 19 (1), 389–407.

Barber, R.T., Chavez, F.P., 1983. Biological consequences of El Niño. Science 222, 1203–1210.

Barton, I.J., 2007. Comparison of in situ and satellite-derived sea surface temperatures in the Gulf of Carpentaria. J. Atmos. Ocean. Technol. 24 (10), 1773–1784.

Basher, R.E., Zheng, X., 1995. Tropical cyclones in the southwest Pacific: Spatial patterns and relationships to Southern Oscillation and sea surface temperature. J. Clim. 8 (5), 1249–1260.

Bauer-Marschallinger, B., Dorigo, W.A., Wagner, W., Dijk, A.I.J.M.v., 2013. How oceanic oscillation drives soil moisture variations over mainland Australia: An analysis of 32 years of satellite observations. J. Clim. 26 (24), 10159–10173.

Beesley, C., Frost, A., Zajaczkowski, J., 2009. A comparison of the BAWAP and SILO spatially interpolated daily rainfall datasets, 18th World IMACS/MODSIM Congress, Cairns, Australia. Citeseer, pp. 17.

Behera, S.K., Yamagata, T., 2001. Subtropical SST dipole events in the southern Indian Ocean. Geophys. Res. Lett. 28 (2), 327–330.

Behera, S.K., Rao, S.A., Saji, H.N., Yamagata, T., 2003. Comments on “A cautionary note on the interpretation of EOFs”. J. Clim. 16 (7), 1087–1093.

Behera, S.K., Luo, J.J., Masson, S., Rao, S.A., Sakuma, H., Yamagata, T., 2006. A CGCM study on the interaction between IOD and ENSO. J. Clim. 19 (9), 1688–1705.

Bjerknes, J., 1966. A possible response of the atmospheric Hadley circulation to anomalies of ocean temperature. Tellus 18, 820–829.

Bjerknes, J., 1969. Atmospheric teleconnections from the equatorial Pacific. Mon. Weather Rev. 97 (3), 163–172.

Boening, C., Willis, J.K., Landerer, F.W., Nerem, R.S., Fasullo, J., 2012. The 2011 La Niña: So strong, the oceans fell. Geophys. Res. Lett. 39 (19).

Brooks, H.E., Lee, J.W., Craven, J.P., 2003. The spatial distribution of severe thunderstorm and tornado environments from global reanalysis data. Atmos. Res. 67–68, 73–94.

Bureau of Meteorology, 2011. The Australian Climate Observations Reference Network - Surface Air Temperature (ACORN-SAT): station catalogue. (112 pp).

Bureau of Meteorology, 2016. Severe storms archive. www.bom.gov.au/australia/stormarchive, Australia, accessed September 2016.

Cai, W., Cowan, T., 2008. Dynamics of late autumn rainfall reduction over southeastern Australia. Geophys. Res. Lett. 35 (9).

Cai, W., Cowan, T., 2009. La Niña Modoki impacts Australia autumn rainfall variability. Geophys. Res. Lett. 36 (12).

Cai, W., van Rensch, P., 2013. Austral summer teleconnections of Indo-Pacific variability: their nonlinearity and impacts on Australian climate. J. Clim. 26 (9), 2796–2810.

Cai, W., Pan, A., Roemmich, D., Cowan, T., Guo, X., 2009. Argo profiles a rare occurrence of three consecutive positive Indian Ocean Dipole events, 2006–2008. Geophys. Res. Lett. 36 (8), L08701.

Cai, W., van Rensch, P., Cowan, T., Hendon, H.H., 2011. Teleconnection pathways of ENSO and the IOD and the mechanisms for impacts on Australian rainfall. J. Clim. 24 (15), 3910–3923.

Cai, W., Lengaigne, M., Borlace, S., Collins, M., Cowan, T., McPhaden, M.J., Timmermann, A., Power, S., Brown, J., Menkes, C., Ngari, A., Vincent, E.M., Widlansky, M.J., 2012. More extreme swings of the South Pacific convergence zone due to greenhouse warming. Nature 488 (7411), 365–369.

Cane, M.A., 2005. The evolution of El Niño, past and future. Earth Planet. Sci. Lett. 230 (3–4), 227–240.

Cecil, D.J., Blankenship, C.B., 2012. Toward a global climatology of severe hailstorms as estimated by satellite passive microwave imagers. J. Clim. 25 (2), 687–703.

Chaudhuri, A.H., Ponte, R.M., Forget, G., Heimbach, P., 2013. A comparison of atmospheric reanalysis surface products over the ocean and implications for uncertainties in air–sea boundary forcing. J. Clim. 26 (1), 153–170.

Chelton, D.B., Schlax, M.G., 1996. Global observations of oceanic Rossby waves. Science 272 (5259), 234–238.

Chen, Y., Ebert, E.E., Walsh, K.J.E., Davidson, N.E., 2013a. Evaluation of TMPA 3B42 daily precipitation estimates of tropical cyclone rainfall over Australia. J. Geophys. Res. Atmos. 118 (21), 11,966–11,978.

Chen, Y., Ebert, E.E., Walsh, K.J.E., Davidson, N.E., 2013b. Evaluation of TRMM 3B42 precipitation estimates of tropical cyclone rainfall using PACRAIN data. J. Geophys. Res. Atmos. 118 (5), 2184–2196.

Chiew, F.H.S., Piechota, T.C., Dracup, J.A., McMahon, T.A., 1998. El Nino/Southern Oscillation and Australian rainfall, streamflow and drought: Links and potential for forecasting. J. Hydrol. 204 (1–4), 138–149.

Chu, J.-H., Sampson, C.R., Levine, A.S., Fukada, E., 2002. The Joint Typhoon Warning Center tropical cyclone best-tracks, 1945–2000. Ref. NRL/MR/7540-02. 16.

Clette, F., Svalgaard, L., Vaquero, J., Cliver, E., 2014. Revisiting the sunspot number. Space Sci. Rev. 186 (1-4), 35–103.

Compo, G.P., Whitaker, J.S., Sardeshmukh, P.D., Matsui, N., Allan, R.J., Yin, X., Gleason, B.E., Vose, R.S., Rutledge, G., Bessemoulin, P., Brönnimann, S., Brunet, M., Crouthamel, R.I., Grant, A.N., Groisman, P.Y., Jones, P.D., Kruk, M.C., Kruger, A.C., Marshall, G.J., Maugeri, M., Mok, H.Y., Nordli, Ø., Ross, T.F., Trigo, R.M., Wang, X.L., Woodruff, S.D., Worley, S.J., 2011. The twentieth century reanalysis project. Q. J. R. Meteorol. Soc. 137 (654), 1–28.

Dahlman, L., 2016. Climate variability: Oceanic Niño Index. https://www.climate.gov/news-features/understanding-climate/climate-variability-oceanic-niño-index/NOAA Climate.gov accessed October 24 2016.

Daley, R., 1993. Atmospheric Data Analysis. Cambridge Atmospheric and Space Science Series Cambridge University Press.

De Jong, A.F.M., Mook, W.G., Becker, B., 1979. Confirmation of the Suess wiggles: 3200–3700 BC. Nature 280 (5717), 48–49.

Dee, D.P., Uppala, S.M., Simmons, A.J., Berrisford, P., Poli, P., Kobayashi, S., Andrae, U., Balmaseda, M.A., Balsamo, G., Bauer, P., Bechtold, P., Beljaars, A.C.M., van de Berg, L., Bidlot, J., Bormann, N., Delsol, C., Dragani, R., Fuentes, M., Geer, A.J., Haimberger, L., Healy, S.B., Hersbach, H., Hólm, E.V., Isaksen, L., Kållberg, P., Köhler, M., Matricardi, M., McNally, A.P., Monge-Sanz, B.M., Morcrette, J.J., Park, B.K., Peubey, C., de Rosnay, P., Tavolato, C., Thépaut, J.N., Vitart, F., 2011. The ERA-Interim reanalysis: configuration and performance of the data assimilation system. Q. J. R. Meteorol. Soc. 137 (656), 553–597.

Della-Marta, P., Collins, D., Braganza, K., 2004. Updating Australia's high-quality annual temperature dataset. Aust. Meteorol. Mag. 53 (2), 75–93.

Deser, C., Wallace, J.M., 1990. Large-scale atmospheric circulation features of warm and cold episodes in the tropical Pacific. J. Clim. 3 (11), 1254–1281.

Diamond, H.J., Lorrey, A.M., Knapp, K.R., Levinson, D.H., 2012. Development of an enhanced tropical cyclone tracks database for the southwest Pacific from 1840 to 2010. Int. J. Climatol. 32 (14), 2240–2250.

Done, S.J., Holbrook, N.J., Beggs, P.J., 2002. The quasi-biennial oscillation and Ross River virus incidence in Queensland, Australia. Int. J. Biometeorol. 46 (4), 202–207.

Draper, C.S., Walker, J.P., Steinle, P.J., de Jeu, R.A.M., Holmes, T.R.H., 2009. An evaluation of AMSR–E derived soil moisture over Australia. Remote Sens. Environ. 113 (4), 703–710.

Drosdowsky, W., 2005. The latitude of the subtropical ridge over Eastern Australia: The *L* index revisited. Int. J. Climatol. 25 (10), 1291–1299.

Dvorak, V.F., 1975. Tropical cyclone intensity analysis and forecasting from satellite imagery. Mon. Weather Rev. 103 (5), 420–430.

Enfield, D.B., Mestas-Nuñez, A.M., Mayer, D.A., Cid-Serrano, L., 1999. How ubiquitous is the dipole relationship in tropical Atlantic sea surface temperatures? J. Geophys. Res. Oceans Atmos. 104 (C4), 7841–7848.

Erlykin, A.D., Wolfendale, A.W., 2011. Cosmic ray effects on cloud cover and their relevance to climate change. J. Atmos. Sol. Terr. Phys. 73 (13), 1681–1686.

Erlykin, A.D., Sloan, T., Wolfendale, A.W., 2010. Correlations of clouds, cosmic rays and solar irradiation over the Earth. J. Atmos. Sol. Terr. Phys. 72 (2–3), 151–156.

Evans, J.L., Allan, R.J., 1992. El Niño/Southern Oscillation modification to the structure of the monsoon and tropical cyclone activity in the Australasian region. Int. J. Climatol. 12 (6), 611–623.

Fedorov, A.V., Brown, J.N., 2009. Equatorial waves. In: Steele, J.H. (Ed.), Encyclopedia of Ocean Sciences. Academic Press, Oxford, pp. 271–287.

Feng, M., Meyers, G., 2003. Interannual variability in the tropical Indian Ocean: a two-year time-scale of Indian Ocean Dipole. Deep-Sea Res. II Top. Stud. Oceanogr. 50 (12–13), 2263–2284.

Folland, C.K., Renwick, J.A., Salinger, M.J., Mullan, A.B., 2002. Relative influences of the Interdecadal Pacific Oscillation and ENSO on the South Pacific Convergence Zone. Geophys. Res. Lett. 29 (13), 1643. http://dx.doi.org/10.1029/2001GL014201.

Franks, S.W., 2002. Assessing hydrological change: deterministic general circulation models or spurious solar correlation? Hydrol. Process. 16 (2), 559–564.

Freeman, E., Woodruff, S.D., Worley, S.J., Lubker, S.J., Kent, E.C., Angel, W.E., Berry, D.I., Brohan, P., Eastman, R., Gates, L., Gloeden, W., Ji, Z., Lawrimore, J., Rayner, N.A., Rosenhagen, G., Smith, S.R., 2017. ICOADS Release 3.0: a major update to the historical marine climate record. Int. J. Climatol. 37 (5), 2211–2232.

Friis-Christensen, E., Lassen, K., 1991. Length of the solar cycle: an indicator of solar activity closely associated with climate. Science 254 (5032), 698–700.
Fröhlich, C., Lean, J., 2004. Solar radiative output and its variability: evidence and mechanisms. Astron. Astrophys. Rev. 12 (4), 273–320.
Gallant, A.J.E., Kiem, A.S., Verdon-Kidd, D.C., Stone, R.C., Karoly, D.J., 2012. Understanding hydroclimate processes in the Murray-Darling Basin for natural resources management. Hydrol. Earth Syst. Sci. 16 (7), 2049–2068.
GCOS, 2013. GSN station summary by region. http://www.wmo.int/pages/prog/gcos/documents/GSN_Stations_Region_2014.pdf, World Meteorological Organization, accessed 29 May 2017.
Gillett, N., Kell, T., Jones, P., 2006. Regional climate impacts of the Southern Annular Mode. Geophys. Res. Lett. 33 (23).
Gleissberg, W., 1939. A long-periodic fluctuation of the sun-spot numbers. Observatory 62, 158–159.
Gruber, A., Krueger, A.F., 1984. The status of the NOAA outgoing longwave radiation data set. Bull. Am. Meteorol. Soc. 65 (9), 958–962.
Haigh, J.D., 1996. The impact of solar variability on climate. Science 272 (5264), 981–984.
Hale, G.E., Ellerman, F., Nicholson, S.B., Joy, A.H., 1919. The magnetic polarity of sunspots. Astrophys. J. 49, 153–178.
Hall, J.D., Matthews, A.J., Karoly, D.J., 2001. The modulation of tropical cyclone activity in the Australian region by the Madden-Julian Oscillation. Mon. Weather Rev. 129 (12), 2970–2982.
Hanley, D.E., Bourassa, M.A., O'Brien, J.J., Smith, S.R., Spade, E.R., 2003. A quantitative evaluation of ENSO indices. J. Clim. 16 (8), 1249–1258.
Harper, B.A., Stroud, S.A., McCormack, M., West, S., 2008. A review of historical tropical cyclone intensity in northwestern Australia and implications for climate change trend analysis. Aust. Meteorol. Mag. 57 (2), 121–141.
Harris, I., Jones, P.D., Osborn, T.J., Lister, D.H., 2014. Updated high-resolution grids of monthly climatic observations – the CRU TS3.10 Dataset. Int. J. Climatol. 34 (3), 623–642.
Hastings, P.A., 1990. Southern Oscillation influences on tropical cyclone activity in the Australian/south-west Pacific region. Int. J. Climatol. 10 (3), 291–298.
Hendon, H.H., Salby, M.L., 1994. The life cycle of the Madden-Julian oscillation. J. Atmos. Sci. 51 (15), 2225–2237.
Hendon, H.H., Thompson, D.W.J., Wheeler, M.C., 2007. Australian rainfall and surface temperature variations associated with the southern hemisphere annular mode. J. Clim. 20 (11), 2452–2467.
Hendon, H.H., Lim, E.-P., Arblaster, J.M., Anderson, D.T., 2014. Causes and predictability of the record wet east Australian spring 2010. Clim. Dyn. 42 (5-6), 1155–1174.
Henley, B., Gergis, J., Karoly, D., Power, S., Kennedy, J., Folland, C., 2015. A Tripole Index for the Interdecadal Pacific Oscillation. Clim. Dyn. 1–14.
Ho, C.-H., Baik, J.-J., Kim, J.-H., Gong, D.-Y., Sui, C.-H., 2004. Interdecadal changes in summertime typhoon tracks. J. Clim. 17 (9), 1767–1776.
Ho, M., Kiem, A.S., Verdon-Kidd, D.C., 2012. The Southern Annular Mode: a comparison of indices. Hydrol. Earth Syst. Sci. 16 (3), 967–982.
Ho, M., Kiem, A.S., Verdon-Kidd, D.C., 2015. A paleoclimate rainfall reconstruction in the Murray-Darling Basin (MDB), Australia: 2. Assessing hydroclimatic risk using paleoclimate records of wet and dry epochs. Water Resour. Res. 51 (10), 8380–8396.
Holgate, C.M., De Jeu, R.A.M., van Dijk, A.I.J.M., Liu, Y.Y., Renzullo, L.J., Vinodkumar, Dharssi, I., Parinussa, R.M., Van Der Schalie, R., Gevaert, A., Walker, J., McJannet, D., Cleverly, J., Haverd, V., Trudinger, C.M., Briggs, P.R., 2016. Comparison of remotely sensed and modelled soil moisture data sets across Australia. Remote Sens. Environ. 186, 479–500.
Holton, J.R., Hakim, G.J., 2013. Tropical dynamics. In: Holton, J.R., Hakim, G.J. (Eds.), An Introduction to Dynamic Meteorology. Academic Press, Boston, pp. 377–411.
Hou, A.Y., Kakar, R.K., Neeck, S., Azarbarzin, A.A., Kummerow, C.D., Kojima, M., Oki, R., Nakamura, K., Iguchi, T., 2014. The Global Precipitation Measurement mission. Bull. Am. Meteorol. Soc. 95 (5), 701–722.
Hsu, K.-L., Gao, X., Sorooshian, S., Gupta, H.V., 1997. Precipitation estimation from remotely sensed information using artificial neural networks. J. Appl. Meteorol. 36 (9), 1176–1190.
Huang, B., Banzon, V.F., Freeman, E., Lawrimore, J., Liu, W., Peterson, T.C., Smith, T.M., Thorne, P.W., Woodruff, S.D., Zhang, H.-M., 2015. Extended reconstructed sea surface temperature version 4 (ERSST. v4). Part I: Upgrades and intercomparisons. J. Clim. 28 (3), 911–930.
Huffman, G.J., Bolvin, D.T., Nelkin, E.J., Wolff, D.B., Adler, R.F., Gu, G., Hong, Y., Bowman, K.P., Stocker, E.F., 2007. The TRMM multisatellite precipitation analysis (TMPA): Quasi-global, multiyear, combined-sensor precipitation estimates at fine scales. J. Hydrometeorol. 8 (1), 38–55.
Hulme, M., Dessai, S., Lorenzoni, I., Nelson, D.R., 2009. Unstable climates: Exploring the statistical and social constructions of 'normal' climate. Geoforum 40 (2), 197–206.
Hung, C.-C., 2007. Apparent relations between solar activity and solar tides caused by the planets. (27 pp).
Jeffrey, S.J., Carter, J.O., Moodie, K.B., Beswick, A.R., 2001. Using spatial interpolation to construct a comprehensive archive of Australian climate data. Environ. Model Softw. 16 (4), 309–330.
Jones, D.A., Wang, W., Fawcett, R., 2009. High-quality spatial climate data-sets for Australia. Aust. Meteorol. Oceanogr. J. 58, 233–248.
Jovanovic, B., Jones, D.A., Collins, D., 2008. A high-quality monthly pan evaporation dataset for Australia. Clim. Chang. 87 (3), 517–535.
Jovanovic, B., Collins, D., Braganza, K., Jakob, D., Jones, D.A., 2011. A high-quality monthly total cloud amount dataset for Australia. Clim. Chang. 108 (3), 485–517.
Joyce, R.J., Janowiak, J.E., Arkin, P.A., Xie, P., 2004. CMORPH: a method that produces global precipitation estimates from passive microwave and infrared data at high spatial and temporal resolution. J. Hydrometeorol. 5 (3), 487–503.
Julian, P.R., Chervin, R.M., 1978. A study of the Southern Oscillation and Walker Circulation phenomenon. Mon. Weather Rev. 106, 1433–1451.
Kållberg, P.W., Simmons, A., Uppala, S., Fuentes, M., 2004. The ERA-40 archive. ECMWF, Shinfield Park, Reading (32 pp).
Kalnay, E., Kanamitsu, M., Kistler, R., Collins, W., Deaven, D., Gandin, L., Iredell, M., Saha, S., White, G., Woollen, J., Zhu, Y., Leetmaa, A., Reynolds, R., Chelliah, M., Ebisuzaki, W., Higgins, W., Janowiak, J., Mo, K.C., Ropelewski, C., Wang, J., Jenne, R., Joseph, D., 1996. The NCEP/NCAR 40-year reanalysis project. Bull. Am. Meteorol. Soc. 77 (3), 437–471.
Kennedy, J.J., Rayner, N.A., Smith, R.O., Parker, D.E., Saunby, M., 2011a. Reassessing biases and other uncertainties in sea surface temperature observations measured in situ since 1850: 1. Measurement and sampling uncertainties. J. Geophys. Res. Atmos. 116 (D14).
Kennedy, J.J., Rayner, N.A., Smith, R.O., Parker, D.E., Saunby, M., 2011b. Reassessing biases and other uncertainties in sea surface temperature observations measured in situ since 1850: 2. Biases and homogenization. J. Geophys. Res. Atmos. 116 (D14).
Kidd, C., Levizzani, V., Bauer, P., 2009. A review of satellite meteorology and climatology at the start of the twenty-first century. Prog. Phys. Geogr. 33 (4), 474–489.
Kidwell, A., Lee, T., Jo, Y.-H., Yan, X.-H., 2016. Characterization of the variability of the South Pacific Convergence Zone using satellite and reanalysis wind products. J. Clim. 29 (5), 1717–1732.
Kiem, A.S., Franks, S.W., 2004. Multi-decadal variability of drought risk, eastern Australia. Hydrol. Process. 18 (11), 2039–2050.
Kiem, A.S., Franks, S.W., Kuczera, G., 2003. Multi-decadal variability of flood risk. Geophys. Res. Lett. 30 (2), 1035.
Kiladis, G.N., Dias, J., Straub, K.H., Wheeler, M.C., Tulich, S.N., Kikuchi, K., Weickmann, K.M., Ventrice, M.J., 2014. A comparison of OLR and circulation-based indices for tracking the MJO. Mon. Weather Rev. 142 (5), 1697–1715.
Kim, W., Yeh, S.-W., Kim, J.-H., Kug, J.-S., Kwon, M., 2011. The unique 2009–2010 El Niño event: A fast phase transition of warm pool El Niño to La Niña. Geophys. Res. Lett. 38 (15), L15809.
King, A.D., Alexander, L.V., Donat, M.G., 2013. The efficacy of using gridded data to examine extreme rainfall characteristics: a case study for Australia. Int. J. Climatol. 33 (10), 2376–2387.
Klingaman, N.P., Woolnough, S.J., Syktus, J., 2013. On the drivers of inter-annual and decadal rainfall variability in Queensland, Australia. Int. J. Climatol. 33 (10), 2413–2430.
Knapp, K.R., Kruk, M.C., Levinson, D.H., Diamond, H.J., Neumann, C.J., 2010. The International Best Track Archive for Climate Stewardship (IBTrACS). Bull. Am. Meteorol. Soc. 91 (3), 363–376.
Kovats, R.S., Bouma, M.J., Hajat, S., Worrall, E., Haines, A., 2003. El Niño and health. Lancet 362 (9394), 1481–1489.
Kuleshov, Y., Fawcett, R., Qi, L., Trewin, B., Jones, D., McBride, J., Ramsay, H., 2010. Trends in tropical cyclones in the South Indian Ocean and the South Pacific Ocean. J. Geophys. Res. Atmos. 115 (D1), D01101.
Kwan, K.F., Samah, A.A., 2003. A conceptual model relating the quasi-biennial oscillation and the tropospheric biennial oscillation. Int. J. Climatol. 23 (3), 347–362.
Larsen, S.H., Nicholls, N., 2009. Southern Australian rainfall and the subtropical ridge: Variations, interrelationships, and trends. Geophys. Res. Lett. 36 (8).
Lau, K.-M., Chan, P.H., 1983. Short-term climate variability and atmospheric teleconnections from satellite-observed outgoing longwave radiation. Part I: Simultaneous relationships. J. Atmos. Sci. 40 (12), 2735–2750.
Lavery, B., Kariko, A., Nicholls, N., 1992. A historical rainfall data set for Australia. Aust. Meteorol. Mag. 40, 33–39.
Lavery, B., Joung, G., Nicholls, N., 1997. An extended high-quality historical rainfall dataset for Australia. Aust. Meteorol. Mag. 46 (1), 27–38.
Liebmann, B., Hendon, H.H., Glick, J.D., 1994. The relationship between tropical cyclones of the western Pacific and Indian Oceans and the Madden–Julian oscillation. J. Meteorol. Soc. Jpn. 72 (3), 401–412.
Lindsay, M., Broom, A.K., Wright, A., Johansen, C.A., Mackenzie, J.S., 1993. Ross River virus isolations from mosquitoes in arid regions of Western Australia: implication of vertical transmission as a means of persistence of the virus. Am. J. Trop. Med. Hyg. 49 (6), 686–696.
Lindsey, R., 2013. In watching for El Niño and La Niña, NOAA adapts to global warming. https://www.climate.gov/news-features/understanding-climate/watching-el-ni%C3%B1o-and-la-ni%C3%B1a-noaa-adapts-global-warming, National Oceanic and Atmospheric Administration, ClimateWatch Magazine, accessed 7 April 2017.
Liu, Y.Y., Parinussa, R.M., Dorigo, W.A., De Jeu, R.A.M., Wagner, W., van Dijk, A.I.J.M., McCabe, M.F., Evans, J.P., 2011. Developing an improved soil moisture dataset by blending passive and active microwave satellite-based retrievals. Hydrol. Earth Syst. Sci. 15 (2), 425–436.
Llewellyn, E.J., Lloyd, N.D., Degenstein, D.A., Gattinger, R.L., Petelina, S.V., Bourassa, A.E., Wiensz, J.T., Ivanov, E.V., McDade, I.C., Solheim, B.H., McConnell, J.C., Haley, C.S., von Savigny, C., Sioris, C.E., McLinden, C.A., Griffioen, E., Kaminski, J., Evans, W.F., Puckrin, E., Strong, K., Wehrle, V., Hum, R.H., Kendall, D.J., Matsushita, J., Murtagh, D.P., Brohede, S., Stegman, J., Witt, G., Barnes, G., Payne, W.F., Piché, L., Smith, K., Warshaw, G., Deslauniers, D.L., Marchand, P., Richardson, E.H., King, R.A., Wevers, I., McCreath, W., Kyrölä, E., Oikarinen, L., Leppelmeier, G.W., Auvinen, H., Mégie, G., Hauchecorne, A., Lefèvre, F., de La Nöe, J., Ricaud, P., Frisk, U., Sjoberg, F., von Schéele, F., Nordh, L., 2004. The OSIRIS instrument on the Odin spacecraft. Can. J. Phys. 82 (6), 411–422.
Madden, R.A., Julian, P.R., 1971. Detection of a 40–50 day oscillation in the zonal wind in the tropical Pacific. J. Atmos. Sci. 28 (5), 702–708.
Magee, A.D., Verdon-Kidd, D.C., Kiem, A.S., 2016. An intercomparison of tropical cyclone best-track products for the southwest Pacific. Nat. Hazards Earth Syst. Sci. 16 (6), 1431–1447.

Magee, A.D., Verdon-Kidd, D.C., Diamond, H.J., Kiem, A.S., 2017. Influence of ENSO, ENSO Modoki, and the IPO on tropical cyclogenesis: a spatial analysis of the south-west Pacific region. Int. J. Climatol. 37, 1118–1137.
Maggioni, V., Meyers, P.C., Robinson, M.D., 2016. A review of merged high-resolution satellite precipitation product accuracy during the Tropical Rainfall Measuring Mission (TRMM) era. J. Hydrometeorol. 17 (4), 1101–1117.
Mantua, N.J., Hare, S.R., 2002. The Pacific Decadal Oscillation. J. Oceanogr. 58 (1), 35–44.
Mantua, M.J., Hare, S.R., Zhang, Y., Wallace, J.M., Francis, R.C., 1997. A Pacific inter-decadal climate oscillation with impacts on salmon production. Bull. Am. Meteorol. Soc. 78, 1069–1079.
Marshall, G.J., 2003. Trends in the southern annular mode from observations and re-analyses. J. Clim. 16 (24), 4134–4143.
Matthews, A.J., Singhruck, P., Heywood, K.J., 2007. Deep ocean impact of a Madden-Julian Oscillation observed by Argo floats. Science 318 (5857), 1765–1769.
Matthews, A.J., Singhruck, P., Heywood, K.J., 2010. Ocean temperature and salinity components of the Madden–Julian oscillation observed by Argo floats. Clim. Dyn. 35 (7), 1149–1168.
McBride, J.L., Nicholls, N., 1983. Seasonal relationships between Australian rainfall and the Southern Oscillation. Mon. Weather Rev. 111 (10), 1998–2004.
McGowan, H.A., Marx, S.K., Soderholm, J., Denholm, J., 2010. Evidence of solar and tropical-ocean forcing of hydroclimate cycles in southeastern Australia for the past 6500 years. Geophys. Res. Lett. 37 (10), L10705.
McPhaden, M.J., 1999. Genesis and Evolution of the 1997–98 El Niño. Science 283 (5404), 950–954.
Meehl, G.A., 1997. The south Asian monsoon and the tropospheric biennial oscillation. J. Clim. 10 (8), 1921–1943.
Meehl, G.A., Arblaster, J.M., 2011. Decadal variability of Asian–Australian monsoon–ENSO–TBO relationships. J. Clim. 24 (18), 4925–4940.
Meneghini, B., Simmonds, I., Smith, I.N., 2007. Association between Australian rainfall and the Southern Annular Mode. Int. J. Climatol. 27 (1), 109–121.
Menne, M.J., Durre, I., Vose, R.S., Gleason, B.E., Houston, T.G., 2012. An overview of the global historical climatology network-daily database. J. Atmos. Ocean. Technol. 29 (7), 897–910.
Meyers, G., McIntosh, P., Pigot, L., Pook, M., 2007. The years of El Niño, La Niña, and interactions with the tropical Indian Ocean. J. Clim. 20 (13), 2872–2880.
Micevski, T., Franks, S.W., Kuczera, G., 2006. Multidecadal variability in coastal eastern Australian flood data. J. Hydrol. 327 (1–2), 219–225.
Miller, G., Mangan, J., Pollard, D., Thompson, S., Felzer, B., Magee, J., 2005. Sensitivity of the Australian Monsoon to insolation and vegetation: Implications for human impact on continental moisture balance. Geology 33 (1), 65–68.
Mo, K.C., 2000. Relationships between low-frequency variability in the Southern Hemisphere and sea surface temperature anomalies. J. Clim. 13 (20), 3599–3610.
Mufti, S., Shah, G.N., 2011. Solar-geomagnetic activity influence on Earth's climate. J. Atmos. Sol. Terr. Phys. 73 (13), 1607–1615.
Murphy, B.F., Timbal, B., 2008. A review of recent climate variability and climate change in southeastern Australia. Int. J. Climatol. 28 (7), 859–879.
Newnham, G.J., Grant, I.F., Martin, D.N., Anderson, S.A.J., 2010. Improved Methods for Assessment and Prediction of Grassland Curing, Melbourne. (86 pp).
Nicholls, N., 1978. Air-sea interaction and the quasi-biennial oscillation. Mon. Weather Rev. 106 (10), 1505–1508.
Nicholls, N., 1984. The Southern Oscillation, sea-surface-temperature, and interannual fluctuations in Australian tropical cyclone activity. J. Climatol. 4 (6), 661–670.
Nicholls, N., 1985. Predictability of interannual variations of Australian seasonal tropical cyclone activity. Mon. Weather Rev. 113 (7), 1144–1149.
Nicholls, N., 1989. Sea surface temperatures and Australian winter rainfall. J. Clim. 2 (9), 965–973.
Nicholls, N., Landsea, C., Gill, J., 1998. Recent trends in Australian region tropical cyclone activity. Meteorog. Atmos. Phys. 65 (3-4), 197–205.
Nicolas, J.P., Bromwich, D.H., 2011. Precipitation changes in high southern latitudes from global reanalyses: a cautionary tale. Surv. Geophys. 32 (4), 475–494.
Oort, A.H., Yienger, J.J., 1996. Observed interannual variability in the Hadley circulation and its connection to ENSO. J. Clim. 9 (11), 2751–2767.
Palmer, J.G., Cook, E.R., Turney, C.S.M., Allen, K., Fenwick, P., Cook, B.I., O'Donnell, A., Lough, J., Grierson, P., Baker, P., 2015. Drought variability in the eastern Australia and New Zealand summer drought atlas (ANZDA, CE 1500–2012) modulated by the Interdecadal Pacific Oscillation. Environ. Res. Lett. 10 (12), 124002.
Parker, D., Folland, C., Scaife, A., Knight, J., Colman, A., Baines, P., Dong, B., 2007. Decadal to multidecadal variability and the climate change background. J. Geophys. Res. Atmos. 112 (D18), D18115.
Peck, E.L., 1997. Quality of hydrometeorological data in cold regions. J. Am. Water Resour. Assoc. 33 (1), 125–134.
Pepler, A., Timbal, B., Rakich, C., Coutts-Smith, A., 2014. Indian Ocean Dipole overrides ENSO's influence on cool season rainfall across the eastern seaboard of Australia. J. Clim. 27 (10), 3816–3826.
Peterson, T., Daan, H., Jones, P., 1997. Initial selection of a GCOS surface network. Bull. Am. Meteorol. Soc. 78 (10), 2145–2152.
Philander, S.G., 1990. El Niño, La Niña, and the Southern Oscillation. Academic Press, London.
Pook, M., Gibson, T., 1999. Atmospheric blocking and storm tracks during SOP-1 of the FROST Project. Aust. Meteorol. Mag. 51–60.
Power, S., Casey, T., Folland, C., Colman, A., Mehta, V., 1999. Inter-decadal modulation of the impact of ENSO on Australia. Clim. Dyn. 15 (5), 319–324.
Power, S., Haylock, M., Colman, R., Wang, X., 2006. The predictability of interdecadal changes in ENSO activity and ENSO teleconnections. J. Clim. 19 (19), 4755–4771.
Ramanathan, V., Crutzen, P.J., Kiehl, J.T., Rosenfeld, D., 2001. Aerosols, climate, and the hydrological cycle. Science 294 (5549), 2119–2124.
Rao, S.A., Behera, S.K., Masumoto, Y., Yamagata, T., 2002. Interannual subsurface variability in the tropical Indian Ocean with a special emphasis on the Indian Ocean Dipole. Deep-Sea Res. II Top. Stud. Oceanogr. 49 (7–8), 1549–1572.
Raspopov, O.M., Dergachev, V.A., Esper, J., Kozyreva, O.V., Frank, D., Ogurtsov, M., Kolström, T., Shao, X., 2008. The influence of the de Vries (~ 200-year) solar cycle on climate variations: results from the Central Asian mountains and their global link. Palaeogeogr. Palaeoclimatol. Palaeoecol. 259 (1), 6–16.
Rayner, N., Horton, E., Parker, D., Folland, C., Hackett, R., 1996. Version 2.2 of the global sea-ice and sea surface temperature data set, 1903–1994. In: Climate Research Technical Note, pp. 74 (43pp).
Rayner, N.A., Parker, D.E., Horton, E.B., Folland, C.K., Alexander, L.V., Rowell, D.P., Kent, E.C., Kaplan, A., 2003. Global analyses of sea surface temperature, sea ice, and night marine air temperature since the late nineteenth century. J. Geophys. Res. Atmos. 108 (D14).
Reager, J.T., Thomas, B.F., Famiglietti, J.S., 2014. River basin flood potential inferred using GRACE gravity observations at several months lead time. Nat. Geosci. 7 (8), 588–592.
Reid, G.C., 1991. Solar total irradiance variations and the global sea surface temperature record. J. Geophys. Res. Atmos. 96 (D2), 2835–2844.
van Rensch, P., Cai, W., 2014. Indo-Pacific induced wave trains during austral autumn and their effect on Australian rainfall. J. Clim. 27 (9), 3208–3221.
Reynolds, R.W., 2009. What's New in Version 2. (10 pp).
Reynolds, R.W., Smith, T.M., Liu, C., Chelton, D.B., Casey, K.S., Schlax, M.G., 2007. Daily high-resolution-blended analyses for sea surface temperature. J. Clim. 20 (22), 5473–5496.
Rintoul, S.R., Sparrow, M., Meredith, M.P., Wadley, V., Speer, K., Hofmann, E., Summerhayes, C., Urban, E., Bellerby, R., Ackley, S., 2012. The Southern Ocean Observing System: Initial Science and Implementation Strategy. Scientific Committee on Antarctic Research.
Risbey, J.S., Pook, M.J., McIntosh, P.C., Ummenhofer, C.C., Meyers, G., 2009a. Characteristics and variability of synoptic features associated with cool season rainfall in southeastern Australia. Int. J. Climatol. 29 (11), 1595–1613.
Risbey, J.S., Pook, M.J., McIntosh, P.C., Wheeler, M.C., Hendon, H.H., 2009b. On the remote drivers of rainfall variability in Australia. Mon. Weather Rev. 137 (10), 3233–3253.
Ropelewski, C.F., Jones, P.D., 1987. An extension of the Tahiti-Darwin southern oscillation index. Mon. Weather Rev. 115 (9), 2161–2165.
Rossby, C.G., 1949. On the dispersion of planetary waves in a barotropic atmosphere. Tellus 1 (1), 54–58.
Rotstayn, L.D., Cai, W., Dix, M.R., Farquhar, G.D., Feng, Y., Ginoux, P., Herzog, M., Ito, A., Penner, J.E., Roderick, M.L., Wang, M., 2007. Have Australian rainfall and cloudiness increased due to the remote effects of Asian anthropogenic aerosols? J. Geophys. Res. Atmos. 112 (D9), D09202.
Roy, I., Haigh, J.D., 2010. Solar cycle signals in sea level pressure and sea surface temperature. Atmos. Chem. Phys. 10 (6), 3147–3153.
Russell, R.C., 1998. Mosquito-borne arboviruses in Australia: the current scene and implications of climate change for human health. Int. J. Parasitol. 28 (6), 955–969.
Russell, P.B., McCormick, M.P., 1989. SAGE II aerosol data validation and initial data use: an introduction and overview. J. Geophys. Res. Atmos. 94 (D6), 8335–8338.
Russell-Smith, J., Yates, C.P., Whitehead, P.J., Smith, R., Craig, R., Allan, G.E., Thackway, R., Frakes, I., Cridland, S., Meyer, M.C.P., Gill, A.M., 2007. Bushfires 'down under': patterns and implications of contemporary Australian landscape burning. Int. J. Wildland Fire 16 (4), 361–377.
Saji, N.H., Yamagata, T., 2003. Possible impacts of Indian Ocean Dipole mode events on global climate. Clim. Res. 25 (2), 151–169.
Saji, N., Goswami, B.N., Vinayachandran, P., Yamagata, T., 1999. A dipole mode in the tropical Indian Ocean. Nature 401 (6751), 360–363.
Salinger, M.J., Basher, R.E., Fitzharris, B.B., Hay, J.E., Jones, P.D., Macveigh, J.P., Schmidely-Leleu, I., 1995. Climate trends in the South-west Pacific. Int. J. Climatol. 15 (3), 285–302.
Salinger, M.J., Renwick, J.A., Mullan, A.B., 2001. Interdecadal Pacific Oscillation and South Pacific climate. Int. J. Climatol. 21 (14), 1705–1721.
Salinger, M.J., McGree, S., Beucher, F., Power, S., Delage, F., 2014. A new index for variations in the position of the South Pacific convergence zone 1910/11–2011/2012. Clim. Dyn. 43 (3-4), 881–892.
Sapiano, M.R.P., Arkin, P.A., 2009. An intercomparison and validation of high-resolution satellite precipitation estimates with 3-hourly gauge data. J. Hydrometeorol. 10 (1), 149–166.
Sato, M., Hansen, J.E., McCormick, M.P., Pollack, J.B., 1993. Stratospheric aerosol optical depths, 1850–1990. J. Geophys. Res. Atmos. 98 (D12), 22987–22994.
Scafetta, N., 2010. Empirical evidence for a celestial origin of the climate oscillations and its implications. J. Atmos. Sol. Terr. Phys. 72 (13), 951–970.
Schneider, U., Becker, A., Finger, P., Meyer-Christoffer, A., Ziese, M., Rudolf, B., 2014. GPCC's new land surface precipitation climatology based on quality-controlled in situ data and its role in quantifying the global water cycle. Theor. Appl. Climatol. 115 (1), 15–40.
Schubert, S.D., Stewart, R.E., Wang, H., Barlow, M., Berbery, E.H., Cai, W., Hoerling, M.P., Kanikicharla, K.K., Koster, R.D., Lyon, B., Mariotti, A., Mechoso, C.R., Müller, O.V., Rodriguez-Fonseca, B., Seager, R., Seneviratne, S.I., Zhang, L., Zhou, T., 2016. Global meteorological drought: a synthesis of current understanding with a focus on SST drivers of precipitation deficits. J. Clim. 29 (11), 3989–4019.
Schwabe, H., 1844. Sonnen-Beobachtungen im Jahre 1843. Astron. Nachr. 21 (15), 234–235.
Sevruk, B., Ondrás, M., Chvíla, B., 2009. The WMO precipitation measurement intercomparisons. Atmos. Res. 92 (3), 376–380.

Sheffield, J., Goteti, G., Wood, E.F., 2006. Development of a 50-year high-resolution global dataset of meteorological forcings for land surface modeling. J. Clim. 19 (13), 3088–3111.
Sinclair, S., Pegram, G., 2005. Combining radar and rain gauge rainfall estimates using conditional merging. Atmos. Sci. Lett. 6 (1), 19–22.
Smith, C.A., Sardeshmukh, P.D., 2000. The effect of ENSO on the intraseasonal variance of surface temperatures in winter. Int. J. Climatol. 20 (13), 1543–1557.
Smith, T.M., Reynolds, R.W., Peterson, T.C., Lawrimore, J., 2008. Improvements to NOAA's historical merged land-ocean surface temperature analysis (1880-2006). J. Clim. 21 (10), 2283–2296.
Solow, A., Nicholls, N., 1990. The relationship between the Southern Oscillation and tropical cyclone frequency in the Australian region. J. Clim. 3 (10), 1097–1101.
Sorooshian, S., Hsu, K.-L., Gao, X., Gupta, H.V., Imam, B., Braithwaite, D., 2000. Evaluation of PERSIANN system satellite–based estimates of tropical rainfall. Bull. Am. Meteorol. Soc. 81 (9), 2035–2046.
Spence, T., Townshend, J., 1995. The Global Climate Observing System (GCOS). Clim. Chang. 31 (2), 131–134.
Stauning, P., 2011. Solar activity–climate relations: a different approach. J. Atmos. Sol. Terr. Phys. 73 (13), 1999–2012.
Stechmann, S.N., Ogrosky, H.R., 2014. The Walker circulation, diabatic heating, and outgoing longwave radiation. Geophys. Res. Lett. 41 (24), GL062257.
Stone, R.C., 2014. Constructing a framework for national drought policy: the way forward – The way Australia developed and implemented the national drought policy. Weather and Clim. Extremes 3 (0), 117–125.
Strangeways, I., 2004. Improving precipitation measurement. Int. J. Climatol. 24 (11), 1443–1460.
Stuecker, M.F., Timmermann, A., Jin, F.-F., Chikamoto, Y., Zhang, W., Wittenberg, A.T., Widiasih, E., Zhao, S., 2017. Revisiting ENSO/Indian Ocean Dipole phase relationships. Geophys. Res. Lett. 44 (5), 2481–2492.
Suess, H.E., 1978. La Jolla measurements of radiocarbon in tree-ring dated wood. Radiocarbon 20 (1), 1–18.
Swenson, S., Wahr, J., 2002. Methods for inferring regional surface-mass anomalies from Gravity Recovery and Climate Experiment (GRACE) measurements of time-variable gravity. J. Geophys. Res. Solid Earth 107 (B9), 2193.
Takahashi, K., Montecinos, A., Goubanova, K., Dewitte, B., 2011. ENSO regimes: Reinterpreting the canonical and Modoki El Niño. Geophys. Res. Lett. 38 (10).
Tanaka, H.L., Ishizaki, N., Kitoh, A., 2004. Trend and interannual variability of Walker, monsoon and Hadley circulations defined by velocity potential in the upper troposphere. Tellus A 56 (3), 250–269.
Tapiador, F.J., Turk, F.J., Petersen, W., Hou, A.Y., García-Ortega, E., Machado, L.A.T., Angelis, C.F., Salio, P., Kidd, C., Huffman, G.J., de Castro, M., 2012. Global precipitation measurement: Methods, datasets and applications. Atmos. Res. 104–105, 70–97.
Tapley, B.D., Chambers, D.P., Bettadpur, S., Ries, J.C., 2003. Large scale ocean circulation from the GRACE GGM01 Geoid. Geophys. Res. Lett. 30 (22).
Tapping, K.F., 2013. The 10.7 cm solar radio flux (F10.7). Space Weather 11 (7), 394–406.
Taschetto, A.S., Ummenhofer, C.C., Gupta, A.S., England, M.H., 2009. Effect of anomalous warming in the central Pacific on the Australian monsoon. Geophys. Res. Lett. 36, L12704. http://dx.doi.org/10.1029/2009GL038416.
Thompson, D.W.J., Wallace, J.M., 2000. Annular modes in the extratropical circulation. Part I: Month-to-month variability. J. Clim. 13 (5), 1000–1016.
Timbal, B., Drosdowsky, W., 2013. The relationship between the decline of Southeastern Australian rainfall and the strengthening of the subtropical ridge. Int. J. Climatol. 33 (4), 1021–1034.
Tinsley, B.A., Yu, F., 2004. Atmospheric ionization and clouds as links between solar activity and climate. In: Pap, J.M., Fox, P., Frohlich, C., Hudson, H.S., Kuhn, J., McCormack, J., North, G., Sprigg, W., Wu, S.T. (Eds.), Solar Variability and Its Effects on Climate. American Geophysical Union, Washington, D. C., pp. 321–339.
Torok, S., Nicholls, N., 1996. A historical annual temperature dataset for Australia. Aust. Meteorol. Mag. 45 (4), 251–260.
Tozer, C.R., Kiem, A.S., 2017. Large-scale ocean-atmospheric processes and seasonal rainfall variability in South Australia: accounting for non-linearity and establishing the hierarchy of influence. Int. J. Climatol. 37, 1180–1198.
Tozer, C.R., Kiem, A.S., Verdon-Kidd, D.C., 2012. On the uncertainties associated with using gridded rainfall data as a proxy for observed. Hydrol. Earth Syst. Sci. 16 (5), 1481–1499.
Tozer, C.R., Verdon-Kidd, D.C., Kiem, A.S., 2014. Temporal and spatial variability of the cropping limit in South Australia. Clim. Res. 60 (1), 25–34.
Tozer, C.R., Kiem, A.S., Verdon-Kidd, D.C., 2017. Large-scale ocean-atmospheric processes and seasonal rainfall variability in South Australia: potential for improving seasonal hydroclimatic forecasts. Int. J. Climatol. 37, 861–877.
Trenberth, K.E., 1997. The definition of El Niño. Bull. Am. Meteorol. Soc. 78 (12), 2771–2777.
Trenberth, K.F., Mo, K.C., 1985. Blocking in the southern hemisphere. Mon. Weather Rev. 113 (1), 3–21.
Trenberth, K.E., Stepaniak, D.P., 2001. Indices of El Niño evolution. J. Clim. 14 (8), 1697–1701.
Trewin, B.C., 2001. Extreme temperature events in Australia. University of Melbourne, Melbourne, Australia.
Trewin, B., 2013. A daily homogenized temperature data set for Australia. Int. J. Climatol. 33 (6), 1510–1529.
Troup, A.J., 1965. The 'southern oscillation'. Q. J. R. Meteorol. Soc. 91 (390), 490–506.
Turk, F.J., Hawkins, J., Smith, E.A., Marzano, F.S., Mugnai, A., Levizzani, V., 2000. Combining SSM/I, TRMM and Infrared Geostationary Satellite Data in a Near-realtime Fashion for Rapid Precipitation Updates: Advantages and Limitations. Proceedings of the 2000 EUMETSAT Meteorological Satellite Data Users' Conferencepp. 705–707.
Ummenhofer, C.C., England, M.H., McIntosh, P.C., Meyers, G.A., Pook, M.J., Risbey, J.S., Gupta, A.S., Taschetto, A.S., 2009a. What causes southeast Australia's worst droughts? Geophys. Res. Lett. 36 (4), L04706.
Ummenhofer, C.C., Gupta, A.S., Taschetto, A.S., England, M.H., 2009b. Modulation of Australian precipitation by meridional gradients in east Indian Ocean sea surface temperature. J. Clim. 22 (21), 5597–5610.
Ummenhofer, C.C., Sen Gupta, A., Briggs, P.R., England, M.H., McIntosh, P.C., Meyers, G.A., Pook, M.J., Raupach, M.R., Risbey, J.S., 2011. Indian and Pacific Ocean influences on southeast Australian drought and soil moisture. J. Clim. 24 (5), 1313–1336.
Ushio, T., Sasashige, K., Kubota, T., Shige, S., Okamoto, K.i., Aonashi, K., Inoue, T., Takahashi, N., Iguchi, T., Kachi, M., Oki, R., Morimoto, T., Kawasaki, Z.-I., 2009. A Kalman filter approach to the Global Satellite Mapping of Precipitation (GSMaP) from combined passive microwave and infrared radiometric data. J. Meteorol. Soc. Jpn. II (87A), 137–151.
Usoskin, I.G., 2013. A history of solar activity over millennia. Living Rev. Sol. Phys. 10 (1), 1–94.
Vance, T.R., Roberts, J.L., Plummer, C.T., Kiem, A.S., van Ommen, T.D., 2015. Interdecadal Pacific variability and eastern Australian megadroughts over the last millennium. Geophys. Res. Lett. 42 (1), 129–137.
Velden, C., Harper, B., Wells II, F., J.L.B, Zehr, R., Olander, T., Mayfield, M., Guard, C.C., Lander, M., Edson, R., Avila, L., Burton, A., Turk, M., Kikuchi, A., Christian, A., Caroff, P., McCrone, P., 2006. The Dvorak tropical cyclone intensity estimation technique: A satellite-based method that has endured for over 30 years. Bull. Am. Meteorol. Soc. 87 (9), 1195–1210.
Ventrice, M.J., Wheeler, M.C., Hendon III, H.H., C.J.S, Thorncroft, C.D., Kiladis, G.N., 2013. A modified multivariate Madden–Julian oscillation index using velocity potential. Mon. Weather Rev. 141 (12), 4197–4210.
Venzke, S., Latif, M., Villwock, A., 2000. The coupled GCM ECHO-2. Part II: Indian Ocean response to ENSO. J. Clim. 13 (8), 1371–1383.
Verdon, D.C., Franks, S.W., 2005. Indian Ocean sea surface temperature variability and winter rainfall: Eastern Australia. Water Resour. Res. 41 (9).
Verdon, D., Kiem, A., Franks, S., 2004a. Multi-decadal variability of forest fire risk—eastern Australia. Int. J. Wildland Fire 13 (2), 165–171.
Verdon, D.C., Wyatt, A.M., Kiem, A.S., Franks, S.W., 2004b. Multidecadal variability of rainfall and streamflow: eastern Australia. Water Resour. Res. 40 (10), W10201.
Vincent, E., Lengaigne, M., Menkes, C., Jourdain, N., Marchesiello, P., Madec, G., 2011. Interannual variability of the South Pacific Convergence Zone and implications for tropical cyclone genesis. Clim. Dyn. 36 (9-10), 1881–1896.
Vuerich, E., Monesi, C., Lanza, L.G., Stagi, L., Lanzinger, E., 2009. WMO field intercomparison of rainfall intensity gauges. In: Instruments and Observing Methods, (96 pp).
Wang, C., Xie, S.P., Carton, J.A., Wang, C., Xie, S.-P., Carton, J.A., 2004. A Global Survey of Ocean-Atmosphere Interaction and Climate Variability, Earth's Climate: The Ocean-Atmosphere Interaction. Geophys. Monogr. Ser. AGU, Washington, DC, pp. 1–19.
Ward, P.J., Jongman, B., Kummu, M., Dettinger, M.D., Sperna Weiland, F.C., Winsemius, H.C., 2014. Strong influence of El Niño Southern Oscillation on flood risk around the world. Proc. Natl. Acad. Sci. 111 (44), 15659–15664.
Weng, H., 2005. The influence of the 11 yr solar cycle on the interannual–centennial climate variability. J. Atmos. Sol. Terr. Phys. 67 (8–9), 793–805.
Whan, K., Timbal, B., Lindesay, J., 2014. Linear and nonlinear statistical analysis of the impact of sub-tropical ridge intensity and position on south-east Australian rainfall. Int. J. Climatol. 34 (2), 326–342.
Wheeler, M.C., Hendon, H.H., 2004. An all-season real-time multivariate MJO index: development of an index for monitoring and prediction. Mon. Weather Rev. 132 (8), 1917–1932.
Wheeler, M.C., Hendon, H.H., Cleland, S., Meinke, H., Donald, A., 2009. Impacts of the Madden-Julian oscillation on Australian rainfall and circulation. J. Clim. 22 (6), 1482–1498.
Whelan, J.A., Frederiksen, J.S., Frederiksen, C.S., Osbrough, S.L., 2013. Synoptic and Dynamical Analyses of ENSO Extreme Events Over Australia, 20th International Congress on Modelling and Simulation, Adelaide, Australia.
White, W.B., Liu, Z., 2008. Non-linear alignment of El Niño to the 11-yr solar cycle. Geophys. Res. Lett. 35 (19), L19607.
Williams, A.A., Karoly, D.J., 1999. Extreme fire weather in Australia and the impact of the El Niño-Southern Oscillation. Aust. Meteorol. Mag. 48 (1), 15–22.
WMO, 1983. Measurement of Surface Wind, Guide to Meteorological Instruments and Methods of Observation. World Meteorological Organization, pp. 121–134.
WMO, 2007. The Role of Climatological Normals in a Changing Climate (WMO/TD-No. 1377, WCDMP-No. 61). World Meteorological Organization, Geneva.
Wolter, K., Timlin, M.S., 1993. In: Monitoring ENSO in COADS With a Seasonally Adjusted Principal Component Index. Proc. of the 17th Climate Diagnostics Workshop. NOAA/NMC/CAC, NSSL, Oklahoma Clim. Survey, CIMMS and the School of Meteor. Univ. of Oklahoma, Norman, OK, pp. 52–57.
Wolter, K., Timlin, M.S., 1998. Measuring the strength of ENSO events: how does 1997/98 rank? Weather 53 (9), 315–324.
Wolter, K., Timlin, M.S., 2011. El Niño/Southern Oscillation behaviour since 1871 as diagnosed in an extended multivariate ENSO index (MEI.ext). Int. J. Climatol. 31 (7), 1074–1087.
Worley, S.J., Woodruff, S.D., Reynolds, R.W., Lubker, S.J., Lott, N., 2005. ICOADS release 2.1 data and products. Int. J. Climatol. 25 (7), 823–842.
Wu, Z., Li, J., Wang, B., Liu, X., 2009. Can the Southern Hemisphere annular mode affect China winter monsoon? J. Geophys. Res. Atmos. 114 (D11), D11107.

Xue, Y., Higgins, W., Kousky, V., 2002. Influences of the Madden Julian Oscillations on Temperature and Precipitation in North America During ENSO-neutral and Weak ENSO Winters. Proc. Workshop on Prospects for Improved Forecasts of Weather and Short-term Climate Variability on Subseasonal (2 Week to 2 Month) Time Scales, NASA Goddard Space Flight Center, MDpp. 1–4.
Yasunaka, S., Hanawa, K., 2011. Intercomparison of historical sea surface temperature datasets. Int. J. Climatol. 31 (7), 1056–1073.
Zeng, J., Chen, K.S., Bi, H., Chen, Q., 2016. A preliminary evaluation of the SMAP radiometer soil moisture product over United States and Europe using ground-based measurements. IEEE Trans. Geosci. Remote Sens. 54 (8), 4929–4940.
Zhang, C., 2005. Madden-Julian Oscillation. Rev. Geophys. 43 (2), RG2003.
Zhang, Y., Wallace, J.M., Battisti, D.S., 1997. ENSO-like interdecadal variability: 1900–93. J. Clim. 10 (5), 1004–1020.